OPTICAL DETECTION OF SPIN-BATH RELAXATION IN SOME PARAMAGNETIC CRYSTALS

by

HANS GLÄTTLI

Dipl. Phys. ETH, Zürich, 1963

A THESIS SUBMITTED IN PARTIAL FULFILMENT OF THE REQUIREMENTS FOR THE DEGREE OF

DOCTOR OF PHILOSOPHY

in the Department

of

Physics

We accept this thesis as conforming to the required standard

THE UNIVERSITY OF BRITISH COLUMBIA

July, 1966

In presenting this thesis in partial fulfilment of the requirements for an advanced degree at the University of British Columbia, I agree that the Library shall make it freely available for reference and study. I further agree that permission for extensive copying of this thesis for scholarly purposes may be granted by the Head of my Department or by his representatives. It is understood that copying or publication of this thesis for financial gain shall not be allowed without my written permission.

Department of Physics

The University of British Columbia
Vancouver 8, Canada

Date August 19, 1966

THE UNIVERSITY OF BRITISH COLUMBIA

FACULTY OF GRADUATE STUDIES

PROGRAMME OF THE

FINAL ORAL EXAMINATION

FOR THE DEGREE OF

DOCTOR OF PHILOSOPHY

of

HANS GLÄTTLI

Dipl.Phys., Swiss Federal Institute

of Technology, (ETH), Zurich, 1963

FRIDAY, AUGUST 19, 1966, at 1:30 P.M.

IN ROOM 301, HENNINGS BUILDING

COMMITTEE IN CHARGE

Chairman: J. H. G. Smith

M. Bloom
J. B. Farmer
W. Opechowski
C. F. Schwerdtfeger
D. L. Williams
R. C. Williams

External Examiner: S. Geschwind

Bell Telephone Laboratories, Incorporated

Murray Hill, New Jersey

Research Supervisor: M. Bloom

OPTICAL DETECTION OF SPIN-BATH RELAXATION IN SOME PARAMAGNETIC CRYSTALS

ABSTRACT

The magneto-optical Faraday effect has been used to observe the spin-bath relaxation at low temperatures in CeES and in Eu-doped CaF_2. The paramagnetic Faraday rotation ϱ is an instantaneous measure of the magnetization M and it is shown that in CeES and Eu^{2+} : CaF_2, $\varrho \sim M$ at the light frequencies employed. The apparatus is the same as that previously described by Rieckoff and by Griffiths. Pulsed MW-power at X-band has been used to disturb the equilibrium between spin system and bath.

In CeES, the observed relaxation time τ is of the order of a few msec, which is several orders of magnitude longer than the theoretical estimate of T_1. This suggests a severe bottleneck in the energy transfer spin-bath. τ is found to be environment-dependent. In HeII, the relaxation is exponential. τ is in good agreement with nonresonant relaxation measurements by Van den Broek and Van der Marel. It is explained as arising from the Kapitza boundary resistance at the CeES-HeII interface. In HeI, the relaxation is non-exponential and is slower than in He gas at the same temperature. This suggests that in this case the thermal diffusion in the helium around the crystal is the bottleneck. The same relaxation behaviour is found when the crystal is heated dielectrically with MW power far off resonance. This supports the assumption that the energy transfer spin-bath is limited by spatial diffusion. If the crystal is surrounded by a He film at a temperature below the λ-point, τ is found to be the same as in HeII up to a well defined average MW power level. For higher powers the relaxation behaviour is similar to that of CeES immersed in HeI.

In Eu^{2+} : CaF_2, T_1 is expected to have the form $T_1 = AT + BT^5$. The observed relaxation time τ, however, is found to be concentration dependent. All measurements have been done on the $+\frac{1}{2} \rightarrow -\frac{1}{2}$ transition with H $\parallel$ [100]. For the three lowest concentrations, the temperature dependence of τ from 1.5 to 4.2°K can be fitted with the expression $\tau^{-1} = CT$ with C = 2.75 (sec°K)$^{-1}$ for 0.02% Eu, C = 3.5 for

0.8% and C = 5 for 0.2%. At a concentration of 2%, τ is shorter and $\tau^{-1} \sim T^2$ from 1.5°K to 7°K. The concentrations given correspond to the total Eu content. The Eu^{2+} concentration has been inferred from the magnitude of the saturation rotation. τ (T) seems to depend on both Eu^{2+} and Eu^{3+} concentrations. It is suggested that exchange coupled pairs of Eu^{2+} and clusters involving Eu^{3+} may account for the concentration dependence of τ. Upper limits of A = 2.5 and B = 5 x 10^{-5} are found for T_1 by extrapolating the lowest concentrations investigated. These values are somewhat lower than both measured and calculated values found by Huang.

GRADUATE STUDIES

Field of Study: Low Temperature Solid State

Elementary Quantum Mechanics	F. A. Kaempffer
Quantum Theory of Solids	W. Opechowski
Advanced Magnetism	M. Bloom
Statistical Mechanics	R. Barrie
Group Theory Methods in Quantum Mechanics	W. Opechowski
Applied Electromagnetic Theory	M. M. Z. Kharadly

AWARDS

1963-64 -Graduate Fellowships, The University of British Columbia.

1965 -National Research Council of Canada Studentship.

PUBLICATIONS

D. J. Griffiths and Hans Glättli, Optical Faraday Rotation Studies of Paramagnetic Resonance and Relaxation in Praseodymium Ethylsulphate. Can. J. Phys. 43, 2361, (1965).

D. J. Griffiths and Hans Glättli, Imprisonment of Phonons by Pr^{3+} Ions in Praseodymium Ethylsulphate. Phys. Letters 21, 275, (1966).

.....
(Prof. W. Opechowski)
for the Supervisor Professor Myer Bloom

ABSTRACT

The magneto-optical Faraday effect has been used to observe the spin-bath relaxation at low temperatures in cerium ethylsulphate (CeES) and in europium doped calcium fluoride ($Eu^{2+}:CaF_2$). The paramagnetic Faraday rotation ϱ is an instantaneous measure of the magnetization M and it is shown that in CeES and $Eu^{2+}:CaF_2$ $\varrho \sim M$ at the light frequencies employed. The apparatus is the same as that previously described by Rieckoff and by Griffiths. Pulsed microwave power at X-band has been used to disturb the equilibrium between spin system and bath.

In CeES, the observed relaxation time τ is of the order of a few msec, which is several orders of magnitude longer than the theoretical estimate of T_1. This suggests a severe bottleneck in the energy transfer spin-bath. τ is found to be environment dependent. In HeII, the relaxation is exponential. τ is in good agreement with nonresonant relaxation measurements by Van den Broek and Van der Marel. It is explained as arising from the Kapitza boundary resistance at the CeES-HeII interface. In HeI, the relaxation is non-exponential and is slower than in He gas at the same temperature. This suggests that in this case the thermal diffusion in the helium around the crystal is the bottleneck. The same relaxation behaviour is found when the crystal is heated dielectrically with microwave power far off resonance. This supports the assumption that the energy transfer spin-bath is limited by spatial diffusion. If the crystal

is surrounded by a He film at a temperature below the λ-point, τ is found to be the same as in HeII up to a well defined average microwave power level. For higher powers the relaxation behaviour is similar to that of CeES immersed in HeI.

In $Eu^{2+}:CaF_2$, T_1 is expected to have the form $T_1 = AT+BT^5$. The observed relaxation time τ, however, is found to be concentration dependent. All measurements have been done on the $+\frac{1}{2} \rightarrow -\frac{1}{2}$ transition with $H \parallel [100]$. For the three lowest concentrations, the temperature dependence of τ from 1.5 to 4.2°K can be fitted with the expression $\tau^{-1} = CT$ with $C = 2.75(\text{sec}\,°K)^{-1}$ for 0.02% Eu, C = 3.5 for 0.8% and C = 5 for 0.2%. At a concentration of 2%, τ is shorter and $\tau \sim T^2$ from 1.5°K to 7°K. The concentrations given correspond to the total Eu content. The Eu^{2+} concentration has been inferred from the magnitude of the saturation rotation. τ (T) seems to depend on both Eu^{2+} and Eu^{3+} concentrations. It is suggested that exchange coupled pairs of Eu^{2+} and clusters involving Eu^{3+} may account for the concentration dependence of τ. Upper limits of A = 2.5 and $B = 5 \times 10^{-5}$ are found for T_1 by extrapolating the lowest concentrations investigated. These values are somewhat lower than both measured and calculated values found by Huang.

TABLE OF CONTENTS

LIST OF ILLUSTRATIONS AND TABLES

Table

ACKNOWLEDGEMENTS

The research described in this thesis was supported by the National Research Council of Canada through grants to Dr. M. Bloom and the award of a studentship to the author.

The author is indebted to the University of British Columbia for the award of two graduate fellowships.

Among the many persons who have contributed to the completion of this work the author would like to thank particularly:

Dr. M. Bloom for his continuous support throughout this work;

Dr. J. B. Brown for his active help and many interesting discussions during the experimental stages;

Professor W. Opechowski for his interest and many helpful suggestions;

Dr. C. F. Schwerdtfeger and Mr. B. J. Slagsvold for checking the samples on their 34 kMc/s spectrometer;

Dr. D. J. Griffiths, from whom I learned most of the experimental know-how;

Mr. T. E. Clarke for his assistance in taking the measurements;

Mr. G. W. Brooks for the construction of the current regulation and the mounting of the dewar cap;

Mr. R. Weissbach for his advice in technical matters and for providing the liquid helium;

Mr. R. F. Trehearne and Mr. Phil West from Nuclear Data

Inc. for lending us an Enhancetron;

Dr. J. A. Wada and Mr. Finn Bauck of the Neurological Institute at U.B.C. for the use of their Mnemotron CAT 400B;

Mrs. R. A. Foreman for her expert typing and advice in questions of language;

and, last but most, my wife Josette, who not only contributed to this work through her continuous moral support, but also helped actively in the time consuming process of evaluating the relaxation traces.

1 INTRODUCTION

Spin-bath relaxation is the mechanism of energy exchange between a system of paramagnetic ions ("spin system") of a crystal and a constant temperature bath of phonons.

Kronig (1939) suggested that a direct energy transfer from the spins to the lattice phonons could take place due to the modulation of the crystal field by the lattice vibrations through the interplay of spin-orbit coupling.

Van Vleck (1939, 1940) calculated the time constant T_1 characterising this direct energy transfer by analysing the normal modes of vibration of an octahedral cluster surrounding the paramagnetic ion. At the lowest temperatures, the one-phonon or direct processes, where the spin makes a transition with the simultaneous emission or absorption of a single phonon, is dominant. At high temperatures, a two-phonon process is dominant. Here, the spin transition is accompanied by inelastic scattering of a phonon into another of different frequency. The energy difference of the two phonons corresponds to the spin transition-frequency. This two-phonon process is known as the Raman process.

Finn, Orbach and Wolf (1961) have shown that a resonant two-phonon process via excited states which are close to the ground state can account for the magnitude and temperature dependence of observed relaxation times which could not be explained in terms of direct and Raman processes. Orbach (1961)

described a phenomenological approach to find the orbit-lattice interaction and from there T_1. This approach avoids the Van Vleck normal-mode expansion, which is very complicated even for cubic symmetry.

The calculation of the relaxation times from the Van Vleck-Orbach theory is reviewed in chapter 2.2. It is in good agreement with many experimental results.

In many cases, however, big discrepancies between theory and experiment are observed and the basic model has to be modified to account for the observed relaxation times.

As early as 1941, Van Vleck has pointed out a possible shortcoming of his model. At the low temperatures, for which the direct process is usually dominant, there exist only very few phonons with energies corresponding to the Zeeman splitting, the so-called phonons "on speaking terms" with the lattice. The assumption of a phonon system in internal equilibrium at constant temperature can be violated. The energy transfer proceeds in two steps, from the spin system via the phonons on speaking terms to the bath. Bath means that part of the phonon system which remains at a constant temperature during the whole relaxation process. The second step can be the limiting process in the energy exchange. This situation is known as the phonon bottleneck. Two-step relaxation processes of this kind show in general nonexponential behaviour and only in limiting cases a single relaxation time is found. The observed relaxation time τ is longer than T_1. (T_1,

called the spin-lattice relaxation time, is used throughout this thesis to characterize the time constant for the direct energy transfer between the spin system and the lattice oscillators by the Van Vleck-Orbach mechanism.)

τ is dependent on the concentration of the paramagnetic ions and approaches T_1 in the limit of low concentration. The phonon bottleneck is studied in more detail in chapter 2.3.

Spin-spin interaction is another complication in real crystals which can lead to observed relaxation times quite different from T_1. This interaction can induce cross-relaxations. The term cross-relaxation, introduced by Bloembergen et al (1959), is used for processes in which energy is transferred directly from one spin system to another spin system or to other levels of the same system. Such processes lead to relaxation paths in parallel to the conventional process of direct energy exchange between the spin system in question and the bath which is characterized by T_1 (in absence of a phonon bottleneck). The observed relaxation time is faster than T_1 and the discrepancy increases with concentration. More details on these cross-relaxation processes are given in chapter 2.4.

Several different methods have been used to observe paramagnetic relaxation and to measure the relaxation times.

In the nonresonant method, developed before World War II and extensively applied by the Leiden group, the absorption and dispersion parts of the magnetic susceptibility are meas-

ured at audio and rf frequency and the value of T_1 deduced.

With the availability of microwave techniques, a number of resonant methods have been developed, eg. the steady state saturation measurements (Eschenfelder and Weidner, 1962), the pulse saturation recovery method (Scott and Jeffries, 1962), and the spin echo techniques (Mims, 1965).

Several optical methods have also been applied successfully. Here, changes in the optical properties of the substance are monitored. Paramagnetic resonance and relaxation in excited states have been detected by Geschwind et al (1961) using optical methods. A discussion of different optical methods is given by Geschwind et al (1965).

The results reported in chapter 4 of this thesis have been obtained using the magneto-optical Faraday effect.

Kramers (1930) and Van Vleck and Hebb (1934) have shown that, under certain circumstances, the direction of polarization of linearly polarized light, after passing through a paramagnetic crystal, can change by an angle which is proportional to the magnetization. It is shown in chapter 2.5 that this proportionality holds for the two substances investigated in this thesis.

Based on Kramers' theory, Becquerel, de Haas and Van den Handel (1937) used the Faraday effect to measure the susceptibility of several rare earth ethylsulphates at low temperatures.

Kastler (1951) pointed out the possibility of an influence of microwave radiation on the optical Faraday rotation. Opechowski (1953) has given a quantum theoretical calculation

of the optical Faraday rotation in presence of microwave resonant radiation. The effect has later been observed in this laboratory by Daniels and Wesemeyer (1958) and has been used to measure spin-bath relaxation times in neodymium ethylsulphate, $Nd(C_2H_5SO_4)_3 9H_2O$ (Rieckoff, 1962), and in praseodymium ethylsulphate (Griffiths, 1965). The same technique as used by the above authors has been applied to study the spin-bath relaxation in undiluted cerium ethylsulphate (CeES) and in europium doped calcium fluoride (Eu^{2+}: CaF_2). Detailed descriptions of the apparatus have been given in the references cited above. A brief review of the experimental set-up and a description of the procedures employed in the present investigations is given in chapter 3.

Both crystals used in the present work have a large Faraday rotation, X-band microwave transitions within the range of our magnet and specimens of reasonable size and optical quality are readily available. They are therefore suitable for investigation with our apparatus.

The relaxation behaviour of the two substances is very different due to a different structure of the ground state of the paramagnetic ions. In neither substance can the observed relaxation times be explained in terms of the Van Vleck-Orbach mechanism. This is due to the fact that T_1 has extreme values in both cases. In CeES, T_1 is very short while in Eu^{2+}: CaF_2 T_1 is very long.

CeES:

Crystal structure and magnetic properties of the CeES are reviewed in chapter 2.1. The cerium ion in an ethylsulphate lattice has as ground state a Kramers doublet. The characteristic feature is an excited doublet $\sim 5\ cm^{-1}$ above the ground state. This close excited doublet leads to an exceptionally strong spin-lattice coupling. T_1 of the Ce ions is expected to be short due to a strong Orbach process. A theoretical estimate of T_1 based on Orbach's phenomenological approach is given in chapter 2.2. This value is several orders of magnitude shorter than the observed relaxation times. It seems likely, therefore, that a phonon bottleneck is observed, even though the spin-lattice relaxation proceeds via the excited doublet at $5\ cm^{-1}$, thus involving phonons with energies of a few times kT.

The experimental results are described and discussed in detail in chapter 4.1. It is seen that the observed relaxation times depend strongly on the environment.

The rate of energy transfer spin-bath is limited by the thermal diffusion from the crystal to its surroundings. The bath in the sense defined earlier is, in this case, the bulk liquid or gaseous helium surrounding the crystal.

If the crystal is immersed in HeI, the thermal diffusion in the liquid seems to limit the rate of energy transfer. The observed relaxation behaviour is slower than in gaseous helium at the same temperature and is nonexponential. This would be expected for thermal diffusion in three dimensions. In HeII,

the thermal diffusion in the bulk liquid is orders of magnitude faster. The limiting process here seems to be the Kapitza boundary resistance at the interface crystal—HeII. The relaxation is exponential, in agreement with the assumption of a surface diffusion process. The Kapitza resistance has been calculated from the measured relaxation times and the known specific heat values. The results agree in magnitude, temperature and field dependence with Kapitza resistance measurements on other substances obtained with conventional heat conduction techniques.

The relaxation behaviour of CeES does not depend on whether the crystal is heated dielectrically in magnetic fields far from resonance or if the energy is transferred to the crystal mainly through the spins as is the case if the magnetic field is on resonance. This indicates that the distribution of excitation among the phonons of different frequencies is the same in both cases.

A conventional heat conduction experiment would give a good test for the validity of the explanations above. Such an experiment should be performed in a simpler geometry such that the thermal diffusion equation can be solved more easily.

Eu^{2+}: CaF_2

The situation in the Eu^{2+}-doped CaF_2 is quite different from the one in CeES.

The Eu^{2+} free ion has a $^8S_{\frac{7}{2}}$ ground state. The cubic field of the fluoride lattice can split the 8-fold degenerate ground state only in higher order through the interplay of spin-orbit

coupling. In magnetic fields of a few kOe, the ground state is split into eight nearly equidistant levels which can be labelled according to J_z, the z-component of the total angular momentum. Magnetic dipole transitions of the form $J_z \rightarrow J_z+1$ can be induced by microwave radiation. The seven paramagnetic resonance lines resulting from these transitions are separated due to the crystal field by an amount which depends upon the relative orientation of the magnetic field with respect to the crystallographic directions. As an additional complication, each line corresponding to a given electronic transition is split into a total of twelve hyperfine lines due to two different isotopes each of which has a nuclear spin $I = 5/2$. In such a complicated multilevel system, cross-relaxations may influence the relaxation behaviour, particularly since the spin-lattice relaxation is expected to be slow for an S-state. A short review of the pertinent theory is given in chapter 2.4. A phonon bottleneck as in CeES cannot occur in Eu^{2+} : CaF_2 since the rate of energy transfer from the spins to the lattice is very small.

We have measured the spin-bath relaxation time of Eu^{2+} ions in CaF_2 by saturating the $J_z = \frac{1}{2} \rightarrow -\frac{1}{2}$ transition. The magnetic field was parallel to the [100] direction in the crystal. This configuration gives minimum cross-relaxation within the single-spin system since the crystal field splitting is maximum and the $\frac{1}{2} \rightarrow -\frac{1}{2}$ transition is quite far removed from the other electronic transitions. The absence of cross-relaxation to other lines has been verified by Huang (1965) using the pulse satura-

tion technique. The results obtained in the present investigation are shown and discussed in chapter 4.2.

The spin bath relaxation times are seen to differ considerably for different specimens, both in magnitude and temperature dependence. The relaxation times get shorter and their temperature dependence becomes steeper with increasing concentration. At the lowest concentration, the relaxation times follow closely a T^{-1}-law suggesting a direct process. At higher concentrations, some mechanism other than the Van Vleck-Orbach relaxation must provide additional channels through which the relaxation can take place.

Exchange coupled pairs or clusters coupled to the single spins by cross-relaxations could provide such mechanisms. This has been first suggested by Van Vleck (1959) and has since been used to explain qualitatively concentration dependent relaxation times of the kind observed in Eu^{2+}: CaF_2.

It is impossible to give more than qualitative arguments in this case. The spectrum of the single ion is already very complicated and the spectrum of exchange coupled pairs or clusters is necessarily even more involved.

An unsuccessful attempt to measure the spin-bath relaxation in undiluted erbium ethylsulphate is described in chapter 4.3. ErES has a smaller Faraday rotation and a larger birefringence than the other rare earth ethylsulphates and an alignment of the crystal-axis sufficiently parallel to the light could not be achieved with our apparatus.

2.1 Cerium Ethylsulphate

2.1.1 Crystal Structure

The ethyl sulphates (ES) form a group of isomorphous substances. Their formula is $M(C_{12}H_5SO_4)_3 \times 9H_2O$ where M stands for all trivalent rare earth ions from La to Yb and for Y. The crystal structure has been determined by Ketelaar (1937) and more recently by Fitzwater and Rundle (1959). Figure 2.1 shows the arrangement of the 9 watermoleoules and of the ethylsulphate radicals around the cerium ion. The crystal is composed of two interlocking lattices of these CeES groups (Figure 2.2). The unit cell contains two magnetically equivalent cerium ions. The point symmetry of the rare earth sites is C_{3h}. Small departures from this symmetry might occur due to arrangement of the protons in the water molecules according to a lower symmetry. In fact, a small admixture of C_{3v} is able to account for the observed transitions between the two lowest doublets (Devor and Hoskins, 1961).

The volume of the unit cell is 1.2×10^{-21} cm^3 which gives a spin concentration of 1.6×10^{21} cm^{-3} for the undiluted salt. The density is $\varrho = 1.9$ gcm^{-3}.

Each cerium ion has two nearest neighbours at a distance of 7.11 Å along the hexagonal axis and six next-nearest neighbours at 8.55 Å at the edges of a triangular prism surrounding the ion.

2.1.2 Groundstate and Paramagnetic Resonance

Cerium is the first ion of the rare earth series which

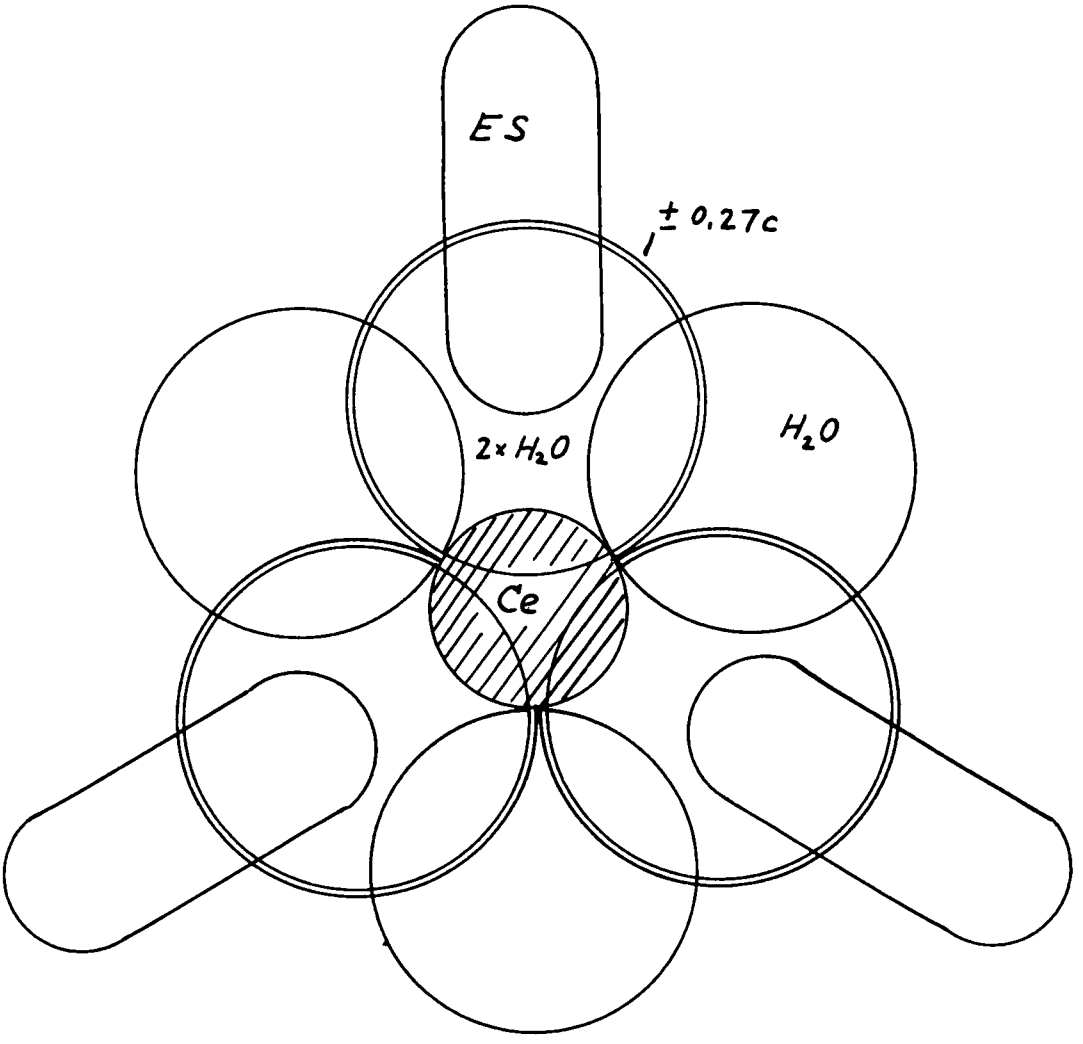

Figure 2.1 Arrangement of H_2O and ES molecules around the Ce ion in CeES

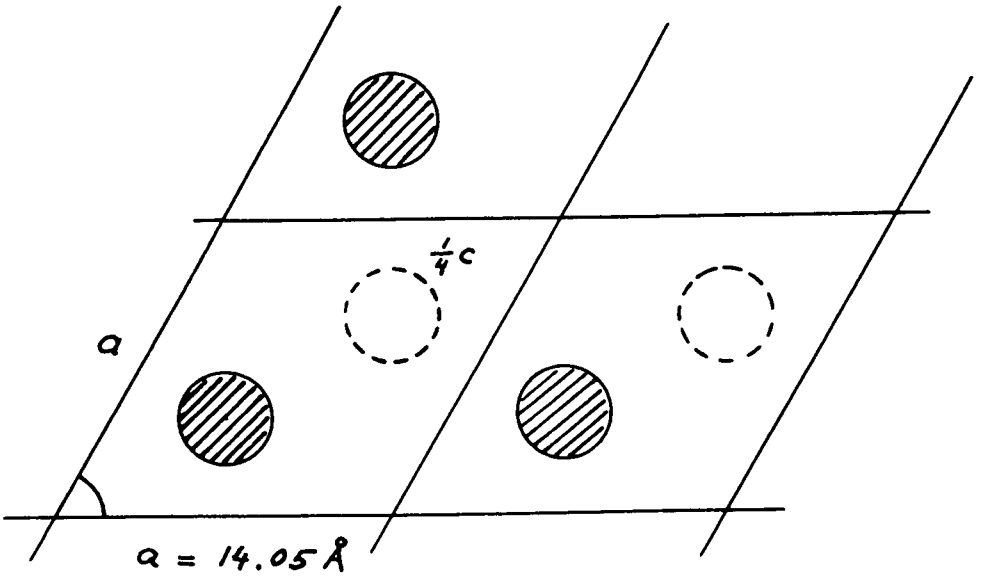

Figure 2.2 Positions of the CeES groups in the unit cell of the CeES lattice

exhibits paramagnetism. It has one 4f electron outside the closed shells. The free ion groundstate $^2F_{\frac{5}{2}}$ is six-fold degenerate.

If placed in a crystal, the free ion is subject to a crystalline electric field V_{cr} of given symmetry. In particular, in the ethylsulphates, the rare earth ion is at a site of C_{3h} symmetry. The crystal field for this symmetry is given in terms of the operator equivalents by Elliott and Stevens (1952):

$$V_{cr} = \alpha A_2^0 \overline{r^2} O_2^0 + \beta A_4^0 \overline{r^4} O_4^0 + \gamma A_6^0 \overline{r^6} O_6^0 + \gamma A_6^6 \overline{r^6} O_6^6 \qquad (2.1)$$

The O_n^m operator equivalents and many of their matrix elements are tabulated in the book by Low (1960).

If one neglects in first approximation the admixture of the $^2F_{\frac{7}{2}}$ multiplet, V_{cr} acts only in a manifold with constant angular momentum J = 5/2 and the terms in A_6^0 and A_6^6 vanish.

For a $^2F_{\frac{5}{2}}$ multiplet, the values of the constants are (Low, 1960):

$$\alpha = -\frac{2}{35} \qquad \beta = \frac{2}{315} \qquad \gamma = 0$$

The operators O_n^0 commute with J_z. V_{cr} splits the $^2F_{\frac{5}{2}}$ multiplet into three Kramers doublets $\langle \pm\frac{1}{2} /$, $\langle \pm\frac{3}{2} /$, and $\langle \pm\frac{5}{2} /$, with the following energies:

$$\begin{aligned}
\langle \pm\tfrac{1}{2} / V_{cr} / \pm\tfrac{1}{2} \rangle &= \frac{16}{35} A_2^0 \overline{r^2} + \frac{16}{21} A_4^0 \overline{r^4} \approx -58 \text{ cm}^{-1} \\
\langle \pm\tfrac{3}{2} / V_{cr} / \pm\tfrac{3}{2} \rangle &= \frac{4}{35} A_2^0 \overline{r^2} - \frac{24}{21} A_4^0 \overline{r^4} \approx 111 \text{ cm}^{-1} \\
\langle \pm\tfrac{5}{2} / V_{cr} / \pm\tfrac{5}{2} \rangle &= -\frac{20}{35} A_2^0 \overline{r^2} + \frac{8}{21} A_4^0 \overline{r^4} \approx -54 \text{ cm}^{-1}
\end{aligned} \qquad (2.2)$$

The values for $A_n^0 \overline{r^n}$ have been extrapolated from the values of the other rare earth ethylsulphates as given by Hüfner (1962). It is seen that the energy difference between the $\langle \pm \frac{1}{2} /$ and the $\langle \pm \frac{5}{2} /$ doublet is very small:

$$\Delta E = E_{\pm\frac{5}{2}} - E_{\pm\frac{1}{2}} \approx 4 \text{ cm}^{-1}$$

A slight change in $A_2^0 \overline{r^2}$ can therefore affect ΔE appreciably and may even reverse its sign.

This is exactly what happens in CeES. The concentrated salt has as lowest state the $\langle \pm \frac{5}{2} /$ doublet with the $\langle \pm \frac{1}{2} /$ doublet lying 4.8 cm^{-1} higher. If Ce^{3+}-ions are diluted into the diamagnetic LaES lattice, the $\langle \pm \frac{1}{2} /$ doublet lies lowest with $\Delta E = 3.94 \text{ cm}^{-1}$ (Bogle, Cooke, and Whitley, 1951). If Ce^{3+} is diluted in YES, the $\langle \pm \frac{1}{2} /$ doublet is still lowest, but with $\Delta E = 17.4 \text{ cm}^{-1}$.

Elliott and Stevens (1952) carried the perturbation calculations to second order. They obtain expressions for the relative energies of the three doublets and the g-values of the two low lying doublets as a function of the crystal field parameters $A_n^0 \overline{r^n}$ (n = 2,4,6) and $A_6^6 \overline{r^6}$. These latter are unknown in the case of Ce. The g-values and the splittings between the doublets have been determined experimentally. This gives 6 pieces of information to determine 4 unknowns, allowing not only to determine the crystal field parameter but also to check the theory. Elliott and Stevens found that the experimental g-values for the diluted Ce:LaES could not be fitted exactly to the theory and suggested a small admixture of C_{3v} symmetry.

In the concentrated salt, the lines are broad and the g-values

cannot be determined accurately. Bogle et al observed paramagnetic resonance absorption due to the lower doublet only at 2.5°K. Absorption due to the upper doublet has not yet been found (Dweck and Seidel, 1966). The g-values found from susceptibility measurements by Bogle et al are $g_{\parallel}(\frac{5}{2}) = 3.80 \pm 0.04$, $g_{\perp}(\frac{5}{2}) = 0 \pm 0.4$, $g_{\parallel}(\frac{1}{2}) = 1.0 \pm 0.2$ and $g_{\perp}(\frac{1}{2}) = 2.25 \pm 0.2$.

The splitting Δ between the two doublets has been deduced from the Schottky peak of the specific heat by Meyer and Smith (1959). They found $\Delta = 6.7$°K. Δ has also been determined by susceptibility measurements. Bogle et al obtained 7.5 ± 1.5°K while Van den Broek and Van der Marel found $\Delta = 6.95$°K. Very recently, direct absorption of infrared radiation between the two Kramers doublets has been observed by Burgiel and Meyer (1966) yielding a value of $\Delta = 7.2$°K.

The splitting of the two doublets in a magnetic field is shown in Figure 2.3.

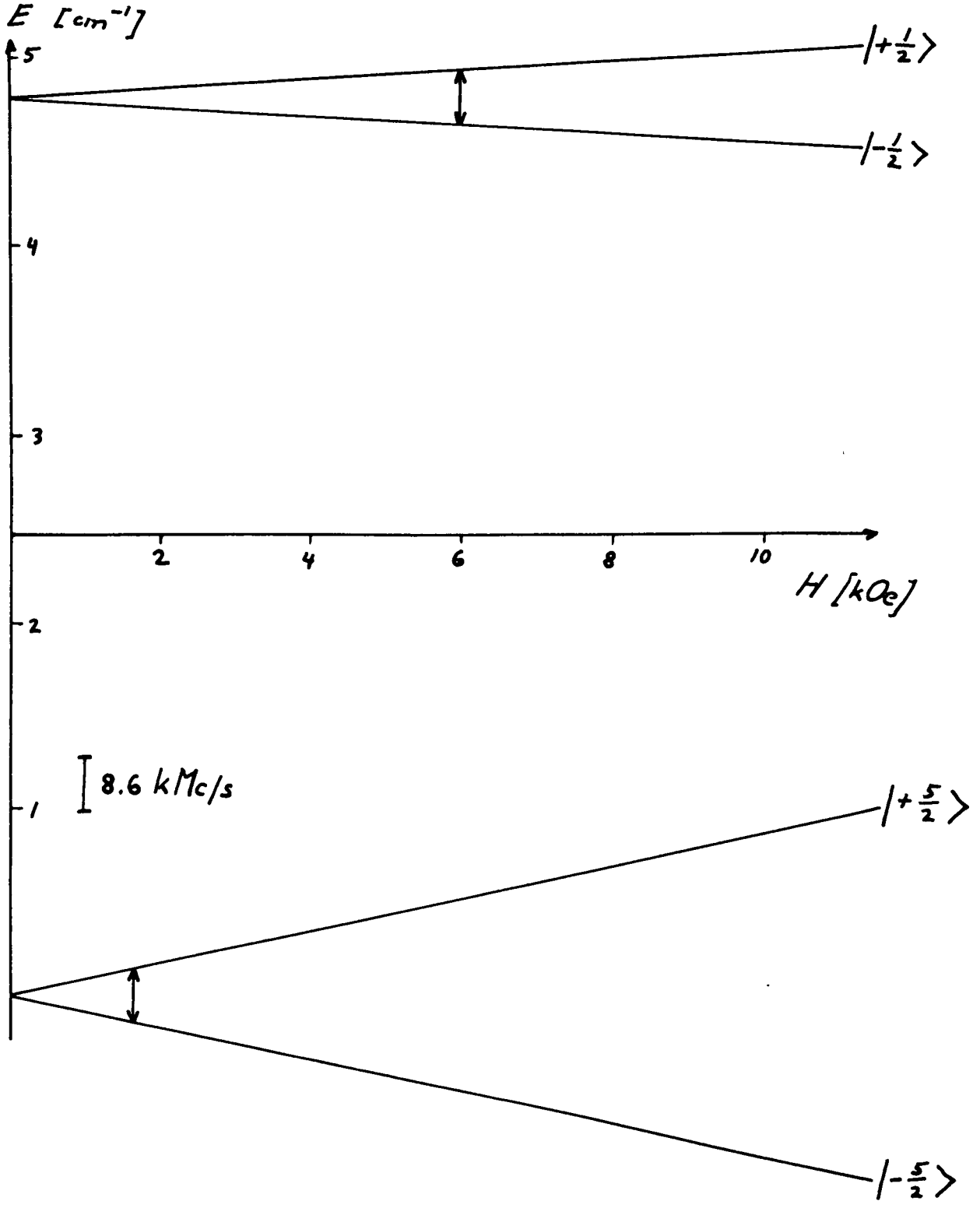

Figure 2.3 Zeeman splitting of the two lowest doublets in CeES

2.2 Spin-Lattice Relaxation

2.2.1 Introduction

Since Finn, Orbach and Wolf (1961) introduced the two phonon resonant process to account for spin-lattice relaxation times which were unexpectedly short and followed an exponential temperature dependence, the mechanism of spin-lattice relaxation seems to be well understood. This is true, if one restricts the term spin-lattice relaxation to the process of energy transfer from a single paramagnetic spin to the surrounding lattice phonons, through modulation of the crystal field by the lattice vibration, i.e. through the orbit-lattice interaction V_{ol}.

Assume a paramagnetic ion in a crystal of low enough symmetry, to lift all degeneracies with exception of the Kramers degeneracy for ions with an odd number of electrons. Assume now that only the ground Kramers doublet is occupied and that the doublet is split by a magnetic field to a separation δ. A spin in the upper level of this doublet can relax to the lower level by means of three different processes:

- the direct process, where the spin makes a transition through the action of the orbit-lattice interaction which creates simultaneously a phonon of energy δ

- the Raman process in which one phonon is scattered inelastically into another phonon while the spin makes simultaneously a transition. The energy difference of the phonons corresponds to the spin transition frequency.

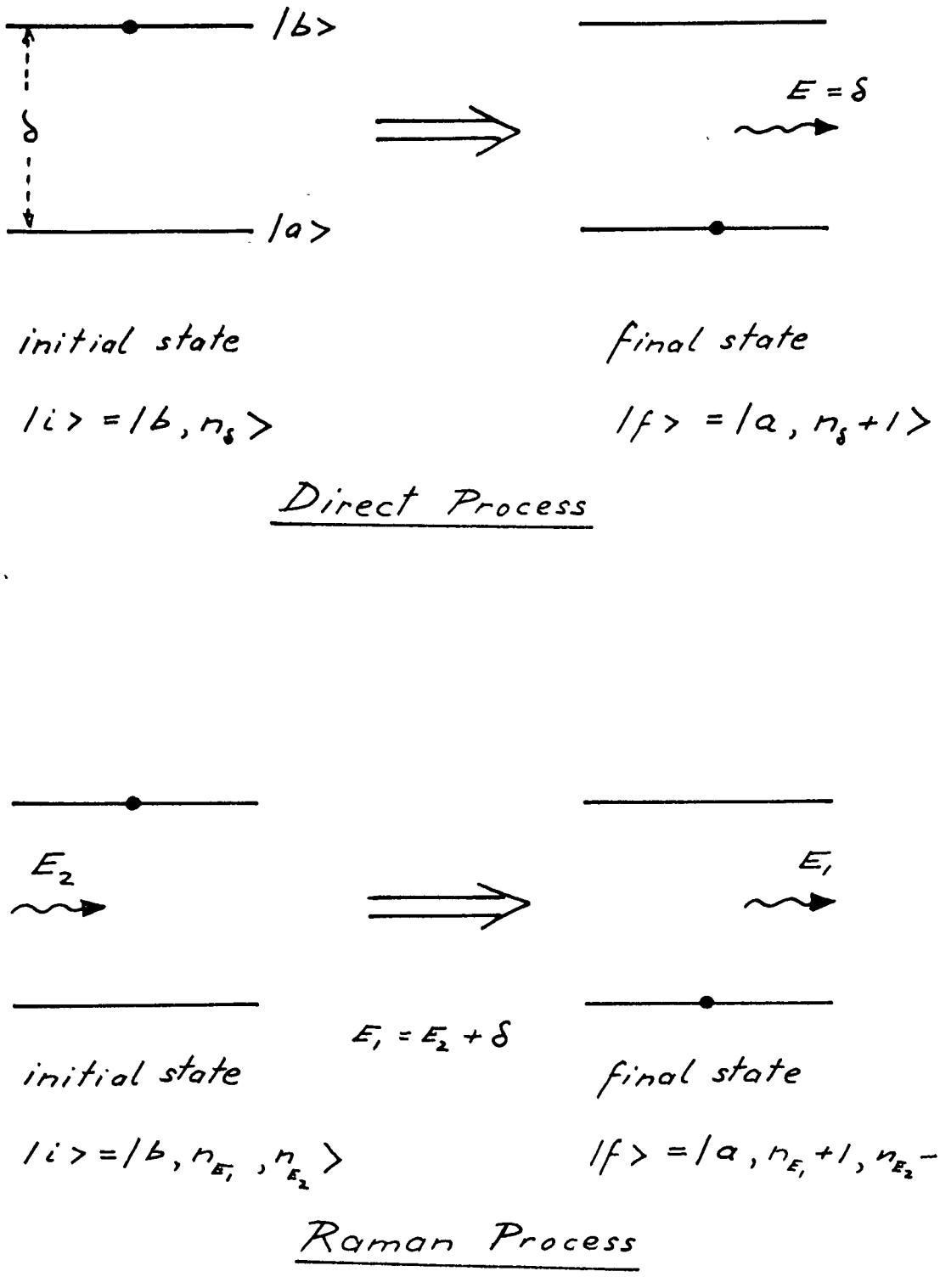

Figure 2.4 Direct and Raman relaxation processes

- the Orbach process which is actually a two-step resonant process via a close excited state. In the case of saturation of an excited doublet, the relaxation proceeds via the ground state, thus making an "inverse" Orbach process which has a different temperature dependence.

A detailed treatment of the three processes has been given by Orbach (1961), in which an easy approach is described to find the matrix elements of the orbit-lattice interaction. In the following, a short review of Orbach's approach is given and is applied to the case of CeES.

2.2.2 The Direct Process

The probability for a spin to make a transition from $|b\rangle$ to $|a\rangle$ (see Figure 2.4) under simultaneous emission of a phonon is

$$W_{b\to a} = \frac{2\pi}{\hbar}\left|\langle f \,|\, V_{ol} \,|\, i\rangle\right|^2 G(f) \tag{2.3}$$

$G(f)$ is the density of final states, which is the number of phonon states with energy δ. A Debye model gives

$$G(f) = \frac{3V\delta^2}{2\pi^2\hbar^3 v^3} \tag{2.4}$$

where V is the volume of the crystal and v is the velocity of sound.

The problem is to find the matrix elements of V_{ol}. In the

same manner, as is customary for the static crystal field, we can expand the orbit-lattice interaction in terms of spherical harmonics.

$$V_{ol} = \sum_{mn} A_{ol_n}^{m} r^n Y_n^m(\vartheta, \varphi) \tag{2.5}$$

For small lattice strains, one can expand the $A_{ol_n}^{m}$ and retaining only the linear term, one has

$$V_{ol} = \sum_{mn} A_n^m \varepsilon_n^m r^n Y_n^m(\vartheta, \varphi) \equiv \sum \varepsilon_n^m V_n^m \tag{2.6}$$

where A_n^m are now the coefficients of the static crystal field expansion.

For not too big anisotropies, the strains ε_n^m can be replaced by an average isotropic strain ε whose matrix elements are known to be (Abragam, 1961)

$$|\langle n_{s+1} | \varepsilon | n_s \rangle|^2 = \frac{s(n_s+1)}{2Mv^2} \tag{2.7}$$

Here M is the crystal mass and n_s the phonon occupation number, which is equal to the Bose-Einstein factor

$$n_s = \left(e^{\frac{s}{kT}} - 1 \right)^{-1} \tag{2.8}$$

The probability for a direct process transition in a crystal with N_b noninteracting spins in the upper state $\langle b|$ is, therefore:

$$W_{b\to a} = \frac{3\delta^3 N_b}{2\pi\hbar^4 \rho v^5}\,(n_\delta + 1)\,V_{ab}^2 \tag{2.9}$$

with

$$V_{ab}^2 \equiv \left| \langle a | \sum_{mn} V_n^m | b \rangle \right|^2 \tag{2.10}$$

$\rho = \frac{M}{V}$ is the crystal density. Using $W_{b\to a}$ from equation (2.9) and the corresponding expression for the reverse process $W_{a\to b}$, the rate equation for the population difference $\Delta N \equiv N_a - N_b$ becomes

$$\frac{d(\Delta N)}{dt} = \frac{3\delta^3 V_{ab}^2}{2\pi\hbar^4 \rho v^5}\left\{ N - \Delta N \coth\left(\frac{\delta}{2kT}\right)\right\} \tag{2.11}$$

The solution of the above differential equation shows an exponential time dependence

$$\Delta N(t) - \Delta N(\infty) = \Delta N(0)\, e^{-\frac{t}{T_{1d}}} \tag{2.12}$$

where

$$T_{1d}^{-1} = \frac{3\delta^3 V_{ab}^2}{2\pi\hbar^4 \rho v^5}\coth\left(\frac{\delta}{2kT}\right) \tag{2.13}$$

is the relaxation rate for the direct process. Our measurements performed at X-band frequencies, give $\delta \approx 0.4\,^\circ K$ and this allows the approximation $\delta \ll kT$. Equation (2.13) can thus be written

approximately

$$T_{1d} = A\,T \qquad \text{with} \qquad A = \frac{3k\,\delta^2 V_{al}^2}{\pi \hbar^4 \rho\, v^5} \tag{2.14}$$

Application to CeES

For Kramers ions in general V_{al} can connect the Kramers conjugate states $|a\rangle$ and $|b\rangle$ only after admixture of higher states through the Zeeman interaction. These matrix elements are proportional to the magnetic field H and we have

$$A \sim H^2 \delta^2$$

or, since $\delta = g\beta H$

$$T_{1d}^{-1} \sim H^4 T \tag{2.15}$$

In CeES, admixture of the $^2F_{\frac{7}{2}}$ multiplet is needed to obtain nonvanishing matrix elements. Since this multiplet is about 2,000 cm^{-1} higher than the groundstate, the direct process is expected to be weak. Larson and Jeffries (1966) estimate relaxation times of the order of seconds at helium temperatures. The Orbach process is much faster in this temperature region and the direct process is therefore not observed.

2.2.3 The Raman Process

A higher order process becomes possible if one considers terms of V_{ol} bilinear in ε , i.e.

$$V_{ol}' = \sum_{mn} \varepsilon_m \varepsilon_n V_n^m \tag{2.16}$$

This operator gives rise to an inelastic scattering of a phonon of energy E_1 into one of energy E_2 with a simultaneous spin flip $|b\rangle \rightarrow |a\rangle$ to take up the energy difference $E_1 - E_2 = \delta$ (Figure 2.4) The transition probability for this process is in close analogy to equation (2.3)

$$W_{b\rightarrow a} = \frac{2\pi}{\hbar} \int |\langle f | V_{ol}' | i \rangle|^2 G(f)\, df \tag{2.17}$$

where $\int df$ means integration over all possible final states. A similar procedure as for the direct process leads to

$$W_{b\rightarrow a} = \frac{9 N_b V_{ab}^2}{8\pi^3 \rho^2 \hbar^7 v^{10}} \int_0^{k\Theta} \frac{E^3 (E+\delta)^3 e^{\frac{E}{kT}}}{\left(e^{\frac{E}{kT}} - 1\right)\left(e^{\frac{E+\delta}{kT}} - 1\right)} dE \tag{2.18}$$

with the Debye cutoff energy $k\Theta$ as the upper limit of the integral. The main contribution to the integral comes from the region where $E \approx kT$ and since $\delta \ll kT$ the integral gives approximately for $\Theta \gg T$ (Ziman, 1954)

$$\int_0^{k\Theta} \frac{E^6 e^{\frac{E}{kT}} dE}{\left(e^{\frac{E}{kT}} - 1\right)^2} \approx 6!\,(kT)^7 \tag{2.19}$$

Again, as for the direct process, the solution of the rate equation for the population difference shows an exponential time dependence

$$\Delta N(t) \sim e^{-\frac{t}{T_{1R}}}$$

with the relaxation rate

$$T_{1R}^{-1} = \frac{9\, 6!\, V_{ab}^2}{4\pi^3 \rho^2 \hbar^7 v^{10}} (kT)^7 \tag{2.20}$$

The comparison with the direct process in CeES gives

$$\frac{T_{1d}^{-1}}{T_{1R}^{-1}} = \frac{\delta^2 \pi^2 \rho \hbar^3 v^5}{540\, k^6 T^6} \approx 6 \times 10^5 T^{-6} \tag{2.21}$$

at X-band frequencies. The direct process is seen to be stronger at helium temperatures.

A second possibility for a Raman process arises from second order time dependent perturbation theory (Orbach, 1961; see also Scott and Jeffries, 1962). Here the orbit-lattice interaction of equation (2.6) acts twice through an intermediate state $|e\rangle$. The transition probability for such a process is

$$W_{b\to a} = \frac{2\pi}{\hbar} N_b \int \left| \sum_e \frac{\langle f | V_{\alpha} | e \rangle \langle e | V_{\alpha} | i \rangle}{E_i - E_e} \right|^2 G(f)\, df \tag{2.22}$$

In the case of a Kramers ion with one excited doublet much closer to the ground state than all the others (as is the case in CeES) and using the same approximations as before, we get from equation (2.22)

$$W_{b\to a} = \frac{9 N_b V_{ac}^2 V_{bc}^2}{8\pi^3 \rho^2 \hbar^7 v^{10}} \int_0^{k\theta} \frac{E^6 e^{\frac{E}{kT}}}{\left(e^{\frac{E}{kT}} - 1\right)^2} \left| \frac{1}{E-\Delta} + \frac{1}{E+\Delta} \right|^2 dE \tag{2.23}$$

c denotes here the lower level of the excited doublet.

For $k\theta \ll \Delta$, the sum of the energy denominators is always small. This is known as Van Vleck cancellation. For $k\theta > \Delta$, as is the case in CeES, the integrand has a singularity for $E = \Delta$. This gives rise to a resonant process which will be treated in chapter 2.24 below.

If one neglects the contribution from the singularity, one obtains another contribution to the Raman relaxation rate, which is

$$T_{1R}'^{-1} = \frac{9!\, V_{ac}^2 V_{bc}^2}{\pi^3 \rho^2 v^{10} \Delta^4 \hbar^7} (kT)^9 \tag{2.24}$$

The ratio of the two contributions to the Raman process is:

$$\frac{T_{1R}^{-1}}{T_{1R}'^{-1}} = \frac{V_{ab}^2}{V_{ac}^2 \, V_{bc}^2} \cdot \frac{\Delta^4}{224(kT)^2} \tag{2.25}$$

V_{ab}^2 , V_{ac}^2 and V_{bc}^2 are of the same order of magnitude as Δ and the T^9 term is therefore dominant for $kT \gtrsim \frac{\Delta}{10}$.

2.2.4 Two Phonon Resonant Processes

The first excited doublet in CeES is so close to the ground state, that it is appreciably populated even at helium temperatures. We consider the rate equations for the whole four-level system shown in Figure 2.5.

If the transitions $\langle a| \rightarrow \langle b|$ and $\langle c| \rightarrow \langle d|$ are neglected, the following rate equations are obtained:

$$\begin{aligned}
\frac{dN_a}{dt} &= W_{c\to a} + W_{d\to a} - \left(W_{a\to c} + W_{a\to d}\right) \\
\frac{dN_b}{dt} &= W_{c\to b} + W_{d\to b} - \left(W_{b\to c} + W_{b\to d}\right) \\
\frac{dN_c}{dt} &= W_{a\to c} + W_{b\to c} - \left(W_{c\to a} + W_{c\to b}\right) \\
\frac{dN_d}{dt} &= W_{a\to d} + W_{b\to d} - \left(W_{d\to a} + W_{d\to b}\right)
\end{aligned} \tag{2.26}$$

In exact analogy to the direct process (equation (2.3)) the

transition probabilities are

$$W_{a\to b} = \frac{3 N_a V_{ad}^2}{2\pi \hbar^4 \rho v^5} \Delta_{ad}^3 \left(n_{\Delta_{ad}} + 1\right)$$

and correspondingly for the other transitions.

The rate equations (2.26) have to satisfy the condition

$$\frac{d}{dt}\left(N_a + N_b + N_c + N_d\right) = 0$$

if no transitions to other levels occur. The solutions of the three remaining independent equations will in general be sums of three exponentials. If $\delta_1, \delta_2 \ll \Delta$ and if $V_{ac}^2 \approx V_{ad}^2 \approx V_{bc}^2 \approx V_{bd}^2 \equiv V^2$ equations (2.26) simplify to

$$\begin{aligned}
\frac{dN_a}{dt} &= c'\left(N_c + N_d\right) - 2c N_a \\
\frac{dN_b}{dt} &= c'\left(N_c + N_d\right) - 2c N_b \\
\frac{dN_c}{dt} &= c'\left(N_a + N_b\right) - 2c' N_c \\
\frac{dN_d}{dt} &= c'\left(N_a + N_b\right) - 2c' N_d
\end{aligned} \tag{2.27}$$

where $$c = \frac{3 V^2 \Delta^3 n_\Delta}{2\pi \hbar^4 \rho v^5}$$

and $$c' = \frac{3 V^2 \Delta^3 (n_\Delta + 1)}{2\pi \hbar^4 \rho v^5}$$

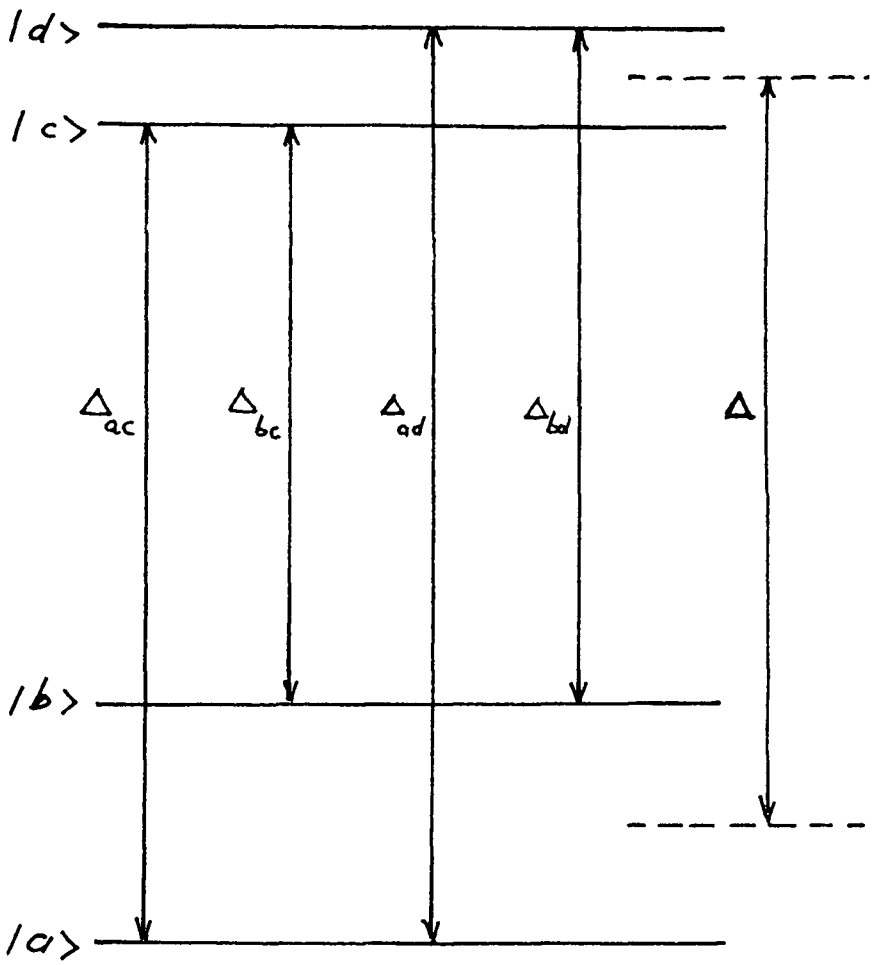

Figure 2.5 Typical energy levels and splittings for two phonon resonant relaxation

In our experiments, either one of the two doublets could be saturated by a microwave pulse. We assume that the Boltzmann distribution between the doublets is not disturbed, which means

$$\frac{d}{dt}\left(N_a + N_b\right) = \frac{d}{dt}\left(N_c + N_d\right) = 0 \tag{2.28}$$

In this case, the equations for the population differences $\Delta N_1 = N_a - N_b$ and $\Delta N_2 = N_c - N_d$ are

$$\frac{d}{dt}\left(\Delta N_1\right) = -2c\,\Delta N_1 \tag{2.29}$$

$$\frac{d}{dt}\left(\Delta N_2\right) = -2c'\Delta N_2 \tag{2.30}$$

Equation (2.29) describes the relaxation of the lower doublet by means of the two-phonon resonant relaxation known as the Orbach process. The relaxation rate is

$$T_{10}^{-1} = \frac{3\Delta^3 V^2}{\pi \hbar^4 \rho v^5} \frac{1}{e^{\frac{\Delta}{kT}} - 1} \tag{2.31}$$

which gives the familiar exponential temperature dependence for $\Delta \gg kT$:

$$T_{10}^{-1} \approx \frac{3\Delta^3 V^2}{\pi \hbar^4 \rho v^5} e^{-\frac{\Delta}{kT}} \tag{2.32}$$

The relaxation of the upper doublet via the lower doublet has been called the inverse Orbach process. Its relaxation rate is found from equation (2.30) to be

$$T_{1i}^{-1} = \frac{3\Delta^3 V^2}{\pi \hbar^4 \rho v^5} \cdot \frac{1}{1 - e^{-\frac{\Delta}{kT}}} \tag{2.33}$$

This gives for the case $kT \ll \Delta$

$$T_{1i}^{-1} \approx \frac{3\Delta^3 V^2}{\pi \hbar^4 \rho v^5} \tag{2.34}$$

It is seen that the relaxation rate for the inverse Orbach process approaches a lower limit at low temperatures and does not decrease exponentially as is the case for the Orbach process. The approximations made in the above derivation of T_{10} and T_{11} are rather rough for CeES. At the resonance-field for the excited doublet, we have $\delta_1 \approx 1.1$ cm^{-1} and $\Delta = 4.7$ cm^{-1}. This is not serious, however, since the matrix elements V_{ac}^2 etc. are not known accurately and the thus obtained values for the relaxation times can at best be regarded as an order of magnitude estimate. In order to estimate the relaxation times T_{10} and T_{11}, we have to know V^2 or more precisely V_{ac}^2 , V_{ad}^2 , V_{bc}^2 and V_{bd}^2 .

We have used the wave functions given by Elliott and Stevens for the dilute Ce : LaES and the static crystal field parameters have been extrapolated from values for other undiluted rare earth ethylsulphates. The values used are:

$$A_2^0 \overline{r^2} = 32 \text{ cm}^{-1}$$

$$A_4^0 \overline{r^4} = -95 \text{ cm}^{-1}$$

$$A_6^0 \overline{r^6} = -55 \text{ cm}^{-1} \tag{2.35}$$

$$A_6^6 \overline{r^6} = 800 \text{ cm}^{-1}$$

In the dynamic case without the C_{3h} symmetry restrictions, other parameters occur (A_2^2 , A_4^2 , A_6^2 , A_4^4 , A_6^4 , A_4^3 and A_6^3). They have been estimated using the Orbach (1961) recipe:

$$A_n^m = A_n^0 \qquad n = 2, 4$$

$$A_6^m = \left(|A_6^0|^{6-m} \cdot |A_6^6|^m \right)^{\frac{1}{6}} \tag{2.36}$$

We have neglected coherence between the different terms, i.e. we assumed that

$$\left| \sum \langle a | V_n^m | b \rangle \right|^2 = \sum \left| \langle a | V_n^m | b \rangle \right|^2 \tag{2.37}$$

With these approximations, the results are

$$V_{ac}^2 = V_{bd}^2 \approx 300 \text{ cm}^{-2}$$

$$V_{bc}^2 = V_{ad}^2 \approx 400 \text{ cm}^{-2} \tag{2.38}$$

Using the value $V^2 \approx 350\ cm^{-2}$ gives for the Orbach relaxation time at 1.5 °K

$$T_{1o} \approx 10^{-5}\ sec \tag{2.39}$$

and for the inverse Orbach relaxation time

$$T_{1i} \approx 10^{-7}\ sec \tag{2.40}$$

Both estimates are several orders of magnitude faster than the measured relaxation times, as will be shown later and we measure therefore not spin-lattice relaxation times as defined at the beginning of this chapter.

2.3 The Phonon Bottleneck

2.3.1 Introduction

In the preceding treatment of spin-lattice relaxation, it has been assumed throughout that the lattice has a constant temperature T_L. This is strictly speaking only the case for a lattice with infinite thermal capacity. However, a real lattice has, in general, a smaller specific heat than the spin system in the low temperature region where relaxation experiments are usually performed and the lattice temperature will not necessarily remain constant.

Casimir (1939) has seen this possibility and has extended the Casimir-duPré formulae used in nonresonant relaxation measurements for the case where T_L is not constant. Van Vleck (1941) studied the energy exchange between the lattice oscillators and postulated the inadequacy of the heat capacity of the lattice oscillators to conduct the spin energy to the bath in a time shorter than the spin-lattice relaxation time T_1. This effect has become known under the name of the phonon bottleneck. A lot of data have been published, which give experimental evidence of a bottleneck, namely by the Leiden group and by Jeffries and his collaborators. The most direct evidence of a bottleneck has been obtained by Brya and Wagner (1965). They observed a phonon avalanche after inversion of a paramagnetic resonance line by adiabatic passage in a bottlenecked lattice.

The bottleneck has been treated in two different ways.

Gorter et al (1955) used a thermodynamical approach to find the time dependence of the spin temperature. Faughnan and Strandberg (1961) used rate equations to determine the change of the spin population with time. Most of the numerous other publications on the subject use one or the other of the above approaches.

In a very interesting and detailed paper, Giordmaine and Nash (1965) showed the analogy between the phonon bottleneck and the imprisonment of resonant photons in gases.

2.3.2 Thermodynamical Treatment

Consider three systems A, B, and C. Each system is assumed to be in internal equilibrium with the respective temperatures T_A, T_B, and T_C. Suppose system A has an infinite specific heat and the internal energy and specific heats of B and C are U_B, C_B and U_C, C_C. Energy is fed into B and C by an external source at the rate W_B and W_C. Suppose that the thermal coupling of the three systems can be described by two time constants τ_{AB} and τ_{BC} as shown in Figure 2.6.

Energy conservation leads to two coupled differential equations

$$\frac{dU_C}{dT} = C_C \frac{dT_C}{dt} = \frac{C_C}{\tau_{BC}}\left(T_B - T_C\right) - W_C \tag{2.40}$$

$$\frac{dU_B}{dt} = C_B \frac{dT_B}{dt} = \frac{C_C}{\tau_{BC}}\left(T_C - T_B\right) + \frac{C_B}{\tau_{AB}}\left(T_A - T_B\right) + W_B \tag{2.41}$$

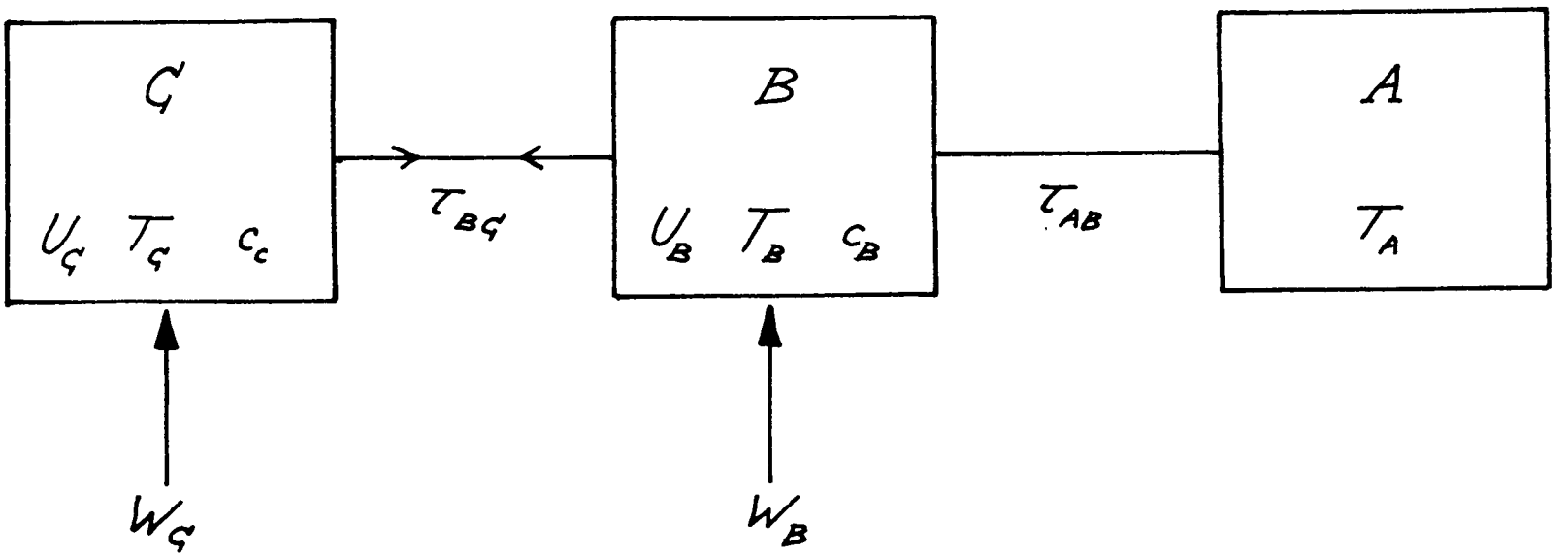

Figure 2.6 Thermodynamical model for the phonon bottleneck

The systems A, B and C can be identified with bath, lattice and spin system respectively. The above equations can be linearized if we assume that the temperature differences are small:

$$|T_B - T_C| \ll T_A$$

$$|T_A - T_B| \ll T_A$$

such that C_C and C_B are independent of time and can be taken at the bath temperature T_A. In our experiments, the temperature differences never exceeded a few m°K and the approximation is reasonable in this case.

Equations (2.40) and (2.41) have to be solved for two different initial conditions applicable in our experiments:

a) The three systems A, B, and C are initially at the same temperature. In this case, the solutions of equations (2.40) and (2.41) describe the warm-up of systems B and C due to simultaneous heating pulses to both systems.

b) The systems B and C are initially at the temperatures T_B^o and T_C^o respectively and $T_B^o \neq T_C^o$ due to a previous heating pulse. The solutions of equations (2.40) and (2.41) with $W_B = W_C = 0$ characterize in this case the relaxations of T_B and T_C towards T_A.

a) $T_C(t = 0) = T_B(t = 0) = T_A$

The differential equation for T_C is obtained by eliminating T_B from equations (2.40) and (2.41) and the solution is

$$T_C(t) - T_C(\infty) = a\, e^{-\frac{t}{\tau_1}} + b\, e^{-\frac{t}{\tau_2}} \qquad (2.42)$$

If terms of the order $\frac{c_B}{c_C}$ are neglected compared to unity, the time constants are

$$\tau_1 = \tau_{BC} + \frac{c_C}{c_B}\tau_{AB} \tag{2.43}$$

and

$$\tau_2 = \tau_{AB} \frac{1}{1 + \frac{c_C \tau_{AB}}{c_B \tau_{BC}}} \tag{2.44}$$

The constants are

$$a = T_A - T_C(\infty) \tag{2.45}$$

$$b = \frac{\tau_2 \tau_{AB}}{\tau_1 c_B} W_B \tag{2.46}$$

$$T_C(\infty) = \frac{\tau_{AB}}{c_B}\left(W_C + W_B\right) + \frac{\tau_{BC}}{c_C} W_C + T_A \tag{2.47}$$

b) Relaxation with $T_B(t' = 0) = T_B^\circ$, $T_C(t' = 0) = T_C^\circ$ and $W_B = W_C = 0$.

The solution for $T_C(t')$ is in this case

$$T_C(t') = T_A = a' e^{-\frac{t'}{\tau_1}} + b' e^{-\frac{t'}{\tau_2}} \tag{2.48}$$

with the same time constants τ_1 and τ_2 as found before in

equations (2.43) and (2.44) and with

$$a' = T_C^{\circ} - T_A + \frac{\tau_2}{\tau_{BC}}\left(T_B^{\circ} - T_C^{\circ}\right) \approx T_C^{\circ} - T_A \qquad (2.49)$$

and

$$b' = \tau_2 T_C^{\circ}\left(\frac{1}{\tau_{BC}} - \frac{1}{\tau_1}\right) + \tau_2\left(\frac{T_A}{\tau_1} + \frac{T_B^{\circ}}{\tau_{BC}}\right) \approx -\frac{\tau_2}{\tau_1} a' \qquad (2.50)$$

It is seen that for both cases a) and b) $\tau_2 \ll \tau_1$ and $b \ll -a$, $b' \ll -a'$ due to the assumption $c_C \gg c_B$.

The longer time constant τ_1 has been derived in this manner by Stoneham (1965) and can be regarded as the effective time constant for the thermal exchange of the combined system B + C and system A.

The time τ_2 which is very much shorter than τ_1 if $c_B \ll c_C$, can be shown to characterize the time needed for systems B and C to come into equilibrium. Peterson (1965) has studied the relaxation of two systems, both with finite heat capacity. τ_2 is identical to his time constant for small temperature differences.

For big disturbances, a whole distribution of time constants are obtained depending upon the functional dependence $c_B(T)$ and $c_C(T)$ and τ_1 , τ_2 are the asymptotic values for $t \to \infty$. This has been shown by Kalbfleisch (1965) using the alternative rate equation approach for the direct process. The corresponding equations for the Orbach process are more involved, but yield

the same result.

From equation (2.43) can be seen how a bottleneck can arise in paramagnetic relaxation. If the systems A, B and C are identified with the constant temperature bath, with the lattice oscillators on speaking terms with the spin system and with the spin system respectively, then τ_{BC} is the spin-lattice relaxation time T_1, and τ_{AB} is the life-time of the phonons with respect to absorption by the bath. A bottleneck arises if

$$\frac{C_C}{C_B}\,\tau_{AB} \gtrsim \tau_{BC} \tag{2.51}$$

and the observed relaxation time given by equation (2.43) is longer than T_1. In severe bottleneck cases

$$\frac{C_C}{C_B}\,\tau_{AB} \gg \tau_{BC} \tag{2.52}$$

It follows that

$$\tau_2 \ll \tau_{AB} \qquad \text{and} \qquad \tau_1 \gg \tau_{AB}$$

and the second relaxation time can be completely neglected, leading to a perfectly exponential time dependence of the system C. This exponential behaviour is based on the assumptions that:

1. the relaxation times describing the energy exchange between the systems are independent of temperature in the interval discussed, and that

2. the systems are in thermal equilibrium, i.e. each system is described by a single temperature.

The nonexponential behaviour of the observed relaxation in CeES above the λ-point can be explained as due to violation of assumption 2.

It is always possible to subdivide a system with inhomogeneous temperature into more subsystems with homogeneous temperature. Each new system in series between C and A contributes a new exponential term in the time dependence of C. In the limit corresponding to spatial diffusion in a medium with a finite diffusion constant, a continuous distribution of relaxation times is needed to describe $T_C(t)$.

It is interesting to know under what condition the above relaxation behaviour can be described by means of two systems only. The actually observed relaxation time is given by equation (2.43)

$$\tau_1 = \tau_{BC} + \frac{C_C}{C_B}\tau_{AB}$$

If

$$\frac{C_C}{C_B}\tau_{AB} \ll \tau_{BC}$$

the lattice can be lumped together with the bath and the observed relaxation time of the spin system is τ_{BC}. No bottleneck occurs and τ_{BC} is the ordinary spin-lattice relaxation time, which is usually denoted as T_1.

If

$$\frac{C_C}{C_B}\tau_{AB} \gg \tau_{BC}$$

the lattice and the spin system can be lumped together and the observed relaxation time is characteristic of the energy exchange between the lattice system and the bath. This happens, to consider a special case, if the dominant resistance to energy exchange is the boundary resistance at the crystal interface due to acoustic mismatch. This behaviour will be treated in more detail below.

2.3.3 Acoustic Mismatch at a Boundary

The Kapitza Resistance

The phonons transporting energy from the crystal into the helium bath experience a boundary resistance R_K at the interface. This is due to the fact that the acoustic impedance $Z = \varrho v$ changes from the crystal to the helium.

This effect has been observed by Kapitza (1941) between HeII and copper. The properties of superfluid helium have been used to explain this Kapitza resistance. A boundary resistance is, however, to be expected quite generally at an interface between two media with different characteristic impedances. It is readily observed between a metal and HeII because there is no temperature drop in HeII and a very small one in the metal, such that the temperature difference across the interface is not masked by big gradients in the bulk solid and liquid. Experimental data are available for the boundary resistance between metals or very few dielectrics and HeII or liquid ^{3}He.

For small heat currents, the temperature drop ΔT across the

surface is proportional to the thermal flux f. Thus

$$\Delta T = R_K f \tag{2.53}$$

and R_K is called the Kapitza resistance. (Kapitza, 1941) Deviation from the linear dependence $\Delta T \sim f$ has been found by Andronikashvili (1956) for high fluxes.

R_K depends strongly on the surface condition of the solid (Johnson and Little, 1963) and differs only slightly for different materials. The known experimental data for R_K can be fitted with the empirical expression

$$R_K = A T^{-n} \qquad \frac{{}^{o}K\ cm^2\ sec}{Joule} \tag{2.54}$$

with $10 < A < 40$

and $2.6 < n < 4.15$.

A highly polished surface has a higher R_K than a rough one. Surface inhomogeneities which are big compared to the acoustic wave length increase the effective area and give a smaller apparent R_K, while surface inhomogeneities comparable to the wavelength serve as impedance transformer by smoothing out the abrupt impedance mismatch at a sharp boundary and hence lead to a decrease in R_K.

The Kapitza resistance was found to be the same for thermal currents in both directions, i.e. with the solid cooler or hotter than the surrounding HeII. (Kuang Wey-Yen, 1962)

Challis (1962) measured R_K between lead and HeII and found

a slight magnetic field dependence. R_K decreases by 7% from 1 kOe to 7 kOe.

Most of the measurements up to date have been made in the temperature range from 1°K to 2°K. Abel et al, however, found an abnormally low Kapitza resistance between cerium magnesium nitrate and He^3 in the m°K region, which does not follow a T^{-n} law. Very little headway has been made to calculate R_K theoretically. The mechanism proposed by Khalatnikov gives approximately the right temperature dependence $R_K \sim T^{-3}$, but does not explain the pressure dependence (Challis, Dransfeld, and Wilks, 1961). No significant progress has been made since (Anderson et al, 1965).

Energy Transport Through an Interface

In order to examine the effect of the Kapitza resistance on the relaxation process in CeES, we consider the idealized system of a perfectly conducting crystal at temperature T_{cr}, separated from the bath at constant temperature T_A by a boundary resistance R_K. This model applies to our measurements below the λ-point, where the abnormally high thermal conductivity of HeII allows no temperature gradient in the bulk liquid. If W is the energy fed to the crystal per second by an external source, we have for the time rate of change of the internal energy V_{cr} of the crystal

$$\frac{dU_{cr}}{dt} = C'_{cr}\frac{dT_{cr}}{dt} = W - fs \qquad (2.55)$$

where c'_{cr} is the total heat capacity of the crystal and f is the thermal flux through the crystal surface s. For small fluxes

$$T_{cr} - T_A = \Delta T = R_K f \tag{2.56}$$

and equation (2.55) becomes

$$c'_{cr} \frac{dT_{cr}}{dt} = W - \frac{T_{cr} - T_A}{R_K} s \tag{2.57}$$

For the case of a heat pulse starting at t = 0 with $T_{cr}(0) = T_A$, the solution of equation (2.57) is

$$T_{cr}(t) - T_A = \frac{R_K W}{s}\left(1 - e^{-\frac{t}{\tau_K}}\right) \tag{2.58}$$

with the relaxation time

$$\tau_K = \frac{R_K c_{cr}}{s} \tag{2.59}$$

If the heat pulse is shut off after attaining the temperature T°_{cr} in the crystal, the relaxation is given by

$$T_{cr}(t) - T_A = \left(T^{\circ}_{cr} - T_A\right) e^{-\frac{t}{\tau_K}}$$

The time constant τ_K is the same in both cases. If c_{cr} is the specific heat of the crystal per g and ρ its density, the time constant becomes

$$\tau_K = R_K \rho c_{cr} \left(\frac{V}{s}\right) \tag{2.60}$$

where $\left(\frac{V}{S}\right)$ is the volume-to-surface ratio of the crystal. The maximum temperature rise in the crystal after a long heating pulse is

$$\Delta T(\infty) = \frac{R_k W}{S} \tag{2.61}$$

It is proportional to the heating power W and inversely proportional to the total surface conductivity $K_S = S/R_K$. If τ_k is the rate determining time constant, it should be equal to τ_1 as calculated with the three system picture in the limiting case of $\tau_{BC} << \frac{c_C}{c_B}\tau_{AB}$

By identification of equations (2.43) and (2.60) one gets

$$\tau_K = R_k \rho c_{cr} \left(\frac{V}{S}\right) = \frac{c_C}{c_B}\tau_{AB} \approx \frac{c_{cr}}{c_B}\tau_{AB} \tag{2.62}$$

τ_{AB} is the lifetime of a phonon against absorption by the helium bath and is given by

$$\tau_{AB} = c_B R_k \rho \left(\frac{V}{S}\right) = \frac{c_B M}{K_S} \tag{2.63}$$

where c_B is the specific heat of the lattice system and K_S is the total conductivity across the surface. A typical value of $R_K = 10$ cm^{2}deg.sec.joules^{-1} gives for our crystal

$$\left(V/S \approx 0.05 \text{ cm.} \;,\; c_B \approx 6 \times 10^{-5} \text{ joules}(\text{g}^\circ\text{K})^{-1} \right)$$

$$\tau_{AB} \approx 6 \times 10^{-5} \text{ sec.}$$

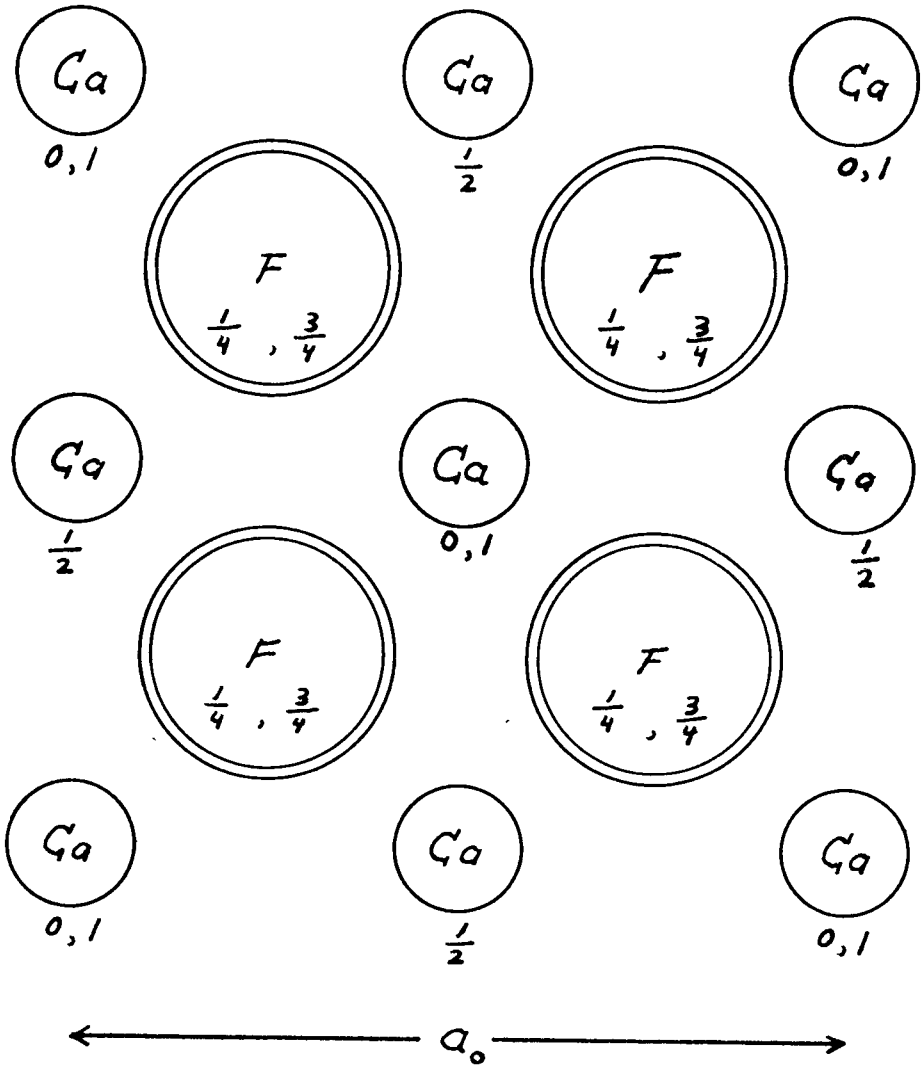

Figure 2.7 Crystal structure of CaF_2

2.4 Europium Doped Calcium Fluoride

2.4.1 Crystal Structure

The position of the calcium and fluorine ions in the CaF_2 crystal lattice is shown in Figure 2.7 (from Wykoff: Crystal Structure). Each unit cell contains 4 Ca^{2+} and 8 F^- ions. The fluorine form a simple cubic lattice with a lattice constant of $\frac{1}{2}a_o$ = 2.72Å. The calcium ions can be found at every other center of the fluorine cubic lattice, thus forming a face centered cubic lattice with the lattice constant a_o . Each Ca^{2+} has 8 F^- nearest neighbours at a distance of 2.36Å and 12 Ca^{2+} nearest neighbours at 3.86Å. Each F^- has 4 Ca^{2+} nearest neighbours at 2.36Å and 6 F^- nearest neighbours at 2.72Å. Divalent europium ions are replacing the calcium ions in CaF_2 without causing noticeable distortion. The crystal field symmetry remains cubic. This is not the case with trivalent rare earth ions which can be found at sites of lower than cubic symmetry.

2.4.2 Ground State and Paramagnetic Resonance

The free-ion ground state of divalent europium is $^8S_{\frac{7}{2}}$. The crystal field V_{cr} cannot lift the eight-fold degeneracy immediately. The spin-orbit coupling admixes, however, in first order the $^6P_{\frac{7}{2}}$ multiplet and in second order the multiplets $^6D_{\frac{7}{2}}$ and $^4D_{\frac{7}{2}}$. A cubic field has only off-diagonal matrix elements between states containing the second order perturbation in spin-

orbit coupling. The matrix elements are, therefore, of the order of $V_{cr}\,\zeta^4$ where ζ is the spin-orbit coupling parameter. The effect is a decomposition of the ground state into two doublets and one quartet with an overall splitting of 0.178 cm^{-1} (Ryter, 1957). This is of the order of magnitude of the Zeeman perturbation $\mathcal{H}_z$. Lacroix (1957) has diagonalized the Hamiltonian considering V_{cr} and $\mathcal{H}_z$ simultaneously. The resulting 8 by 8 secular determinant is rather complicated.

An alternative procedure is to describe the ground state by a phenomenological spin-Hamiltonian as has been done by Baker, Bleaney and Hayes (1958):

$$\mathcal{H} = g\beta(\underline{H}\cdot\underline{S}) + B_4\left(O_4^0 + 5\,O_4^4\right) + B_6\left(O_6^0 - 21\,O_6^6\right) + A(\underline{S}\cdot\underline{I}) \qquad (2.64)$$

S = 7/2 is the effective spin and the O_n^m are the operator equivalents corresponding to the Legendre-polynomials in the crystal field expansion and are tabulated by Baker <u>et al</u>. g, B_4, B_6 and A are parameters determined by fitting the spin Hamiltonian to the observed ground state splittings.

We neglect for the moment the hyperfine interaction $A(\underline{S}\cdot\underline{I})$. In magnetic fields of a few kOe, the ground state consists then of 8 levels which can be described approximately by the magnetic quantum number $M = +\frac{7}{2}, +\frac{5}{2} \ldots -\frac{7}{2}$

There are seven allowed magnetic dipole transitions $\Delta M = 1$ with the following frequencies:

$$
\begin{aligned}
\pm\tfrac{7}{2} &\rightarrow \pm\tfrac{5}{2} & h\nu &= g\beta H \pm 20 p b_4 \pm 6 q b_6 \\
\pm\tfrac{5}{2} &\rightarrow \pm\tfrac{3}{2} & h\nu &= g\beta H \mp 10 p b_4 \pm 14 q b_6 \\
\pm\tfrac{3}{2} &\rightarrow \pm\tfrac{1}{2} & h\nu &= g\beta H \mp 12 p b_4 \pm 14 q b_6 \\
\tfrac{1}{2} &\rightarrow -\tfrac{1}{2} & h\nu &= g\beta H
\end{aligned}
\tag{2.65}
$$

where $b_4 = 60\,B_4$, $b_6 = 1260\,B_6$

and
$$p = 1 - 5(l^2m^2 + m^2n^2 + n^2l^2)$$
$$q = \frac{21}{2}\left\{11\,l^2m^2n^2 - (l^2m^2 + m^2n^2 + n^2l^2) + \frac{2}{21}\right\}$$

l,m,n are the direction cosines of the magnetic field with respect to the four-fold cubic axes. The experimental values are (Ryter, 1957):

$$|b_4| = 55.75 \times 10^{-4}\,\mathrm{cm}^{-1}, \quad |b_6| = 0.25 \times 10^{-4}\,\mathrm{cm}^{-1},$$
$$\frac{b_4}{b_6} < 0 \quad \text{and} \quad g = 1.9927$$

There are two stable isotopes, Eu^{151} and Eu^{153}, of approximately the same natural abundance. Both have a nuclear spin I = 5/2. The hyperfine interaction therefore splits each electronic transition into twice six hyperfine lines. The hyperfine splitting constants are $A^{151} = 34.1 \times 10^{-4}\,\mathrm{cm}^{-1}$ and $A^{153} = 15.1 \times 10^{-4}\,\mathrm{cm}^{-1}$. The resonance fields for the different transitions have been calculated at the constant frequency of 8500 Mc/s and are plotted in Figure 2.8 for the two directions [100] and [111] . The sign of b_4 has been assumed negative in anticipation of our own results.

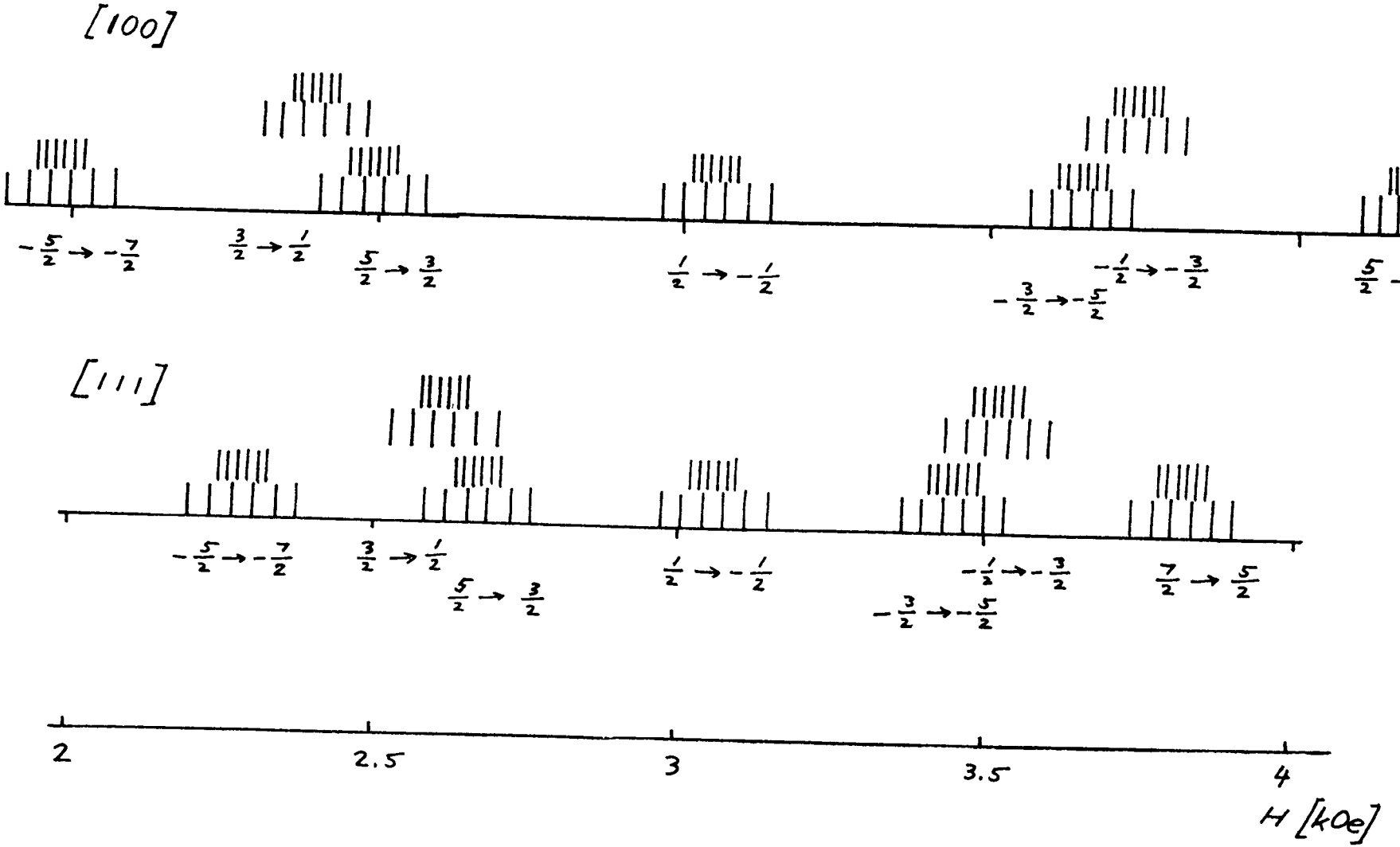

Figure 2.8 Paramagnetic resonance spectrum of $Eu^{2+}:CaF_2$ calculated line positions

2.4.3 Interactions Between Europium Ions

In the preceding paragraph, we have treated the problem of a single Eu^{2+} ion, substituted for a Ca^{2+} ion in the CaF_2 lattice. With increasing concentration the probability for one Eu^{2+} ion to have another Eu^{2+} in the close neighbourhood becomes appreciable and the interaction between the electronic spins of such pairs has to be taken into account.

The Hamiltonian $\mathcal{H}_{pr}$ for a pair of paramagnetic ions with spins $\underline{S}_1$ and $\underline{S}_2$ separated by a distance r_{12} can be written

$$\mathcal{H}_{pr} = \mathcal{H}_1 + \mathcal{H}_2 + \mathcal{H}_{int} \tag{2.66}$$

where $\mathcal{H}_1$ and $\mathcal{H}_2$ are the single-ion Hamiltonians, which are, in our case

$$\mathcal{H}_i = g\beta(\underline{H}\cdot\underline{S}_i) + \mathcal{H}_{cr} + A_i(\underline{S}_i\cdot\underline{I}_i) \qquad (i = 1,2) \tag{2.67}$$

Note that $\mathcal{H}_{cr}$ will in general be different from the single-ion case, since the crystal field at one ion site might be distorted due to the neighbouring ion. As an example, the crystal field for a nearest neighbour Eu^{2+} pair in CaF_2 will have axial rather than cubic symmetry.

The interaction Hamiltonian can be written approximately as

$$\mathcal{H}_{int} = J(\underline{S}_1\cdot\underline{S}_2) + D\left[(\underline{S}_1\cdot\underline{S}_2) - \frac{3(\underline{S}_1\cdot\underline{r}_{12})(\underline{S}_2\cdot\underline{r}_{12})}{r_{12}^2}\right] \tag{2.68}$$

The first term is the isotropic exchange interaction and J is

the exchange integral due to the overlap of the electron wave functions of the two ions. The second term contains classical dipolar interaction $\left(D_d = \frac{g^2\beta^2}{r_{12}^3} \right)$ and a pseudo-dipolar term (D_p) known as the anisotropic exchange interaction (Van Kranendonk and Van Vleck, 1958). For spins $S > \frac{1}{2}$, higher order terms are possible (quadrupole, octupole, etc.).

The pair-Hamiltonian can now be written (Owen, 1961)

$$\begin{aligned} \mathcal{H}_{pr} = g\beta(\underline{H}\cdot\underline{S}) + J(\underline{S}_1\cdot\underline{S}_2) + \mathcal{H}_{cr}^{(1)} + \mathcal{H}_{cr}^{(2)} + A_1(\underline{S}_1\cdot\underline{I}_1) \\ + A_2(\underline{S}_2\cdot\underline{I}_2) + D\left[(\underline{S}_1\cdot\underline{S}_2) - \frac{3(\underline{S}_1\cdot\underline{r}_{12})(\underline{S}_2\cdot\underline{r}_{12})}{r_{12}^2}\right] \end{aligned} \tag{2.69}$$

where $\underline{S} = \underline{S}_1 + \underline{S}_2$

If the isotropic exchange interaction is the dominant term in the Hamiltonian, the pair-states can be grouped into multiplets of total spin $\underline{S}$ ($S = S_1 + S_2$, $S_1 + S_2 - 1$, ..., 0) with energies $J\,\frac{S(S+1)}{2}$. The effect of the dipolar and crystal field terms is to lift the (2S+1)-fold degeneracy (even in zero field). For an antiferromagnetic exchange interaction, ($J > 0$), the lowest pair state is a singlet and the paramagnetic absorption lines due to pairs will disappear at low temperatures. This has been observed in copper acetate by Bleaney and Bowers (1952). If the remaining terms in the Hamiltonian are small compared to the Zeeman interaction, the lines of the pair spectrum will be close to the lines of the single-ion spectrum.

For Eu^{2+} pairs $S_1 = S_2 = 7/2$ and this gives a total of 64 lines without considering the hyperfine interaction.

EuF_2 has been observed to remain paramagnetic down to 1.6°K (Lee et al, 1965). A molecular field model for nearest neighbour (nn) interaction gives

$$|J_{nn}| = \frac{3T_c}{2z\,S(S+1)} \tag{2.70}$$

where T_c is the transition temperature and z is the number of nearest neighbours. This gives $|J_{nn}| < 0.08$°K

There is the possibility that J_{nn} is not very different in magnitude and opposite in sign as compared to next nearest neighbour interaction J_{nnn}. This would raise the upper limit for the exchange integral. It is, however, likely that the overall splitting of the pair lines does not exceed a few °K. Due to the complicated single ion spectrum, it seems hopeless to find and identify pair transitions in Eu^{2+} : CaF_2 as has been possible in ruby by Statz et al (1961) and by Gill (1961).

2.4.4 Spin-Lattice Relaxation of Eu^{2+}

The calculation of the spin-lattice relaxation time T_1 as reviewed in chapter 2.2 cannot be applied to the case of Eu^{2+} in a cubic field without modifications.

The transition probability for a one phonon process between two levels of the ground state manifold has still the form of equation (2.9)

$$W_{b\to a} = N_b A T \tag{2.71}$$

The matrix elements of the orbit-lattice interaction contained in A vanish between the states of the $^8S_{\frac{7}{2}}$ multiplet in first approximation and only combined action of V_{01} and spin-orbit coupling give non-zero matrix elements. The direct process is therefore weaker for S-state ions than for ions with $J > 0$ in the ground state.

The two-phonon Raman process has to be modified. Equation (2.23) for the transition probability is still valid but care must be taken in integrating. Previously, equation (2.23) was integrated approximately by assuming $\Delta \gg kT$. The two energy denominators were almost equal in magnitude but opposite in sign, thus leading to the Van Vleck cancellation. In the case of a multilevel ground state, however, the opposite approximation $\Delta \ll kT$ applies in the Raman region, if the intermediate state $|c\rangle$ belongs to the ground state multiplet. The two energy denominators in equation (2.23) are still approximately equal in magnitude, but of the same sign and no cancellation occurs. The transition probability becomes

$$W_{b\to a} = \sum_c \frac{9 N_b V_{ac}^2 V_{bc}^2}{4\pi^3 \rho^2 \hbar^7 v^{10}} \int_0^{k\Theta} \frac{E^4 e^{\frac{E}{kT}}}{\left(e^{\frac{E}{kT}} - 1\right)^2} dE \tag{2.72}$$

The integral gives for $T \ll \Theta$

$$W_{b\to a} \approx \frac{36 \cdot 4! N_b \sum_c V_{ac}^2 V_{bc}^2}{\pi^3 \rho^2 v^{10} \hbar^7} (kT)^5 \equiv N_b B T^5 \tag{2.73}$$

Such a temperature dependence has first been suggested by Orbach and Blume (1962).

In order to find the relaxation time characterizing the return to equilibrium of two levels, one has to solve the rate equations for the whole 8-level multiplet.

$$\frac{dN_i}{dt} = \sum_{\substack{j \neq i \\ j = -\frac{7}{2}}}^{+\frac{7}{2}} W_{j \to i} - W_{i \to j} \qquad \left(i = \tfrac{7}{2}, \tfrac{5}{2}, \cdots -\tfrac{7}{2}\right) \tag{2.74}$$

This leads, in general, to seven time constants (since $\sum_i \frac{dN_i}{dt} = 0$). It is easy to show that the relaxation is exponential if all nonvanishing transition probabilities per electron $\frac{W_{ij}}{N_i}$ are equal. In this case, the relaxation time can be written approximately

$$T_1^{-1} \approx AT + BT^5 \tag{2.75}$$

Orbach's approach to calculate the matrix elements of the orbit-lattice interaction does not work for cubic crystals. A cubic field has only terms in A_4^m and A_6^m (equation 2.64) and thus the A_2^m terms of the dynamic crystal field expansion cannot be estimated from the coefficients for the static crystal field.

Huang (1964) obtained an expression for V_{01} by examining the normal modes of vibration of a cluster containing the Eu^{2+} ion at the center of a cube formed by eight F^- ions. This approach has been used first by Van Vleck (1939, 1940). From the normal mode expansion of V_{01}, Huang obtained the relaxation time

$$T_1^{-1} \approx 3T + 4 \times 10^{-4} T^5 \ (\mathrm{sec}^{-1}) \tag{2.76}$$

2.4.5 Cross-relaxation

The Van Vleck-Orbach theory used to calculate T_1 in CeES and in Eu^{2+} : CaF_2 assumes noninteracting spins. At high concentrations spin-spin interactions (dipolar and exchange interactions) can play an important role in redistributing the populations of the different levels in the spin system thus leading to cross-relaxation effects.

Three different types of crossrelaxations may affect the relaxation behaviour of Eu^{2+} : CaF_2. These processes will be examined in the following:

a) cross-relaxation between different hyperfine components of a given electronic transition.

If the hyperfine splitting of a given electronic transition is not large compared to the dipolar width of the single components, the hyperfine structure is not resolved. This is the case in an inhomogeneously broadened resonance line. In such a line, a short microwave pulse may saturate only parts of the line. Bloembergen et al (1959) have used a random walk model to estimate the time τ_d it takes for the excitation to diffuse through the whole line.

If $\Delta\nu^*$ is the width of the whole resonance line and $\Delta\nu$ the width of its homogeneously broadened components, the diffusion time τ_d is given by

$$\tau_d = \frac{(\Delta\nu^*)^3}{(\Delta\nu)^4} \tag{2.77}$$

In Eu^{2+} : CaF_2 the line width of one hyperfine component is approximately 5 gauss, as measured from the spectrum at 34 Gc/s and the total splitting is 180 gauss. This gives $\tau_d \approx 2$ msec. This value should be too low, since the hyperfine components are partly resolved and the overlap is small. Huang has detected the influence of crossrelaxations due to inhomogeneous saturation of the $+\frac{1}{2} \rightarrow -\frac{1}{2}$ line up to pulse lengths of 0.5 msec. This time is somewhat shorter than the estimate from the random walk model. A shorter time could be due to increased intensity of the wings of the single components or to multiple spin flips as proposed by Bloembergen <u>et al</u> (1959).

b) cross-relaxation between different electronic transitions

There are many possibilities for multiple spin flips between the different electronic levels of Eu^{2+} : CaF_2. Consider crossrelaxation processes which spread the excitation from the center $+\frac{1}{2} \rightarrow -\frac{1}{2}$ transition to the other lines. One process which conserves energy is shown in Figure 2.9a. (The level distances in Figure 2.9 correspond to the actual splittings of the $^8S_{\frac{7}{2}}$ multiplet with $H \parallel [100]$.) Processes of lower order than this quadruple spin flip are possible only through the far wings of the resonance lines and are therefore weak. As an example, a double spin flip is shown in Figure 2.9b. Processes a) and b)

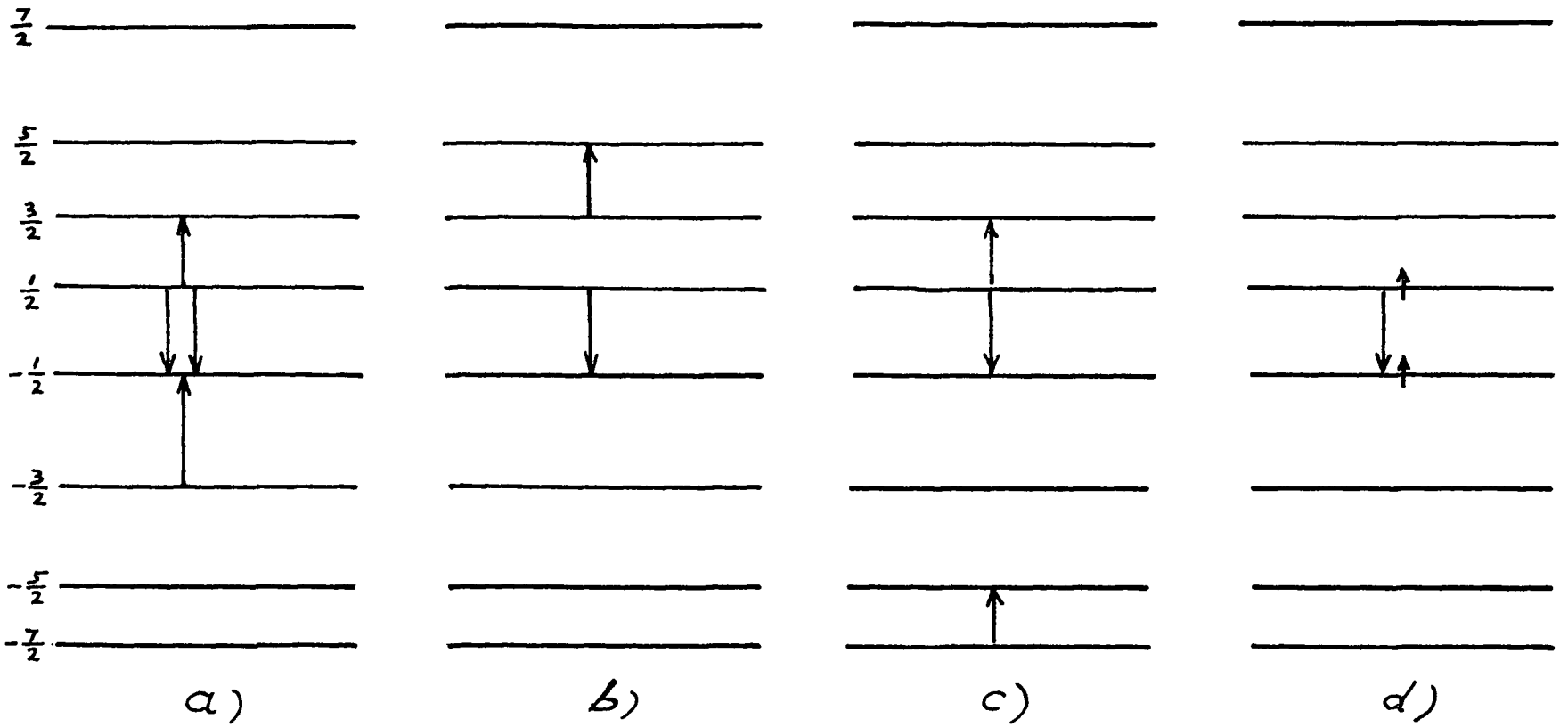

Figure 2.9 Energy levels and cross-relaxations in $Eu^{2+}:CaF_2$ H = 3100 Oe
H ∥ [100]

conserve angular momentum. Figure 2.9c and 2.9d show the triple spin-flips which do not conserve angular momentum. All processes except a) can take place only through the wings of the lines, if $H \parallel [100]$, and can be expected to be weak. The process 2.9d involves two nuclear spin flips together with an electronic transition.

The actual calculation of the transition probabilities due to all the above mentioned processes is not possible without the knowledge of the line shapes and would be extremely involved in our case due to the complicated hyperfine structure.

c) cross-relaxation to other spin systems

Consider two different spin systems 1 and 2 with two levels of almost equal spacing. Let the crossrelaxation rate between the two systems be $W_{12} = 1/T_{12}$. If $W_1 = 1/T_1$ and $W_2 = 1/T_1$ are the spin-lattice relaxation rates in the respective systems, the rate equations for the population differences n_1 and n_2 are:

$$\begin{aligned} \frac{dn_1}{dt} &= -W_1(n_1 - n_1^\circ) - W_{12}(N_2 n_1 - N_1 n_2) \\ \frac{dn_2}{dt} &= -W_2(n_2 - n_2^\circ) - W_{12}(N_1 n_2 - N_2 n_1) \end{aligned} \tag{2.78}$$

N_1 and N_2 are the populations in the two levels of each system and $n_1^\circ \approx n_2^\circ$ are the equilibrium population differences.

Rannestad and Wagner (1963) have discussed the solutions of the above rate equations in detail. In general, two decay constants are found which reduce to one in the limit of $N_1 \gg N_2$.

This is the observed relaxation rate τ^{-1} if system 1 relaxes through spin-lattice relaxation and cross-relaxation with system 2.

$$\tau^{-1} = W_1 + \frac{W_{12}(W_2 - W_1)}{W_{12} + W_2 - W_1} \cdot \frac{N_2}{N_1} \tag{2.79}$$

If either one of the relaxation rates is dominant we obtain three special cases:

a) $W_1 \gg W_2, W_{12}$

The spin-lattice relaxation is dominant and cross-relaxation can be neglected: $\tau^{-1} \approx W_1$

b) $W_{12} \gg W_1 W_2$

The cross-relaxation is very fast compared to both spin-lattice relaxation rates. We obtain

$$\tau^{-1} = W_1 + W_2 \frac{N_2}{N_1} \tag{2.80}$$

c) $W_2 \gg W_1, W_{12}$

System 2 relaxes very rapidly to the bath and the observed relaxation rate is

$$\tau^{-1} = W_1 + W_{12} \frac{N_2}{N_1} \tag{2.81}$$

It is seen that the energy exchange of system 1 via 2 with the bath is limited by the slower of the two relaxation rates in series and its efficiency is diminished by the ratio of the populations in both systems $\frac{N_2}{N_1}$.

From equation (2.79), a great variety of temperature and concentration dependences are possible. W_1 and W_2 can have any of the temperature dependences of the spin-lattice relaxation rates and also N_2 might depend on temperature through the Boltzman factor, if the cross-relaxation takes place to an excited state of system 2. $\frac{N_2}{N_1}$ depends on the relative concentration of the two systems and W_{12} can also be concentration dependent through the line shapes.

If there are several levels of the same system or several systems to which cross-relaxations are possible, it does not seem possible to solve the rate equations except in limiting cases. Rannestad and Wagner find for the time constant τ of system 1 in presence of cross-relaxation to (m-1) other systems:

$$\tau^{-1} = W_1 + \sum_{i=2}^{m} W_{1i} N_i \tag{2.82}$$

for the case of dominant spin-lattice relaxations and

$$\tau^{-1} = \frac{N_1 W_1 + \sum_{2}^{m} N_i W_i}{N_1 + \sum_{2}^{m} N_i} \tag{2.83}$$

for the case of dominant cross-relaxation. Equation (2.83) reduces for $\sum_{2}^{m} N_i \ll N_1$ to

$$\tau^{-1} = W_1 + \frac{\sum_{2}^{m} N_i W_i}{\sum_{2}^{m} N_i} \tag{2.84}$$

The influence of the above discussed processes on the observed spin-bath relaxation times in Eu^{2+} : CaF_2 will be discussed in chapter 4.

2.5 The Magneto-optical Faraday Effect

2.5.1 Introduction

The direction of polarization of linearly polarized light after passing through a medium, can change as a function of an externally applied magnetic field. This is known as the magneto-optical Faraday effect.

Kramers (1930) showed that the rotation of the plane of polarization, called the Faraday rotation ϱ , can be proportional to the magnetization M of the medium under certain general conditions. This proportionality $\varrho \sim M$ leads to a simple method of measuring changes in magnetization. One can measure the time dependence of the light intensity $I(t)$ transmitted by an analyser and if the transmission law of the analyser $I(\varrho)$ is known, the magnetization can be calculated. The time resolution of this method is only limited by the response time of the light detection system.

Under suitable conditions, microwave radiation can induce magnetic dipole transitions between the energy levels of paramagnetic ions thus causing a redistribution of the populations in the various levels. A change in population will affect the magnetization and consequently the Faraday rotation. Opechowski (1954) has given a quantum mechanical treatment of the influence of microwave radiation on the Faraday rotation. No attempt has been made to apply this rigorous treatment to the crystals studied in this thesis.

We are mainly interested in the relaxation process, i.e. in the recovery of the magnetization from a non-equilibrium value. The microwave radiation is only used to disturb the spin system in a well defined manner by equalizing the population differences in certain levels.

Microwave radiation is not the only way of establishing non-equilibrium populations. Kalbfleisch (1964) pulsed the DC magnetic field from a low to a higher value. If this is done in a time short enough such that the populations in the Zeeman levels do not change appreciably, the effective temperature T_s of the spin system will be raised. This can be seen from the definition of T_s, the so-called spin temperature

$$n_2 = n_1 e^{-\frac{\delta_{12}}{kT_s}}$$

Here n_1 and n_2 are the populations in two levels with an energy difference of δ_{12}. The two methods establish different initial conditions for the relaxation which follows the microwave pulse or the DC magnetic field step.

In the following, the conditions for the proportionality $\varrho \sim M$ are examined and it is shown that for the substances investigated in this thesis, this proportionality holds at the light frequencies employed.

2.5.2 Faraday Rotation of Rare Earth Ions in Solids

Shen (1964) has generalized the Kramers formula for the Faraday rotation to include not only electric-dipole transi-

tions. He gets the following expression for the complex Faraday rotation:

$$\rho = \frac{\pi \omega e^2 N(n^2+2)}{9mcn} \sum \frac{\frac{1}{\omega_{ba}}\left(\omega - \frac{i}{2}\Gamma_{ba}\right)}{\left(\omega_{ba}^2 - \omega^2 + \frac{1}{4}\Gamma_{ba}^2\right) - i\omega\Gamma_{ba}} \left(f_{ba}^{+} - f_{ba}^{-}\right) \qquad (2.85)$$

n is the average refractive index of the medium; N is the number of atoms per unit volume; ω is the light frequency; $\omega_{ba} = \frac{E_b - E_a}{\hbar}$ is the transition frequency between states $|b\rangle$ and $|a\rangle$; Γ_{ba} is the associated damping term and $f_{ba}^{\pm}$ are the oscillator strengths for right and left circularly polarized light. For electric dipole transitions, we can write

$$f_{ba}^{\pm} = -\frac{2\omega_{ba}^3 m}{\hbar \omega^2} \left|\langle b | r_{\pm} | a \rangle\right| \rho_a^0 \qquad (2.86)$$

where $r_{\pm} = x \pm iy$ and ρ_a^0 is the Boltzmann factor $e^{-\frac{E_a}{kT}}$.
If the light frequency is far from resonance, the damping terms can be neglected and equation (2.85) becomes

$$\rho = -\frac{2\pi e^2 N(n^2+2)}{9\hbar c n} \sum \frac{\omega_{ba}^2 \rho_a^0}{\omega_{ba}^2 - \omega^2}\left(\left|\langle b | r_+ | a \rangle\right|^2 - \left|\langle b | r_- | a \rangle\right|^2\right) \qquad (2.87)$$

In order to simplify the above expression, we have to specify the states. For free ions, the states can be specified by $|n, J, m_s\rangle$ in the Russell-Saunders approximation, which is quite good for rare earths. For the ground state of rare earth ions in solids, J remains a good quantum number, but m_J has to

be replaced by the symmetric quantum number μ . In the excited states, the effect of the crystal field can be strong. J is no longer a good quantum number and is replaced by ζ . For illustration, a part of the level diagram for a hypothetical ion is shown in Figure 2.10. If the crystal field and Zeeman splittings are small compared to the difference between the average transition frequency and the light frequency, i.e. if

$$\left|\Delta\omega_{n'\zeta'\mu'-nJ\mu}\right| \ll \left|\overline{\omega}_{n'-nJ} - \omega\right| \tag{2.88}$$

where

$$\Delta\omega_{n'\zeta'\mu'-nJ\mu} = \omega_{n'\zeta'\mu'} - \overline{\omega}_{n'-nJ}$$

the frequency factor in equation (2.87) can be expanded in terms of $\Delta\omega$:

$$\frac{\omega^2_{n'\zeta'\mu'-nJ\mu}}{\omega^2_{n'\zeta'\mu'-nJ\mu} - \omega^2} = \frac{\left(\overline{\omega}_{n'-nJ} + \Delta\omega_{n'\zeta'\mu'-nJ\mu}\right)^2}{\left(\omega_{n'-nJ} + \Delta\omega_{n'\zeta'\mu'-nJ\mu}\right)^2 - \omega^2}$$

$$= \frac{\overline{\omega}^2_{n'-nJ}}{\overline{\omega}^2_{n'-nJ} - \omega^2}\left\{1 - 2\Delta\omega_{n'\zeta'\mu'-nJ\mu}\left[\frac{\omega^2}{\overline{\omega}_{n'-nJ}\left(\overline{\omega}^2_{n'-nJ} - \omega^2\right)}\right] + \dots\right\}$$

$$\equiv D^{(0)}_{n'-nJ}(\omega) + \Delta\omega_{n'\zeta'\mu'-nJ\mu}\, D^{(1)}_{n'-nJ}(\omega) + \dots$$

(2.89)

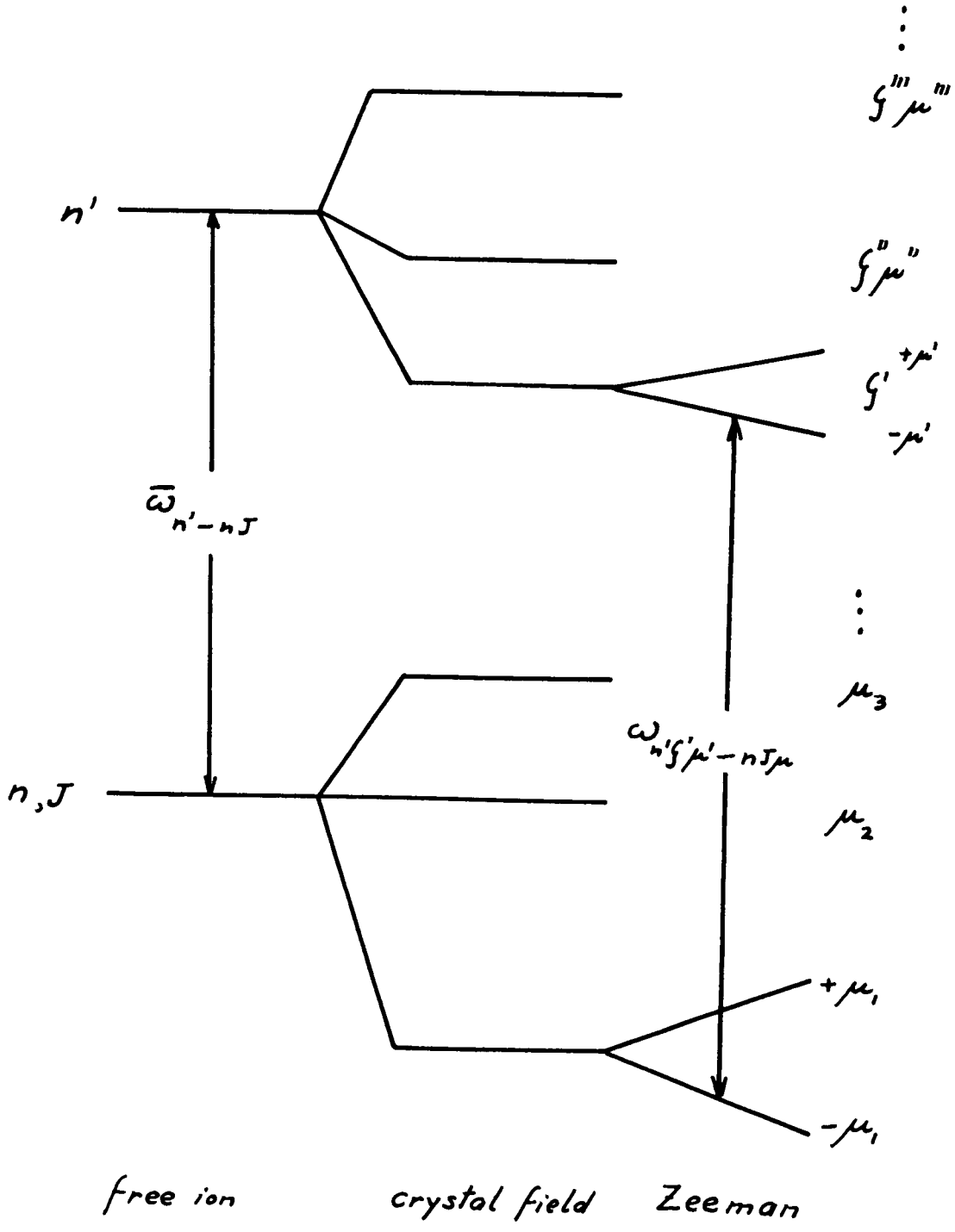

Figure 2.10 Typical levels of rare earth ions in solids

If one retains only the first term of expansion (2.89), equation (2.87) for the Faraday rotation gives

$$\rho_0 = C \sum_{\substack{n n' \\ J}} D^{(0)}_{n'-nJ}(\omega) \sum_{\zeta' \mu' \mu} \left(|\langle n'\zeta'\mu' | r_+ | nJ\mu \rangle|^2 - |\langle n'\zeta'\mu' | r_- | nJ\mu \rangle|^2 \right) \rho^0_{nJ\mu} \quad (2.90)$$

with

$$C = - \frac{2\pi e^2 N (n^2+2)^2}{9 \hbar c n}$$

Following Van Vleck and Hebb (1934), we change from the $|n'\zeta'\mu'\rangle$ and $|nJ\mu\rangle$ to the $|nJm\rangle$ representation and apply the Kronig-Hönl formula for the electric dipole moment operator. The result is

$$\rho_0 = C \sum_{\substack{n n' \\ J}} D^{(0)}_{n'-nJ}(\omega) \sum_{J'} |T(nJ; n'J')|^2 \sum_m m \, \rho^0_{nJm} \quad (2.91)$$

At the low temperatures employed in our experiments, only the lowest J-multiplet is occupied and equation (2.91) can be written

$$\rho_0 = A_{nJ} \sum_m m \, \rho^0_{nJm} = A \langle J_z \rangle \quad (2.92)$$

with

$$A_{nJ} \equiv C \sum_{n'} D^0_{n'-nJ} \sum_{J'} |T(nJ; n'J')|^2$$

It is seen that ρ_0 is proportional to the magnetization. Shen (1963) has calculated the contribution to the Faraday rotation from the $D^{(1)}_{n'-nJ}(\omega)$ term, which arises from the Zeeman

perturbation on the frequencies $\omega_{n'J'\mu' - nJ\mu}$. He gets two additional terms to the rotation, one diamagnetic and one paramagnetic. They are small to the extent that approximation (2.88) holds. Finally, both the crystal field and Zeeman interactions perturb the ground J multiplet such that J is no longer a good quantum number. The former gives a small paramagnetic contribution while the latter causes a diamagnetic rotation, which is the analogue to the so-called Van Vleck paramagnetism.

Application to CeES

CeES crystals are completely transparent down to a wavelength of 2700Å and the absorption bands due to the strong electric dipole transitions start at 2500Å. The light frequencies used are around $\omega = 20{,}000\ cm^{-1}$. We have, therefore

$$\bar{\omega} - \omega \approx 20\,000\ cm^{-1}$$

Since the crystal field splitting is relatively small (Van Vleck and Hebb, 1934) $\Delta\omega$ becomes

$$\Delta\omega \approx 1000\ cm^{-1}$$

Therefore, the coefficients for the dominant terms in equation (2.87) due to the strong electric dipole transitions (4f) → (5d) are $D^{(0)} \approx \frac{4}{3}$ and $D^{(1)}\Delta\omega \approx \frac{1}{60}$. The approximation (2.88) thus holds to within one percent.

Application to $Eu^{2+} : CaF_2$

The strong absorption bands for Eu^{2+} are in the visible region and the approximation (2.88) is not valid. However, the

transitions which contribute mainly to the sum in (2.87) are the allowed electric dipole transitions $S \rightarrow P$. If the Eu^{2+} ion is at a cubic site, the crystal field splittings of the P multiplets are only of the order of 10 cm^{-1} (Van Vleck and Penney, 1934) and J remains a good quantum number even in the excited P states (Figure 2.11).

It is then possible to expand the frequency dispersion factors using a much less stringent requirement, namely

$$\left| \Delta\omega_{n'J'\mu'-nJ\mu} \right| \ll \left| \bar{\omega}_{n'J'\mu-nJ} - \omega \right| \tag{2.93}$$

with

$$\Delta\omega_{n'J'\mu'-nJ\mu} = \omega_{n'J'\mu'-nJ\mu} - \bar{\omega}_{n'J'-nJ}$$

This yields the expansion

$$\frac{\omega^2_{n'J'\mu'-nJ\mu}}{\omega_{n'J'\mu'-nJ\mu} - \omega^2} = \frac{\bar{\omega}^2_{n'J'-nJ}}{\bar{\omega}^2_{n'J'-nJ} - \omega^2}\left\{ 1 - 2\Delta\omega_{n'J'\mu'-nJ\mu}\left[\frac{\omega^2}{\bar{\omega}_{n'J'-nJ}\left(\bar{\omega}^2_{n'J'-nJ} - \omega^2\right)}\right] + \cdots \right\}$$

$$\equiv D^{(0)}_{n'J'-nJ}(\omega) + \Delta\omega_{n'J'\mu'-nJ\mu}\, D^{(1)}_{n'J'-nJ}(\omega) \tag{2.94}$$

If only the ground J multiplet is occupied and if only the first term in expansion (2.94) is retained, the same procedure as used before gives the Faraday rotation

$$\rho_0 = A_{nJ} \langle J_z \rangle \tag{2.95}$$

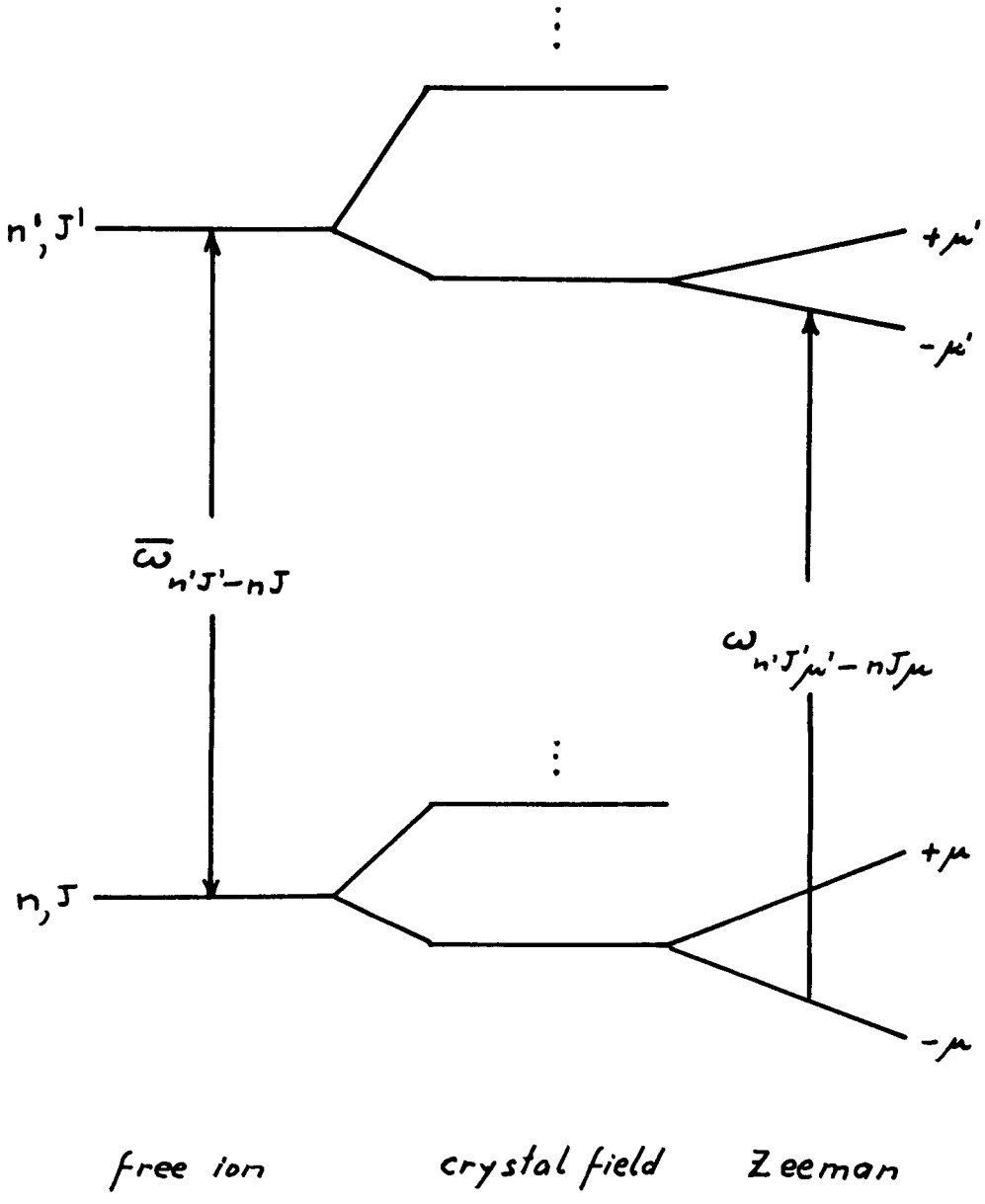

Figure 2.11 Typical levels for rare earth ions in solids: S-state ion in a cubic field

with

$$A_{nJ} \equiv C \sum_{n'J'} D^{(0)}_{n'J'-nJ} \left| T(n'J'; nJ) \right|^2$$

The Faraday rotation is again proportional to the magnetization M, which, in this approximation, is given by the Brillouin function

$$B_J(x) = \frac{2J+1}{2J} \coth\left[\frac{(2J+1)x}{2J}\right] - \frac{1}{2J} \coth\left[\frac{x}{2J}\right] \qquad (2.96)$$

with $x = \frac{g\beta JH}{kT}$ and $J = 7/2$ for Eu^{2+}

J is a good quantum number and departure of the magnetization from the Brillouin curve is small. In fact, higher J-states are admixed to the ground state only in second order as mentioned in chapter 2.4. As mentioned above, the splitting of the excited P-states by a cubic crystal field is of the order of 10 cm^{-1}. Hence, the frequency difference $\Delta\omega_{n'J'\mu'-nJ\mu}$ is small, corresponding to ≈ 3Å at the light frequencies used. The approximation (2.93) is valid even for light frequencies very close to the absorption bands due to the electric dipole $S \rightarrow P$ transitions which begin below 4200Å (Feofilov and Kaplyanskii, 1963). The frequency factor $D^{(0)}_{n'J'-nJ}$ enhances, in this case, the Faraday rotation considerably due to its small denominator, without spoiling the proportionality between Faraday rotation and magnetization.

3 EXPERIMENTAL ARRANGEMENT

3.1 Apparatus

The basic apparatus required for the optical detection of paramagnetic resonance and relaxation described in this thesis include

- a helium cryostat to maintain the sample at the low temperatures needed to obtain long enough spin-lattice relaxation times and appreciable paramagnetic rotation.
- a magnet to provide strong enough fields to split the ground levels of the paramagnetic ions by an amount corresponding to convenient microwave frequencies.
- a microwave system capable of saturating transitions between the ground levels.
- an optical system to produce a collimated beam of linearly polarized monochromatic light.
- a detection system to analyse the state of polarization of the light after passing through the crystal.

The apparatus used in our experiments is basically the same as that described in great detail by Rieckoff (1962) and Griffiths (1965). We review, therefore, only briefly the general features, describing at the same time in more detail the few adaptions which have been made for our experiments. A block diagram of the apparatus is shown in Figure 3.1.

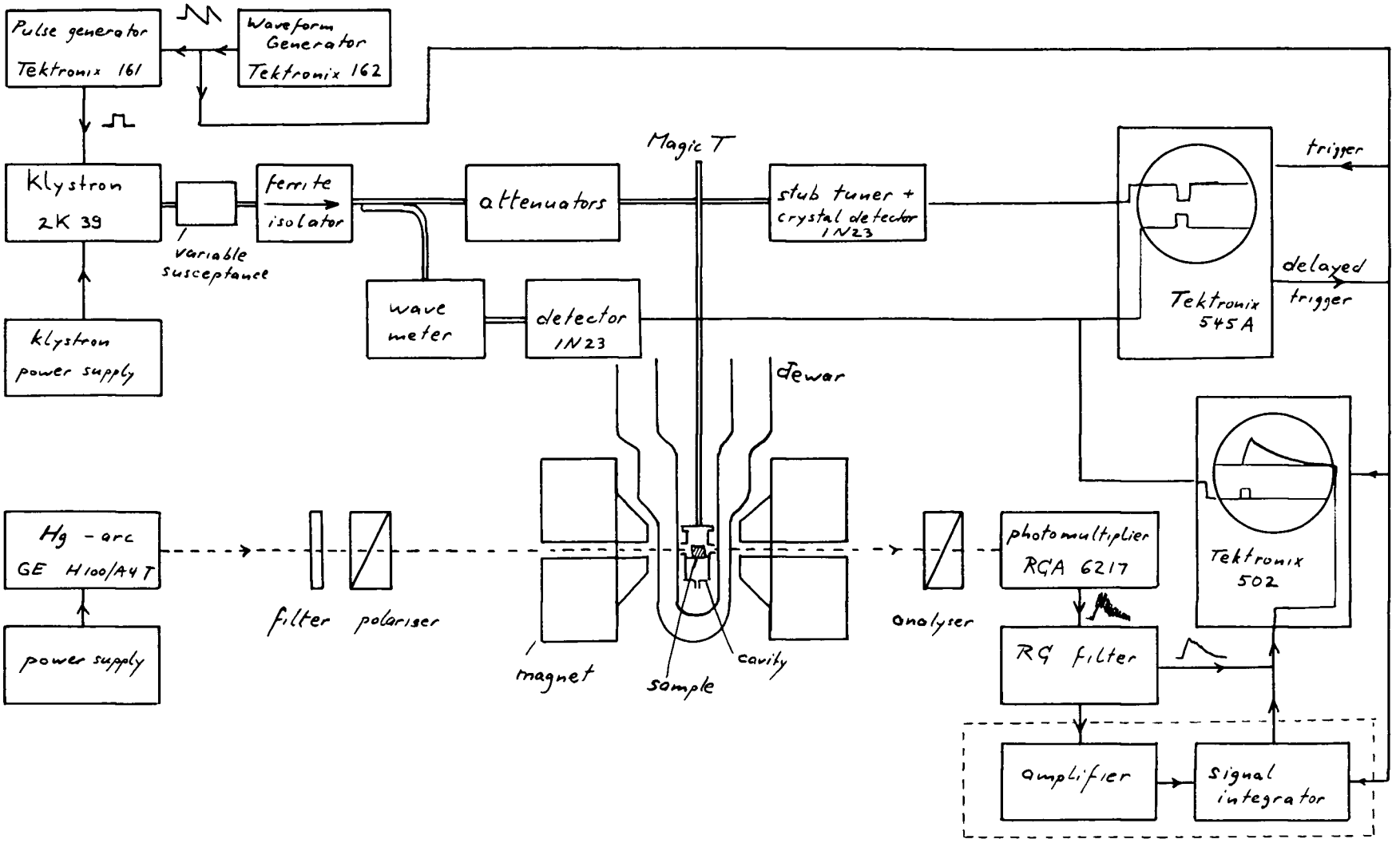

Figure 3.1 Block diagram for the apparatus

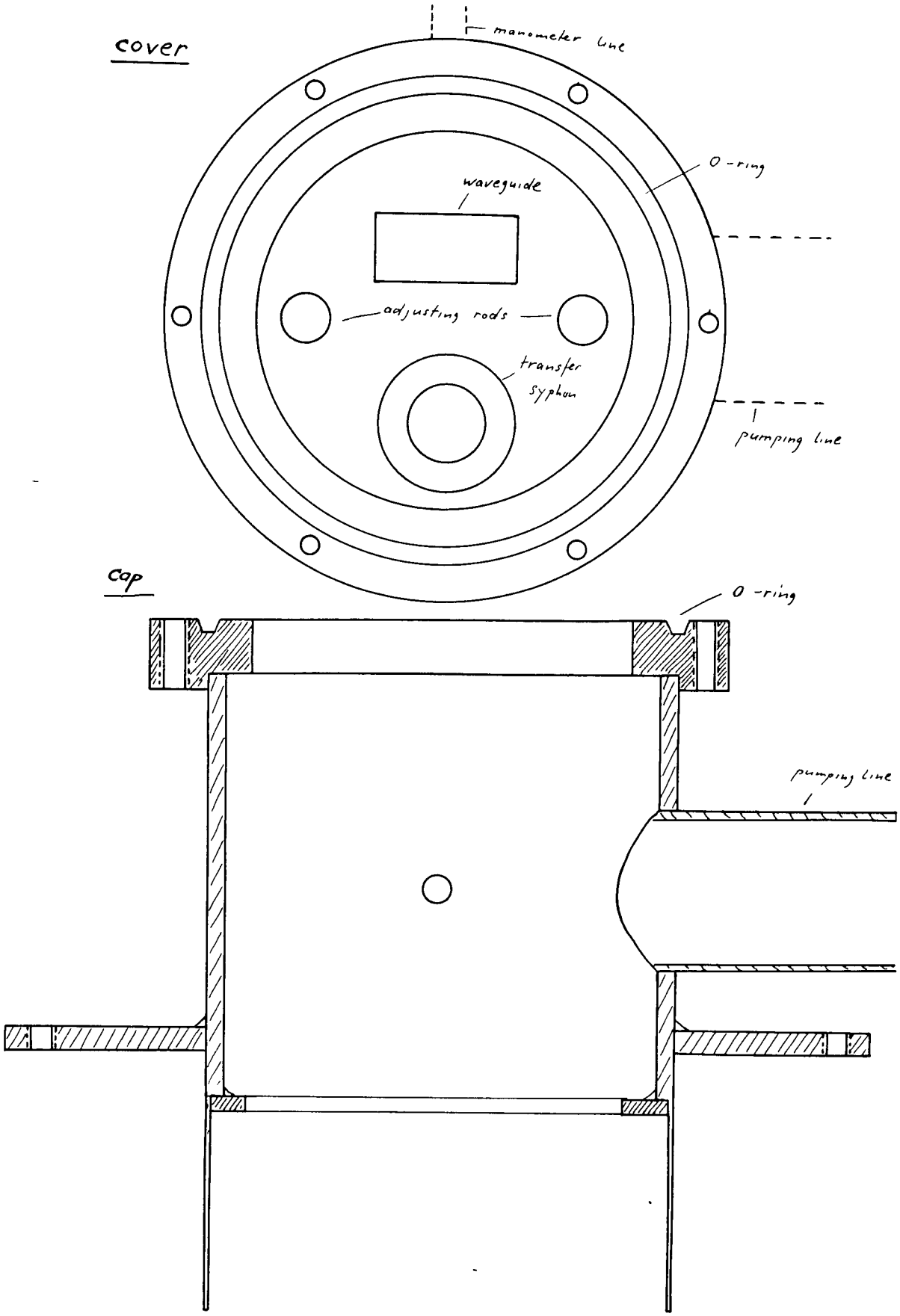

Figure 3.2 The dewar cap

3.1.1 The Cryostat

The helium dewar, whose diameter is just large enough for the microwave cavity and the adjusting mechanisms, is placed into an oversize nitrogen dewar. Both dewars are made of pyrex glass and strip silvered. Two windows, cut out of several layers of plastic tape and held to the inner dewar by a copper sleeve, kept the liquid nitrogen out of the light path. This eliminates noise in the light signal arising from boiling nitrogen.

A new dewar cap was used, which is of the same basic design as those used currently in our low temperature laboratory. The details are shown in Figure 3.2. The pumping line and the connections to the helium return line and manometers enter the brass cap from the side. The cover is screwed on top of the cap and contains the feedthrough for waveguide, transfer syphon and adjusting rods. A combination of forepump and Hg-diffusion pump was used to pump out the transfer syphon jacket, the manometers and the wall of the helium dewar to a hard vacuum. A Kinney high-speed pump was employed to reduce the pressure over the liquid helium surface in order to obtain temperatures down to 1.4 °K.

3.1.2 The Magnet

The low-impedance watercooled electromagnet was custom made to specifications from Dr. J.M. Daniels by the Tatena Electric Mfg. Co. in Tokyo. An axial hole through the magnet per-

mits optical investigations with a light beam parallel to the magnetic field as required for our experiments. The magnet produces a field of 12 kOe at 40 amperes. This is large enough at X-band frequencies to investigate substances with g-values as low as 0.5. The current through the magnet was provided by a DC generator and regulated by means of water cooled rheostats. The generator ripple was reduced through a filter of two 5600 Mfd capacitors in parallel. The magnet current was stabilized by power transistors, whose base current was regulated by combined current and voltage feedback loops. This stabilization has been described by Garwin et al (1959). A diagram of the circuit is shown in Figure 3.3. A long term stability of at least ±1 gauss was achieved, which is certainly less than the line width of the hyperfine components of the Eu^{2+} lines and is better than the resolution limit set by the inhomogeneity of the magnetic field. The value of the magnetic field was determined by measuring the current through the magnet. The field values could then be taken from a calibration curve H vs I.

3.1.3 The Microwave System

A 2K39 reflex klystron produced 250 mW microwave power at X-band frequencies. The klystron heater current was taken from a 6 Volt car battery and the high voltages were provided by a home made regulated power supply. The klystron was matched to the rectangular waveguide transmission line by a variable sus-

ceptance. A ferrite isolator protected the klystron from reflected power. The microwave power was then passed through a 30 db flap attenuator, two variable precision attenuators and the magic T, before reaching the sample cavity. The reflected power from the cavity was monitored in the fourth branch of the magic T, which contained a stub tuner and a crystal detector (1N23).

A cavity wavemeter followed by a crystal detector was coupled to the microwave system with a 20 db directional coupler inserted just after the ferrite isolator (see Figure 3.1). It served to measure the resonance frequency of the sample cavity.

The cylindrical sample cavity was coupled to the waveguide by a circular iris. Two screws extending into the waveguide were used to match the loaded cavity to the transmission line at room temperature. Usually the matching deteriorated considerably at liquid N_2 temperature, but at helium temperatures, the match was again satisfactory.

The cavity was operated in the TE 112 mode. The field configuration in a horizontal plane through the sample is shown in Figure 3.4. This particular mode permits a simple solution to the problem of adjusting the crystal at helium temperatures. A teflon plug fills the lower half of the cavity. A cylindrical teflon rod is inserted in a horizontal slot in the upper part of the plug. The plug was turned through a gear drive while the rod was tilted by pulling on one end of the nylon thread passing through the rod. This allowed the crystal to

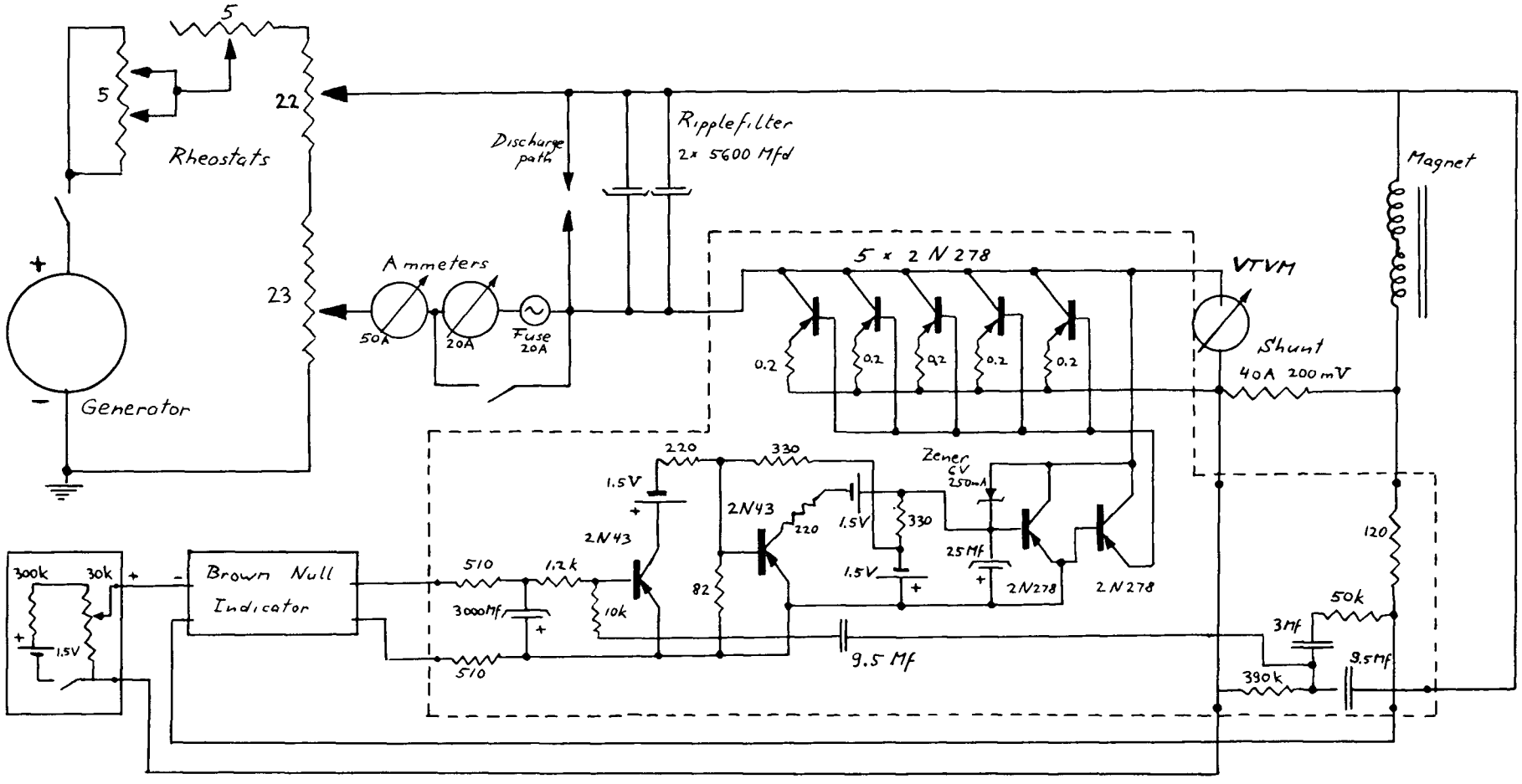

Figure 3.3 The current regulation

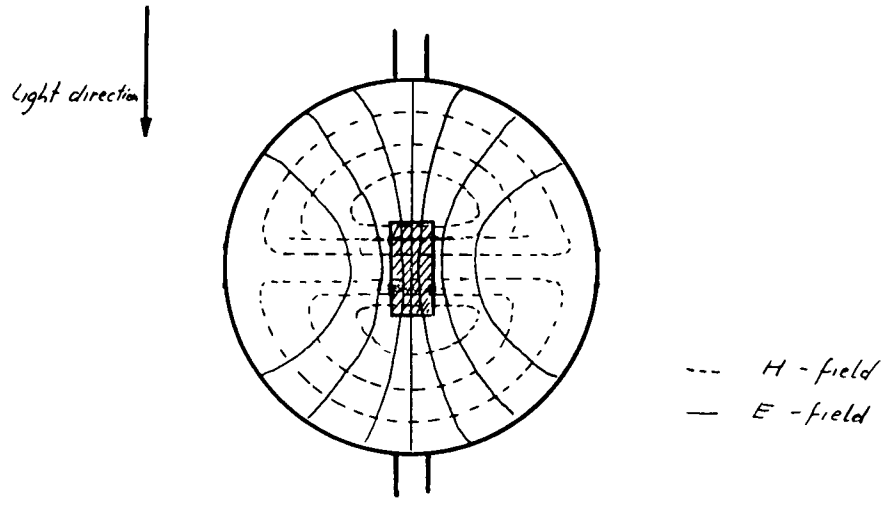

Figure 3.4 Field configuration in the microwave cavity

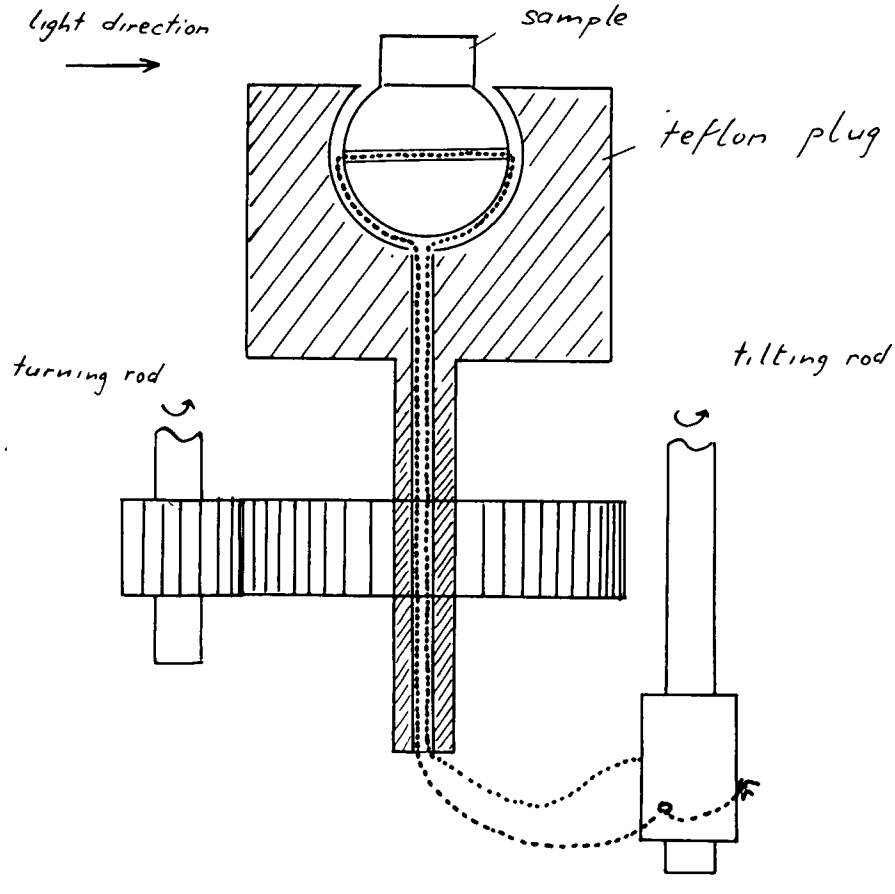

Figure 3.5 Crystal adjusting mechanism

rotate about two perpendicular axes. The strength of the nylon is not very great at helium temperatures and it breaks very easily. It has been found that imperfections in the nylon thread (ordinary 12 pound fishing line) occur fairly often. Breaking has occurred less often when the nylon thread was examined under a low power microscope to find a perfect piece. A new piece of nylon thread was used for each experimental run since repeated use was found to weaken the thread. A schematic drawing of the cavity with the adjusting mechanism is shown in Figure 3.5. For more details, we refer to Rieckoff and Weissbach (1962).

For that section of the transmission line, which extends into the dewar, a thin-wall material with low thermal conduction is required. The home made german-silver waveguide used previously was replaced by a stainless steel waveguide obtained from Superior Tube Co., Norristown, Pa. The heat leak was found to be smaller and thus the helium lasted several hours longer. Since in all substances investigated in this thesis, magnetic-dipole transitions are induced by a microwave magnetic field perpendicular to the DC magnetic field, the H-plane of the wave guide was set perpendicular to the DC field.

Pulse modulation of the microwaves was achieved by applying a pulse from a Tektronix 161 pulse generator to the reflector electrode of the klystron via a 1 Mfd condensor. The pulse width used varied between 1 msec and 100 msec and the repetition rate was in all cases at least ten times the relaxation

time in order to achieve complete recovery before applying a new pulse. To tune the microwave system, a sawtooth voltage from a Tektronix 162 waveform generator was applied to the reflector. This permitted the klystron frequency to be swept through the cavity resonance.

3.1.4 The Optical System

The light source was a General Electric H100 A4/T mercury-arc lamp cooled by forced air. The current was taken from a DC generator and passed through a choke and a current regulator tube Amperite 10-4C in order to keep the light intensity as constant and free from ripple as possible.

A series of lenses collimated the light to a narrow and nearly parallel beam at the sample site. Corning glass filters were used to select single lines from the Hg-spectrum.

Both analyser and polarizer were of the Glan-Thompson type and mounted in a divided circle which allowed angle readings of five minutes of arc. In many cases, the light intensity at the detecting end was too high for the photomultiplier to operate in its linear region. An iris was improvised using plastic tape in these cases and was inserted between the light source and the condenser lens.

Even with optimum alignment, a halo due to scattered light could be seen around the image of the cavity hole at the detecting side of the optical bench. This scattered light was eliminated by another iris narrow enough to pass only the light

coming directly from the cavity. The contribution of scattered light to the photo signal was thus minimized.

3.1.5 Signal Detection

The light passing through the analyser was detected by an RCA 6217 photomultiplier. A bank of twelve 90-volt radio batteries delivered the necessary stable voltages. The photocurrent was passed through a 10 kΩ resistor. The resulting photo signal V_{ph} was found to be proportional to the light intensity up to V_{ph} = 700 mV. The relaxation signals were filtered with a variable RC network. A time constant long enough not to distort the signals, but as short as possible to cut down the noise was chosen.

The signals were usually displayed directly on a Tektronix 502 oscilloscope using the built-in differential DC-amplifier. The required opposite bias to cancel the DC-component of the light was taken from a No. 6 dry cell regulated by a 10 kΩ helipot. In the case of CeES, the signals were very weak, especially at high temperatures, and use was made of signal averaging devices.

An enhancetron was kindly lent to us for an overnight run by Mr. R.F. Trehearne and Mr. Phil West from Nuclear Data Inc. Subsequently, a CAT 400B (Technical Measurement Corp, Mnemotron Div.) was used for which thanks are given to Dr. J.A. Wada and Mr. Finn Bauck from the neurological institute at the University of British Columbia. With both of these averaging devices, we

could increase the signal-to-noise ratio considerably. Signals completely immersed in the noise yielded reasonable traces after integration for only a few minutes (Figure 3.6).

The box-car integrator used in previous work by Griffiths (1965) is unsuitable in the case of CeES because of its dependence on zero-line shifts. Appreciable zero-line shifts over the long time periods necessary for integration by the box-car could not be avoided due to the very large Faraday rotation, which is extremely sensitive to temperature changes.

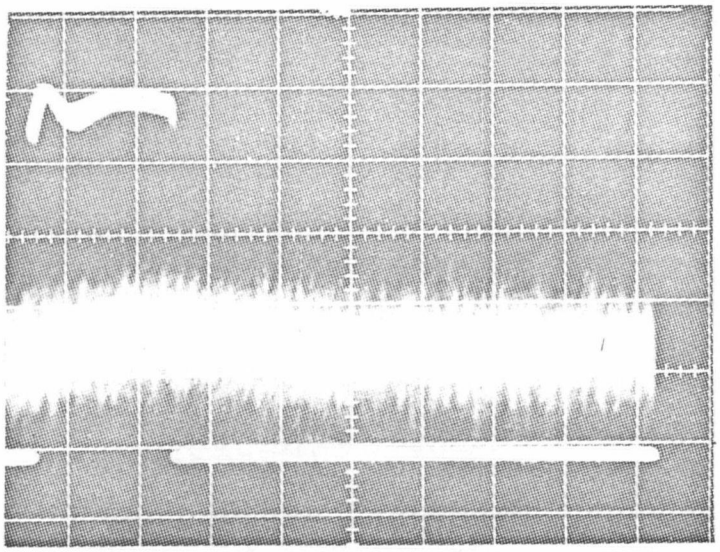

a) before averaging

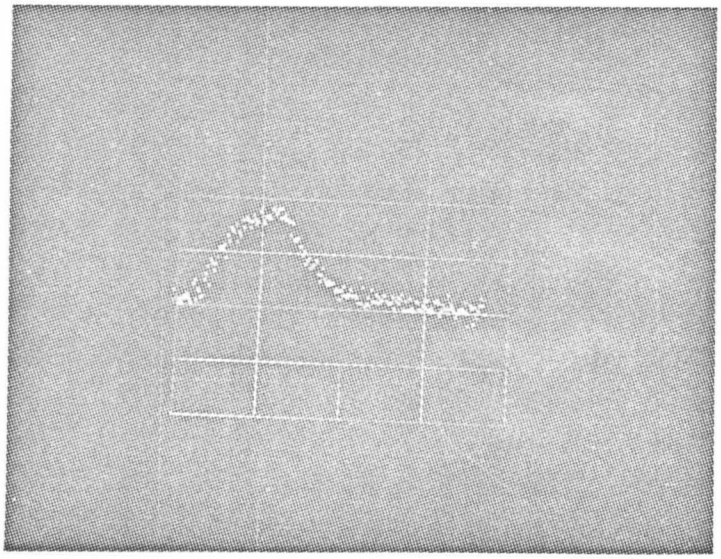

b) after averaging (CAT 400B)

Figure 3.6 Relaxation trace in CeES

3.2 Experimental Procedure

3.2.1 Preparations for the Measurements

The ethylsulphate samples were grown in this laboratory from aqueous solution by slow evaporation at ice temperature. The growing, orienting and polishing procedure has been described in detail by Griffiths (1965). The europium-doped CaF_2 samples were purchased ready cut and oriented from Optovac Inc., North Brookfield and were polished in our laboratory.

The samples were cooled to helium temperatures by standard low temperature techniques described in detail by Griffiths (1965). The ethylsulphate samples dehydrate under reduced pressure or in a dry atmosphere. At the pressure of a few mm Hg, the surfaces of the crystals dehydrate in seconds sufficiently to depolarize the light and thus reduce the signal-to-noise ratio appreciably. It is therefore important to pump the air quickly out of the inner dewar and replace it immediately with dry helium at atmospheric pressure. After that, the precooling should be started without delay.

After having reached the desired low temperature, the crystals are aligned for maximum light transmission. In the ethylsulphates, the alignment is very critical. If the light direction and the hexagonal axis of the crystal are not parallel, birefringence occurs which may diminish the Faraday rotation appreciably. This effect is investigated in some detail in chapter 4.3. A good check of the proper alignment is the Faraday

rotation at low magnetic fields, which should be linear with field.

3.2.2 Faraday Rotation

To determine the Faraday rotation, the analyser was adjusted to minimum light transmission for a given field. If the angle of the analyser is $\varphi_{min}(H)$, then the total Faraday rotation is given by

$$\varrho_{tot}(H) = \varphi_{min}(H) - \varphi_{min}(0) \tag{3.1}$$

Each value of φ was averaged from several readings. The mean deviation of the average varied between 0.3 deg and 1 deg depending on the degree of polarization of the light. ϱ_{tot} has to be corrected for the Faraday rotation of the glass walls of the dewar ϱ_c and for the diamagnetic rotation of the sample ϱ_d to obtain the paramagnetic contribution ϱ_p. Since ϱ_c and ϱ_d are of opposite sign with respect to ϱ_p, we have

$$|\varrho_p| = |\varrho_{tot}| + |\varrho_c| + |\varrho_d| \tag{3.2}$$

ϱ_d is independent of temperature and has been determined at room temperatures, where ϱ_p is negligible. ϱ_c turned out to be also independent of temperature down to 1.5 °K. The Faraday rotation of our dewar is shown in Figure 3.7.

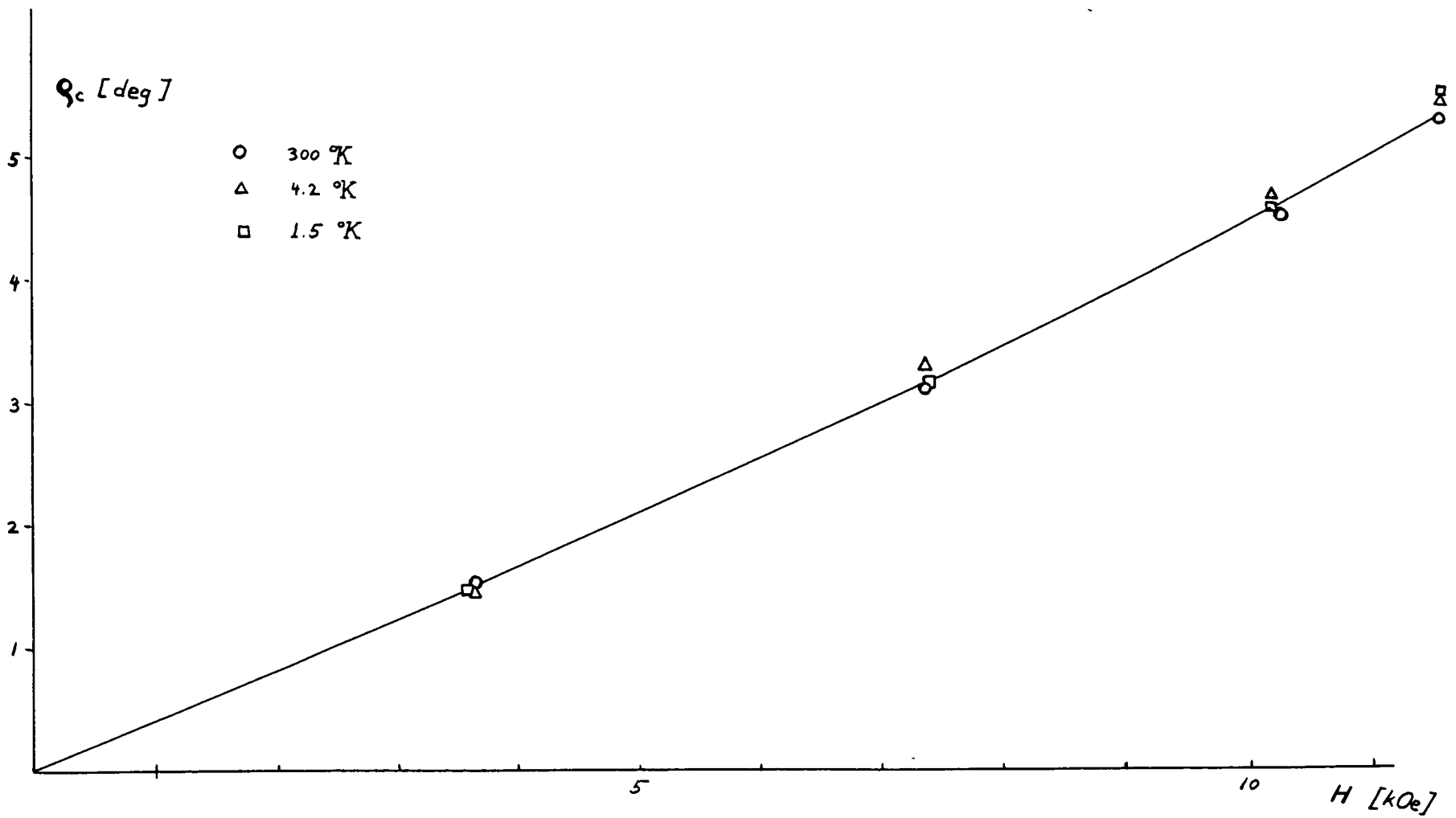

Figure 3.7 Faraday rotation of the glass walls of the dewar

3.2.3 Determination of the Resonance Spectrum

The relative change in the population difference of a two level spin system due to a microwave radiation field is usually called the saturation s.

$$S = \frac{\Delta n_0 - \Delta n}{\Delta n_0} \tag{3.3}$$

Δn and Δn_0 are the population differences between the two levels in presence and in absence of microwaves respectively. The population difference of a two level spin system is proportional to the magnetization M and we can write

$$S = \frac{M_0 - M}{M_0} \tag{3.4}$$

If the magnetization is in turn proportional to the Faraday rotation, the saturation becomes

$$S = \frac{\varrho_0 - \varrho}{\varrho_0} \tag{3.5}$$

where ϱ and ϱ_0 are the paramagnetic Faraday rotations in presence and in absence of the microwave radiation respectively.

In a multilevel system, equation (3.4) can be used to define the saturation s, since equation (3.3) does, in general, not hold. The saturation of a spin system is therefore defined as the relative change in magnetization due to microwave radiation. s is a measure for the microwave absorption and a plot of s versus the applied DC magnetic field H yields, therefore, the para-

magnetic resonance spectrum.

Equation (3.5) has been used to determine the resonance spectrum for CeES and Eu^{2+}: CaF_2. The experimental procedure is very tedious. It requires reading the angles of minimum light transmission with and without microwaves for each field value. This step-by-step procedure is incapable of giving details of a spectrum with closely spaced lines as in the Eu^{2+} spectrum, since the minimum step possible with our rheostat is 30 gauss at medium fields. It is sufficient, however, to determine the spectra found in undiluted rare earth salts which exhibit broad resonance lines.

If the microwave power required to produce a measurable saturation heats the sample a pulse method can be used to determine the saturation. The light intensity I transmitted by an analyser is

$$I(\varphi) = \left(I_0 - I_{\frac{\pi}{2}}\right) \cos^2\varphi + I_{\frac{\pi}{2}} \tag{3.6}$$

φ is the angle of the analyser with respect to the plane of polarization of the light. I_0 is the maximum transmitted light intensity ($\varphi = 0$) and $I_{\frac{\pi}{2}}$ is the minimum ($\varphi = \frac{\pi}{2}$). A small change $\Delta\varphi$ around the angle $\varphi = \left(\frac{\pi}{4}, \frac{3\pi}{4} \ldots\right)$ gives from equation (3.6)

$$|\Delta I| = \left(I_0 - I_{\frac{\pi}{2}}\right)\Delta\varphi = \left(I_0 - I_{\frac{\pi}{2}}\right)\Delta\rho \tag{3.7}$$

since $|\Delta\varphi| = |\Delta\rho|$ if $\Delta\rho$ is the change in Faraday rotation,

eg. due to a microwave pulse.

The saturation due to a microwave pulse can now be determined from equation (3.7)

$$S = \frac{\Delta \varrho}{\varrho_0} = \frac{\Delta I}{\varrho_0 (I_0 - I_{\frac{\pi}{2}})} \tag{3.8}$$

Equation (3.8) has been used to determine the saturation in CeES. The procedure is the following:

The DC photosignal V_{ph} was measured for maximum and mimimum light transmission and the angle corresponding to minimum light intensity was recorded. Then the microwaves were pulsed into the cavity at long repetition rates (generally 2 sec) in order to avoid heating. The saturation signal height ΔV_{ph} was determined from the oscilloscope or from a photo of the saturation trace. Care was taken to stay in the linear region of the photomultiplier such that $V_{ph} \sim I$. For all measurements in CeES $\Delta \varrho$ was small enough to keep equation (3.7) valid.

3.2.4 Relaxation Time Measurements

For the substances investigated in this thesis, the Faraday rotation is proportional to the magnetization. Hence, we have $\Delta \varrho(t) \sim \Delta M(t)$ and the decay of the photosignal ΔV_{ph} observed after a microwave pulse is a linear measure of the recovery of the magnetization. This is true if $\Delta V_{ph} \sim \Delta I$ and $\Delta I \sim \Delta \varrho$. The first proportionality is assured by the photomultiplier characteristic if $V_{ph} < 700$ mV. The deviation from the propor-

tionality $\Delta I(t) \sim \Delta\varrho(t)$ is smallest if the analyser is set at $\varphi_\infty + \frac{\pi}{4} - \frac{1}{2}\Delta\varrho_{tot}$ where φ_∞ is the angle of minimum light transmission without the microwave signal. A microwave pulse rotates the direction of polarization by an angle $\Delta\varrho_{tot}$ from $\varphi_\infty - \frac{1}{2}\Delta\varrho_{tot}$ to $\varphi_\infty + \frac{1}{2}\Delta\varrho_{tot}$ and the decay will proceed in the reverse direction after shutting off the microwaves. For $\Delta\varrho_{tot} < 20$ deg, we have $\Delta I(t) \sim \Delta\varrho(t)$ within the measuring accuracy of the relaxation trace. For larger values $\Delta\varrho_{tot}$, Rieckoff has computed tables to correct $\Delta\varrho$ for the deviation from the proportionality $\Delta I(t) \sim \Delta\varrho(t)$. The correction procedure is, however, time consuming and values of $\Delta\varrho_{tot} > 20$ deg did not give a better signal-to-noise ratio. Care was taken, therefore, not to exceed $\Delta\varrho_{tot} = 20$ deg by attenuating the microwave power. This was only needed in $Eu^{2+} : CaF_2$, the signals in CeES being always small. The relaxation traces were recorded from the oscilloscope screen on polaroid or 35 mm film. The traces were measured point for point and plotted on semilogarithmic paper. The slopes of the obtained straight lines give the relaxation time. If no straight line is obtained, the relaxation is nonexponential and cannot be characterized by a single relaxation time. This occurred only in CeES above the λ-point as will be mentioned in chapter 4.1.

A second scope (Tektronix 545A) was used to monitor the pulse response of cavity and wavemeter. This allowed to observe constantly the tuning of the klystron during the pulse and to correct its frequency for small shifts in the cavity resonance during warm-up by adjusting the height of the pulse

applied to the reflector electrode.

The 545A oscilloscope provided at the same time a delayed trigger which was used to trigger the 502 oscilloscope a second time after the pulse had died out in order to obtain the zero-line of the exponential trace.

3.2.5 Temperature Measurements

From 1.4°K to 4.2°K, the crystal was immersed in liquid helium and the temperature could be measured by monitoring the helium vapour pressure. Up to 2.3°K, an oil manometer and above this temperature a mercury manometer were used.

In order to reach temperatures above 4.2°K, the liquid helium level had to drop below the cavity. In this case, the Faraday rotation was used to measure the crystal temperature. This was only done in the $Eu^{2+} : CaF_2$ samples at higher concentrations. The paramagnetic Faraday rotation can be written as

$$\rho_p = f\left(\frac{H}{T}\right) \tag{3.9}$$

ρ_p has been determined for each specimen as a function of H at 4.2°K as shown in Figure 4.15 and 4.16 and the ρ_p vs $\frac{H}{T}$ curve was used to obtain temperatures T > 4.2°K from the known ρ_p and H values. The accuracy of this method to find T depends on the magnitude of the Faraday rotation of the sample. The decrease in Faraday rotation towards higher temperatures decreases the accuracy of the T value. At the same time, however, the

signal-to-noise ratio of the relaxation trace deteriorates and the inaccuracy in τ is of the same magnitude as the temperature inaccuracy. An estimate of these inaccuracies is shown in Figure 4.18 as error flags at the high temperature point of crystal No. 2. This is an extreme case. The signal-to-noise ratio is exceptionally good for such a high temperature owing to the long relaxation time. On the other hand, the Faraday rotation is relatively small due to the low Eu^{2+} content of sample No. 2.

A slight temperature dependence of the function $\varrho_F = f(\frac{H}{T})$ has been found for Eu^{2+} : CaF_2 between 1.5 °K and 4.2 °K. This is presumably due to the fact that J is not a perfectly good quantum number, a fact which also gave rise to a deviation of ϱ_F from the Brillouin curve. In this case, f would change with the relative population in the different levels of the $^8S_{\frac{7}{2}}$ multiplet. The overall splitting is 2 °K at the field employed and hence the populations change strongly between 1.5 °K and 4.2 °K. At 4.2 °K, the levels are almost equally populated and the function f should not change any more with increasing temperature. We checked the error introduced in the T-values for the unlikely case that f still changes with temperature above 4.2 °K at the same rate as between 1.5 °K and 4.2 °K. It was found that this error was below the measuring inaccuracy for all values.

In some cases, the temperature of the crystal between the λ-point and 4.2 °K was also measured by means of the Faraday rotation. This allowed a check of the reliability of the me-

thod by monitoring simultaneously helium vapour pressure and Faraday rotation. Once this reliability was established, the crystal was warmed up slower than the helium surface. In this way, no bubbles are formed in the lower part of the cryostat even above the λ-point. Such bubbles introduce a huge noise in the light signal which makes relaxation measurements impossible. They do not always appear and in some cases, we were able to avoid bubbling even when the crystal was at the same temperature as the helium surface. However, this seemed to be a matter of luck and was in no way systematically reproducible.

4. EXPERIMENTAL RESULTS

4.1 Cerium Ethylsulphate

4.1.1 Faraday Rotation

In order to make sure the crystal was properly aligned, the Faraday rotation was measured in each run. The Faraday rotation of CeES has been studied in detail by Becquerel, DeHaas and VanDenHandel (1938) using the green Hg-line (5460Å). In Figure 4.1, our measurements at 5460Å and 4350Å are plotted along with Becquerel's results as a function of H/T. The rotation at the highest fields used in our measurements have been normalized to fit the Becquerel values.

The very high rotation of CeES can be used to detect small temperature changes with great accuracy. The Faraday rotation at a given temperature is

$$\varrho = A \tanh \frac{\mu H}{kT}$$

with A = -430 deg mm^{-1}.

This gives for our crystals, which have a typical length of 8 mm :

at 2 kOe and 1.5 °K $\frac{\Delta\varrho}{\Delta T} = 400$ deg $(°K)^{-1}$

and at 2 kOe and 4.2 °K $\frac{\Delta\varrho}{\Delta T} = 50$ deg $(°K)^{-1}$

The angle of minimum light transmission can easily be determined with an accuracy of 1 deg. This corresponds to an accuracy in determining the temperature of 2 m°K at 1.5 °K and of 20 m°K at 4.2 °K.

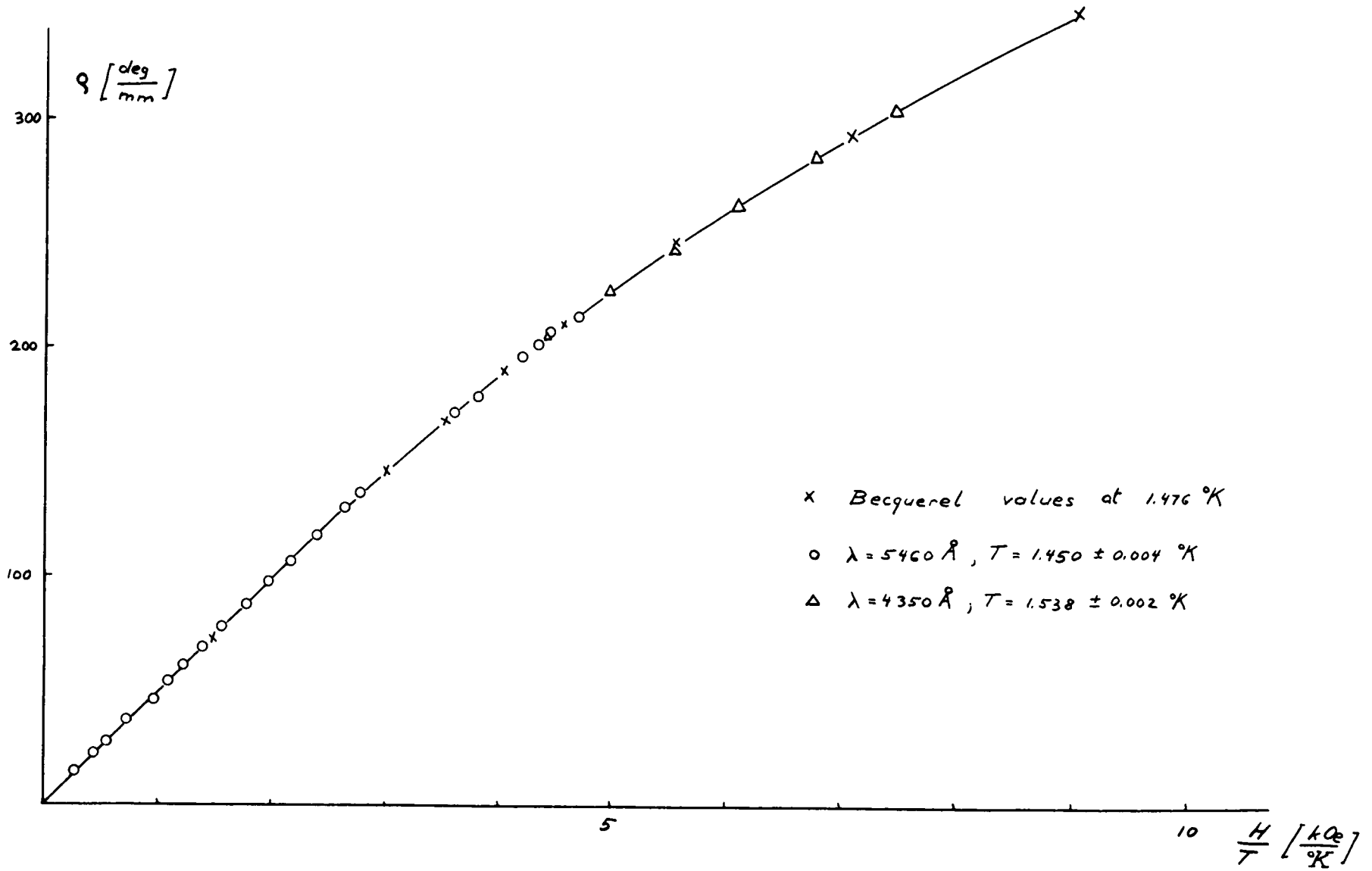

Figure 4.1 Paramagnetic Faraday rotation of CeES

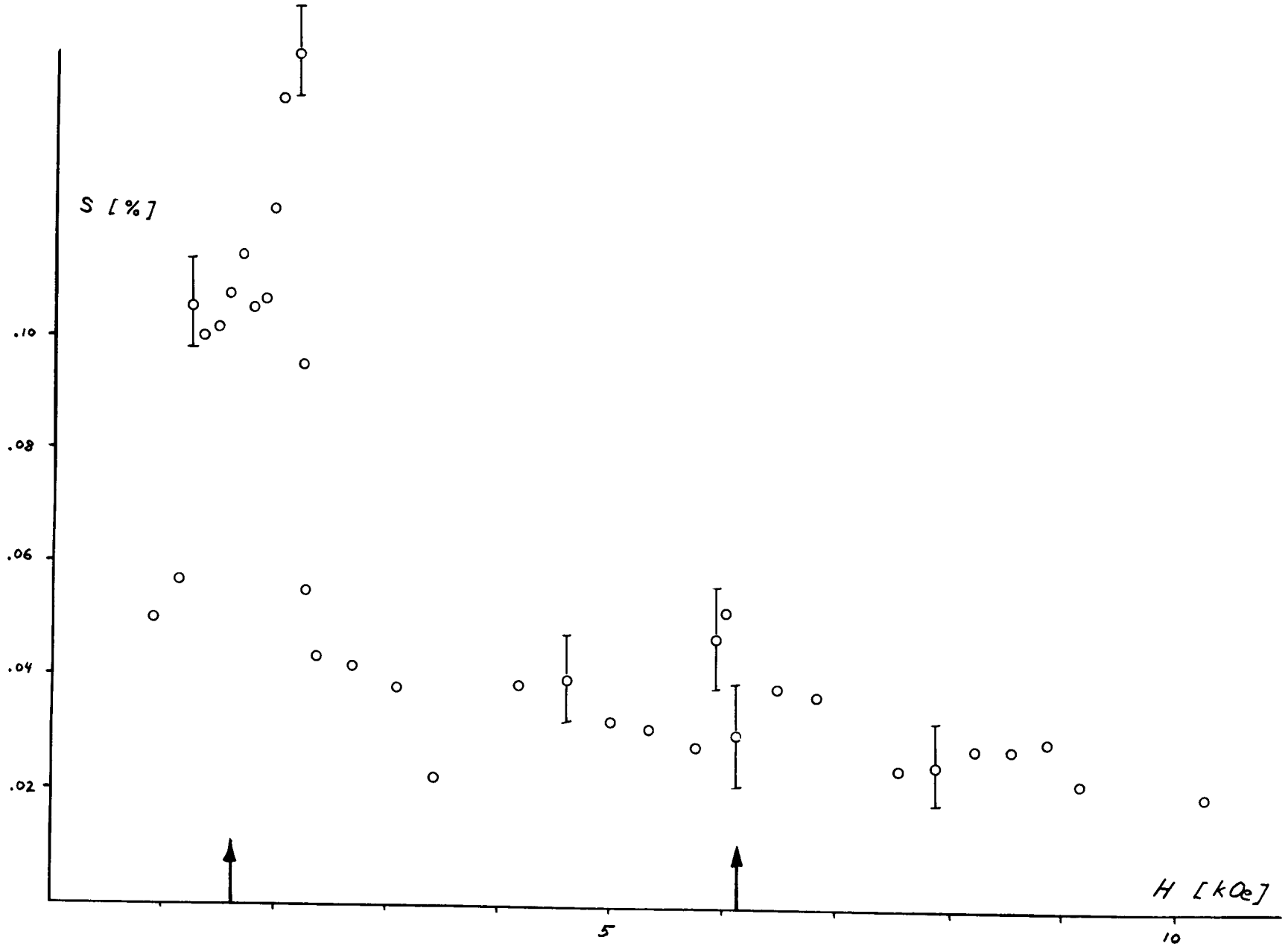

Figure 4.2 Saturation versus magnetic field in CeES

4.1.2 Resonance Spectrum

The paramagnetic resonance spectrum can be determined by measuring the saturation of the spin system due to a microwave field as a function of the DC magnetic field at a given temperature. If ϱ is the paramagnetic rotation in presence of the microwave field and ϱ_0 the rotation in absence of microwave, the saturation is given by equation (3.5) derived in chapter 3.2:

$$S = \frac{\varrho_0 - \varrho}{\varrho_0}$$

In CeES, the microwave power required to obtain a measurable change in rotation is very high and heats both the sample and the helium bath at the rate of about 2 m°K per second independent of magnetic field. This temperature change affects the paramagnetic Faraday rotation so strongly that it was not possible to obtain the paramagnetic saturation by means of Faraday rotation measurements.

It is, however, possible to pulse the microwave power with long enough repetition rates to keep the temperature of the liquid helium constant, while still attaining the same saturation values in the pulse as with DC-microwaves. The saturation values can be calculated from the height of the photomultiplier signal as described in chapter 3.2. The obtained saturation is plotted in Figure 4.2 as a function of magnetic field together with the expected resonance line centers corresponding to $g_{\parallel}(\frac{5}{2})=3.8$, $g_{\parallel}(\frac{1}{2})= 1.0$. A definite resonance is seen to coincide quite well with $g = 3.8$ and is identified as due to the satu-

ration of the lower doublet $|\pm\frac{5}{2}\rangle$.

The line width is about 1,000 gauss. This is 50% higher than the value given by Bogle, Cooke and Whitley (1951) measured by conventional paramagnetic resonance absorption.

Saturation of the higher doublet has not been observed with certainty. The few higher lying points around 6.5 kgauss coincide with the background within measuring accuracy.

The most remarkable feature of the spectrum is the almost constant "background saturation" attaining roughly 1/3 of the resonance saturation.

It does not seem possible to explain this broad, structureless background in terms of paramagnetic saturation.

A small crystal from the same growing solution was used to check the paramagnetic resonance spectrum with a conventional 34 Gc/s spectrometer. No microwave absorption was detected except for a few lines around g = 2 due to impurities. These could yield to some cross saturation, but this would show a marked field dependence characteristic of the impurity levels and can not give a broad structureless band.

It is, however, possible to explain the observed background as due to dielectric heating of the crystal lattice. Such a heating would affect both Kramers doublets and only one spin-temperature is required in this case to describe the whole spin system as opposed to paramagnetic resonance saturation of one doublet, where the spin temperatures in both doublets may be different.

Referring to chapter 2.3, we can identify system A as the

liquid helium surrounding the crystal, B as the crystal lattice and C as the spin system. The temperature increase ΔT_c in the spin system due to a long pulse is given be equation (2.47) where $W_c \approx 0$ off resonance.

$$\Delta T_c(\infty) = \frac{\tau_{AB}}{c_B} W_B$$

τ_{AB} is the time constant associated with the thermal exchange between crystal and helium-bath, c_B is the specific heat of the crystal lattice and W_B is the power fed to the lattice through dielectric heating.

We can estimate the energy ΔU dissipated in the crystal:

$$U = c_V \Delta T$$

Typical values for our crystal are

$$T = 2 \times 10^{-3}\,{}^\circ K$$

$$c_V = 5 \times 10^3 \text{ erg } ({}^\circ K)^{-1}$$

This gives for a pulse of 10 msec an average dissipation of 0.1 mW.

If one uses the Kapitza resistance picture, assuming that spin and lattice are in equilibrium at all times, equation (2.61) gives the temperature rise after a long pulse

$$\Delta T(\infty) = \frac{R_k W}{S}$$

With $R_k \approx \frac{10 \text{ cm}^2 \text{deg sec}}{\text{joules}}$ and $S \approx 0.5 \text{ cm}^2$ the power needed to create the above temperature rise is

$$W = \frac{S\,\Delta T}{R_k} \approx 0.1 \text{ Watt} .$$

Two experimental observations support the idea of spin heating via the lattice:

a) As will be discussed in more detail below, the lattice-bath relaxation time increases by approximately a factor of 15 in passing from HeII to HeI. From equation (2.47) follows that $\Delta T_s(\infty)$ should increase by the same amount. The microwave pulses available were too short to determine $\Delta T_s(\infty)$ accurately above the λ-point. Extrapolation of the short heating curves to $t \rightarrow \infty$ shows, however, a minimum increase of $\Delta T_s(\infty)$ by a factor 10 over the value below the λ-point.

b) Further evidence of a strong heat dissipation in the crystal due to microwave radiation is given by the fact that the bath temperature increases under the influence of DC-microwave by an amount of about 10 m°K off resonance. This temperature increase is very slow, initially about 2 m°K per second and does not affect the pulsed measurements. The time constant associated with this slow temperature increase is a measure for the energy transport through the helium surface due to evaporation and is thus a function of the pumping speed. This slow heating effect can be clearly observed on the oil manometer as an increase in the helium vapour-pressure.

4.1.3 Relaxation Times

Figure 4.3 shows the dependence of the observed relaxation time τ on the magnetic field at 1.48°K. Figure 4.4 shows the temperature dependence of τ from 1.4 to 4.2°K at the resonance field of the lower doublet. A sharp increase in τ is observed in passing from the HeII region through the λ-point. Above

this point, the relaxation traces can be resolved into two time constants. Both stay approximately constant from 2.2°K to 4.2°K. It has to be pointed out that the interpretation of the measured relaxation traces as composed of two exponentials is not quite unique. Some distribution of relaxation times would probably fit the data as well.

Also in Figure 4.4, a point is shown which represents the relaxation time of the crystal surrounded by helium gas at 4.2°K. τ is about three times smaller than the smaller of the two values which are found when the crystal is immersed in liquid helium at the same temperature. Only one relaxation time is found indicating that the relaxation process is exponential.

Figure 4.5 shows the temperature dependence of the relaxation time below the λ-point for two different field values, together with some values obtained from non-resonant dispersion-absorption measurements by Van den Broek and Van der Marel (1963). The latter seem to exhibit a slightly stronger temperature dependence at low magnetic fields than our measurements. In all cases, our relaxation traces show a very good exponential behaviour from 1.4°K up to the sudden rise at the λ-point.

Discontinuities of the same type as those at the λ-point have been observed at 1.5°K, when the liquid helium level was allowed to drop below the crystal.

With small microwave power, the crystal stays at the same temperature and exhibits the same relaxation behaviour as when it is immersed in HeII. As soon as the microwave power exceeds

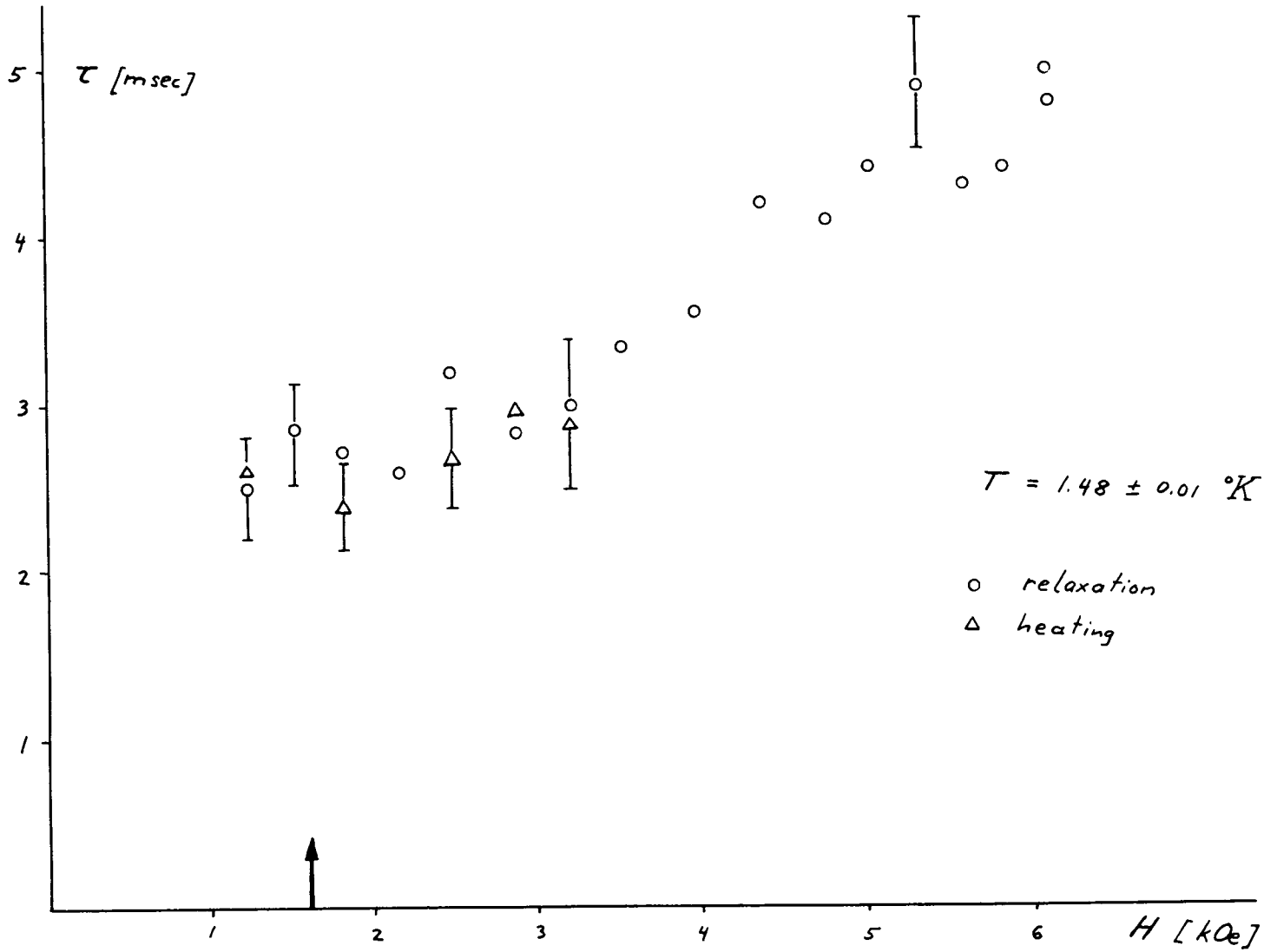

Figure 4.3 Relaxation time in CeES: Magnetic field dependence

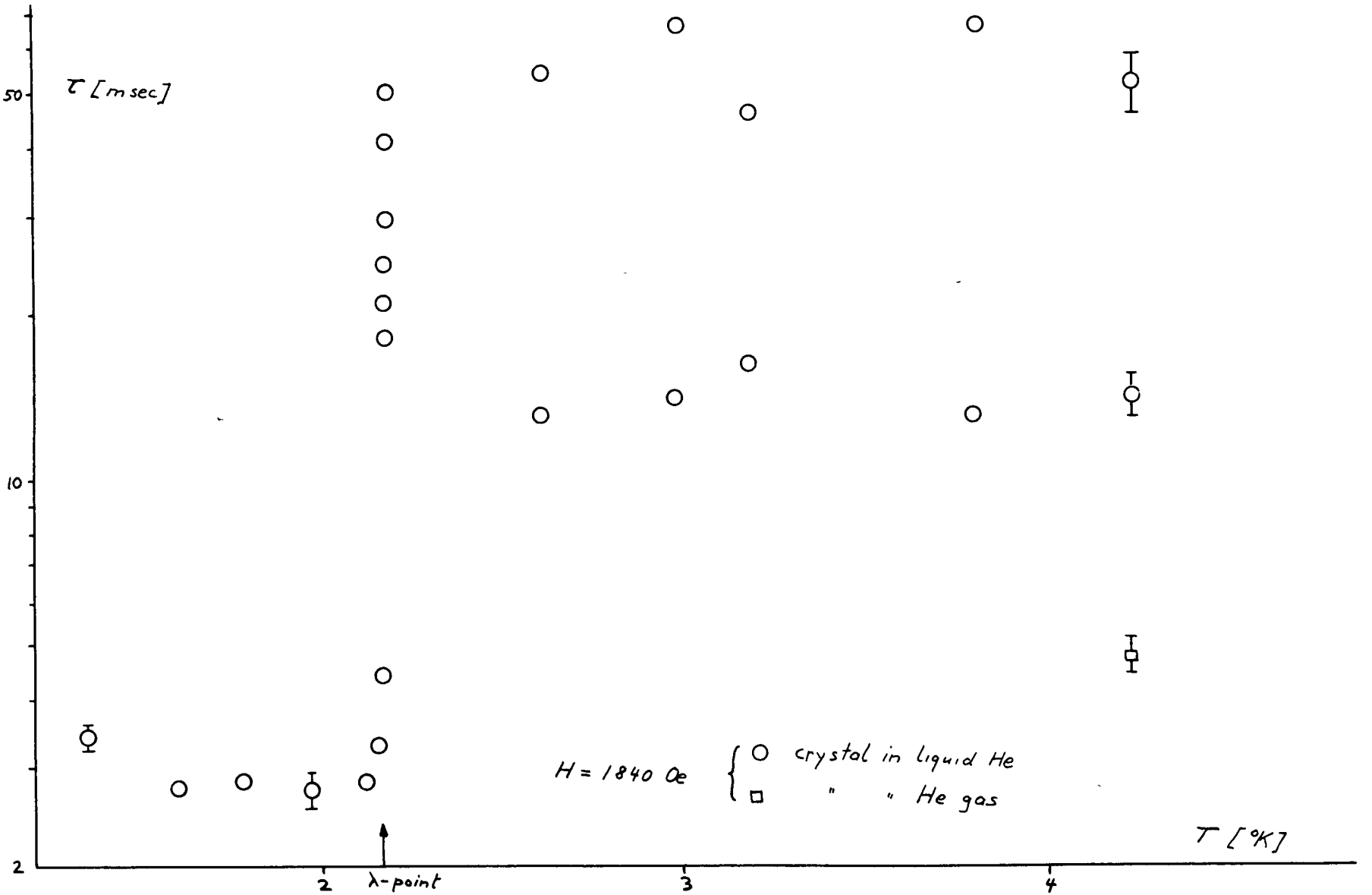

Figure 4.4 Relaxation time in CeES: Temperature dependence

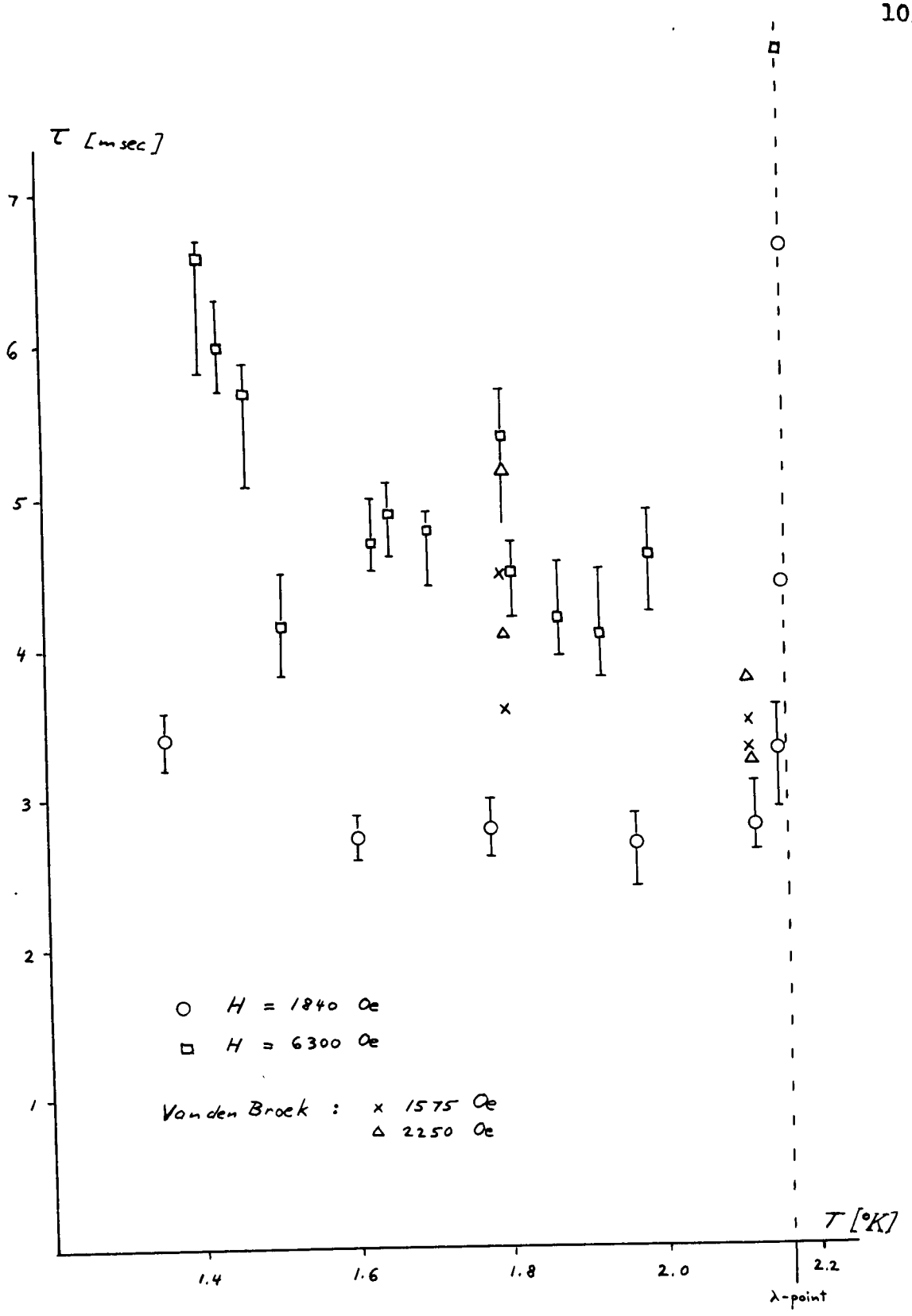

Figure 4.5 Relaxation time in CeES: Temperature dependence below the λ-point

a well defined threshold value, a very sharp increase in τ is observed, very much similar to the one seen in passing through the λ-point. The effect is reversible. The fast relaxation is again established, if the average microwave power fed into the cavity is decreased. This can be done by decreasing either one of pulse power, repetition rate or pulse length. The threshold value of the average power seems to decrease with time in one single run, i.e. with increasing distance between the crystal and the liquid helium level.

Table I

Relaxation time discontinuities below the λ-point

Observation No.	MW pulse rep. rate msec	MW pulse-length msec	MW-power attenuation db	Average MW power at discontinuity in db (0 db=full DC-MW)
1	100	8	0	-11
2	200	8	0	-14
3	200	7 - 20	3.7	(-13.7)-(-18.2)
4	250	8	0.8 - 1.7	(-15.7)-(-16.7)
5	250	40	11.0 - 11.9	19.0 - 19.9
6	320	40	8.4 - 8.8	17.5 - 17.9

In Table 4-I, the microwave data for the different discontinuities observed during the same run are assembled and the corresponding relaxation times are plotted in Figure 4.5 as a function of average microwave power (in db attenuation from full DC-microwave power).

An attempt has been made to detect any change of τ with pulse length or microwave power, while the crystal was immersed in liquid helium. A variation of both microwave pulse power and pulse length by a factor 10 did not produce any change in τ below the λ-point. At 4.2 °K, a change in power by 6 db and a change in pulse length by a factor 10 gave the same relaxation times. Due to generally weak signals, it was impossible to extend these rather narrow limits and still get measurable traces.

For several traces, the time constant for the approach to saturation, which is better called the heating time constant, has been measured. Within the accuracy of our measurements, this time constant is the same as the corresponding τ for relaxation. This is in agreement with the solution of the rate equations treated in chapter 2.3.

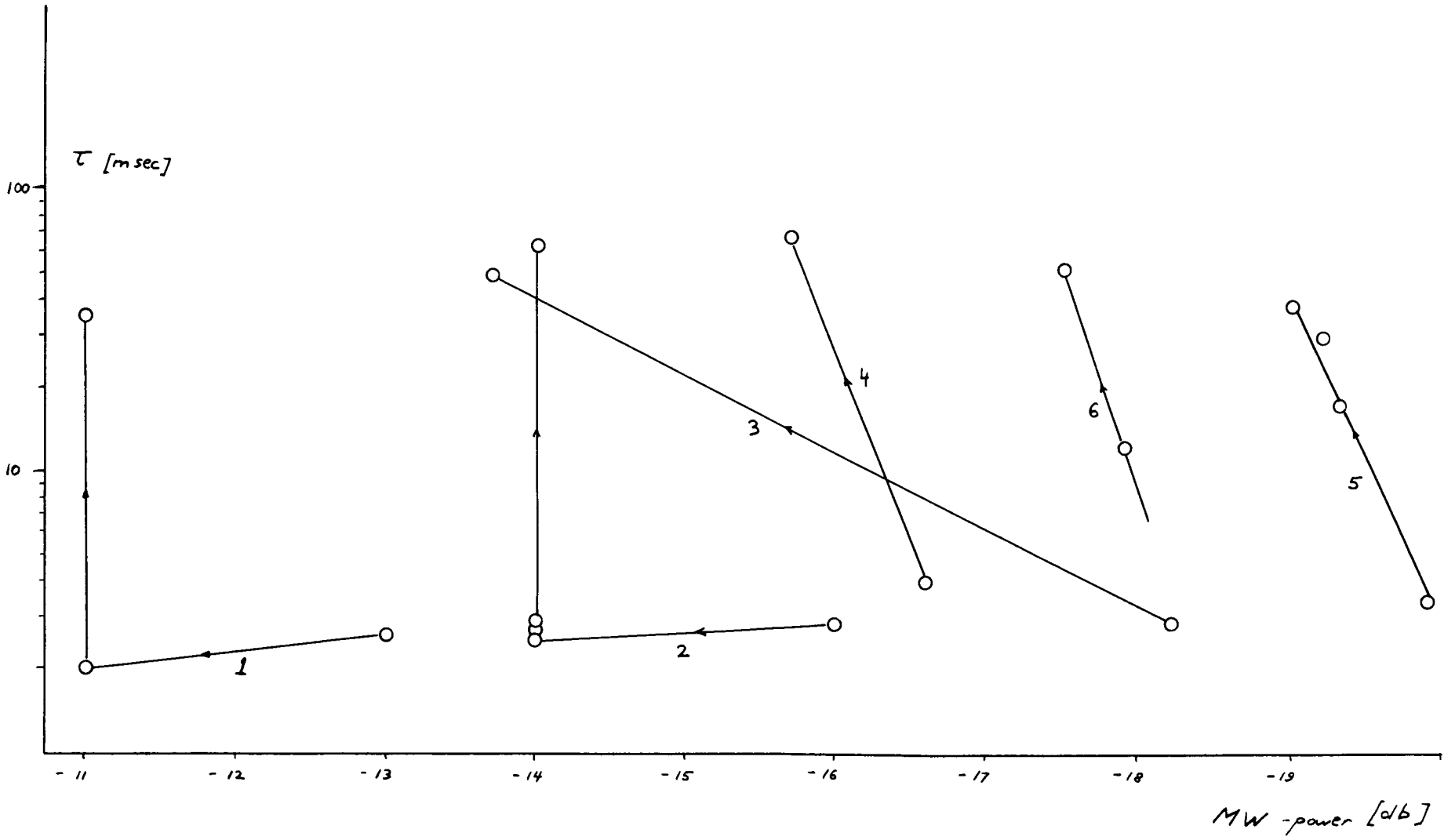

Figure 4.6 Relaxation time discontinuities below the λ-point

4.1.4. Discussion

a) Thermodynamical model

In order to understand the relaxation behaviour in CeES the model shown in Figure 4.7 is used to describe the crystal and its surroundings. The basic assumption is that there are at most four systems in series, and that each of these systems is in internal equilibrium described by a temperature.

T_1 is the usual spin-lattice relaxation time, i.e. the time constant measured if the phonon system of the crystal which we call the lattice is a perfect heat reservoir remaining always at the bath temperature.

τ_f is the time constant associated with the spreading out of the excitation from the phonons "on speaking terms" (Van Vleck, 1941) to the other lattice modes. τ_{lH} and τ_{pH} are time constants associated with the spatial diffusion of the lattice excitation away from the crystal. This time may be quite different for the phonon modes on speaking terms with the spins, for which the lattice is "opaque", than for the other lattice modes, since the modes in the vicinity of the paramagnetic resonance line may have a very much smaller group velocity (Persico et al, 1963). The phonons interacting with the spins are effectively imprisoned by the paramagnetic ions. This problem has been considered in great detail by Giordmaine and Nash (1965) and found to be analogous to the imprisonment of resonant photons in gases. W_s and W_l are the energies fed to the spin and the lattice system respectively during a microwave pulse. The

hot phonon system consists of the excess number of phonons over the equilibrium value at the lattice temperature.

We have now to consider two different heating and relaxation processes, depending on whether the magnetic field is at the resonance value ($W_s > W_1$) or off resonance ($W_s = 0$). These considerations will show that the model of Figure 4.7 can be simplified by elimination of the hot phonon system.

At resonance, the two doublets of the spin system are not in equilibrium, the lower doublet being saturated and therefore at a higher temperature than the upper doublet. It relaxes via an Orbach process, thus forming two phonon spikes around Δ and $\Delta+\delta$. The hot phonon system would, therefore, contain a negative occupation number of phonons in a band around Δ and a positive number of the same magnitude in a band around $\Delta+\delta$. T_p is determined by the difference of the two occupation numbers and $T_p = T_\ell$ for vanishing difference, i.e. for the case, that no hot phonons are produced. The bottlenecked Orbach process has been studied in a similar way by Stoneham (1965).

The relaxation will proceed via crystal lattice through frequency diffusion, since τ_{pH} is long due to resonant reabsorption of the hot phonons as pointed out earlier. Knowing that T_1 is very short, we assume $T_s \approx T_p$ and equation (2.43) gives for the observed relaxation time

$$\tau = \tau_f + \frac{C_s}{C_\ell}\tau_{\ell H} \approx \frac{C_s}{C_\ell}\tau_{\ell H}$$

since $C_s \gg C_\ell$ and $\tau_f \ll \tau$.

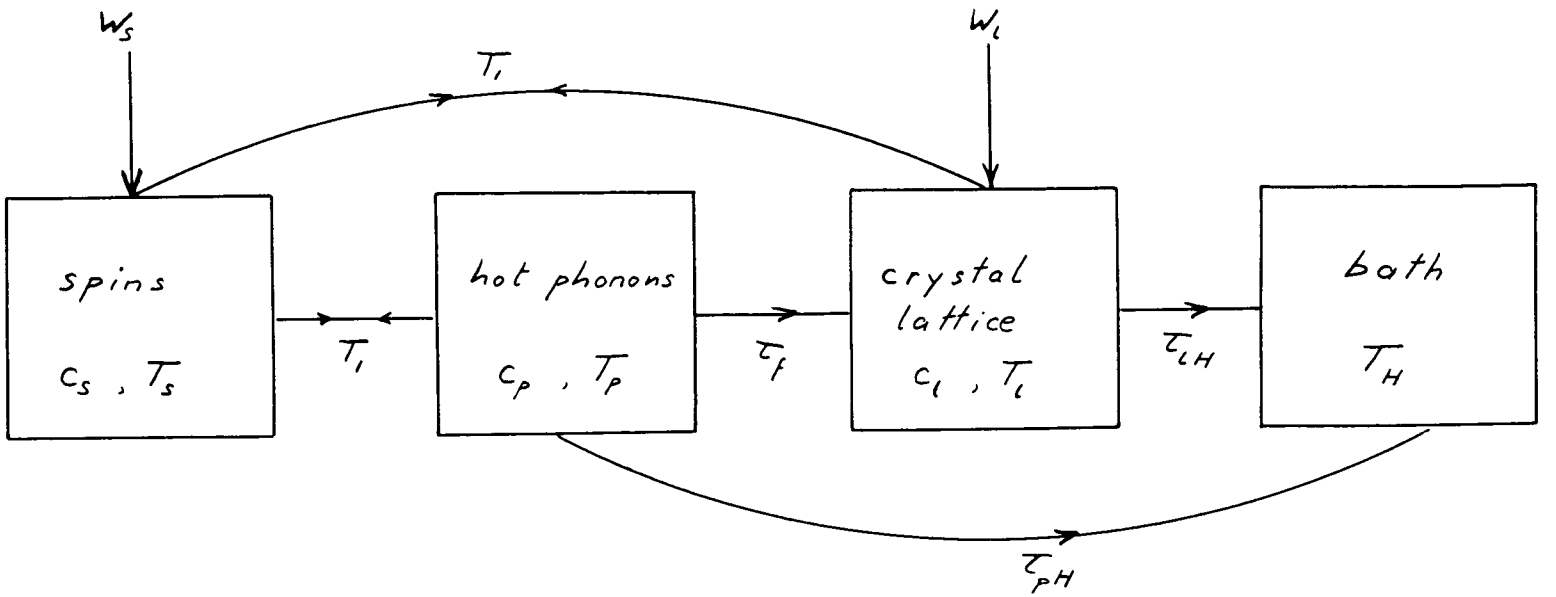

Figure 4.7 Thermodynamical model for CeES-He system

c_s here is the specific heat of the doublet which is at resonance.

$$C_s = \frac{dU_s}{dT_s} = -\frac{d}{dT_s}\left\{\frac{\delta}{2}(N_a - N_b)\right\} \approx \frac{Nk}{4}\left(\frac{\delta}{kT_s}\right)^2$$

With $N = 1.6 \times 10^{21}$ spins cm^{-3} (lower doublet) $\delta = 0.4\,^\circ K$ and $T_s = 1.5\,^\circ K$, we have for a crystal of 0.05 cm^3

$$c_s = 2 \times 10^2 \text{ erg}(^\circ K)^{-1}$$

Off resonance, the hot phonon system cannot exist, since no part of the spin system is saturated. The population of all four levels are rearranged by means of the spin-lattice interaction to follow the lattice temperature. This latter is increased by lattice heating during the microwave pulse.

The relaxation time is given by

$$\tau = T_1 + \frac{c_s}{c_l}\tau_{lH} \approx \frac{c_s}{c_l}\tau_{lH}$$

as before. But now, c_s has to be taken as the specific heat of the whole spin system, not only the doublet which is being saturated as in the previous case. c_s can be taken from the specific heat measurements of Meyer and Smith (1959) and is at $1.5\,^\circ K$ for our crystal

$$c_s = 2 \times 10^3 \text{ erg}(^\circ K)^{-1}$$

This is ten times larger than the value used previously for the field on resonance. We expect, therefore, a distinctly different value of the relaxation time at resonance than off resonance.

The experimental results show, however, a smooth field dependence of τ. This indicates that the energy distribution in the spin and lattice system is the same for heating as for saturation and that in no case are hot phonons produced. This conclusion is confirmed by experiments of Dransfeld (1958), Shiren and Tucker (1959) and Faughnan and Strandberg (1961). These authors have tried without success to detect hot phonons produced in bottleneck situations.

We conclude, therefore, from the insensitivity of the relaxation times to magnetic field, that at all times, all four levels of the spin systems as well as the systems of lattice oscillators are in equilibrium, i.e. determined by a single temperature and the relaxation time for the spin system via lattice to the bath is given by

$$\tau = \frac{C_s}{C_l} \tau_{lH}$$

where τ_{lH} is the time constant for absorption of a lattice phonon by the bath.

The relaxation problem is now reduced to the problem of spatial diffusion of thermal energy through the crystal lattice, across the boundary and into the surrounding helium. The observed strong dependence of τ on the environment suggests that the limiting factor in this energy exchange is not the spatial diffusion in the crystal.

Cracks in the crystal, into which HeII might penetrate, are able to explain only the discontinuities in relaxation time at or below the λ-point. In that region superfluid hel-

ium might shorten out a thermal diffusion bottleneck inside the crystal. However, cracks cannot explain the decrease of the relaxation time in gaseous helium at 4.2°K to nearly the value in HeII.

We suggest, therefore, that the limiting factor in thermal exchange is either the boundary resistance between the crystal and the surrounding helium bath or the limited diffusion in the helium itself. This is supported by the fact that κ_{Ce}, the thermal diffusion constant in CeES, is orders of magnitude higher than the diffusion constants of helium gas or HeI.

b) τ below the λ-point

Since the thermal conductivity of HeII is abnormally high (the diffusion constant κ is of the order of 10^3 $cm^2 sec^{-1}$), we can regard the temperature in the helium bath below the λ-point as constant. We have, therefore, the situation treated in chapter 2.3 with the Kapitza boundary resistance as limiting factor. The relaxation in this case is exponential and τ_K is independent of pulse length or power, as confirmed by our measurements.

The observed time constant τ_K is according to equation (2.62)

$$\tau_K = R_K \rho c_{cr} \left(\frac{V}{S}\right)$$

It should be the same for heating and relaxation, which is consistent with our experimental results.

Equation (2.62) can be used to determine the Kapitza boun-

dary resistance R_K from our measured relaxation times, if the specific heat is known. We have calculated c_{cr} as the sum of the Schottky specific heat c_s and the lattice specific heat c_l.

c_s has been calculated from the partition function Z by means of the formula

$$\frac{C_s}{R} = T \frac{\partial^2}{\partial T^2}\left(T \cdot \ln Z\right)$$

where $R = 1.987$ cal(Mole °K)$^{-1}$, $Z = \sum_i \exp(-\frac{\Delta_i}{kT})$ and the sum is taken over all four populated levels with Δ_i determined by $g_{\parallel}(\frac{5}{2}) = 3.8$, $g_{\parallel}(\frac{1}{2}) = 1.0$ and $\Delta = 6.95$ °K.

c_l has been taken as the difference between the experimentally determined total specific heat in zero field as measured by Meyer and Smith (1959) and the theoretical Schottky value at zero field. c_l gives only a small contribution to c_{cr} at liquid helium temperatures.

Figure 4.8 shows the temperature dependence of c_{cr}/R for two different fields and Figure 4.9 is a plot of the field dependence of c_{cr}/R at two different temperatures. The Kapitza resistance R_K has been obtained from these values for c_{cr} and from the experimental relaxation times. The results are plotted in Figure 4.10 for the temperature dependence and in Figure 4.11 for the field dependence. The obtained R_K can be described by the relation

$$R_K = AT^{-n} \frac{\text{cm}^2\text{degsec}}{\text{joule}}$$

with $A = 30$ and $n = 2.4$. R_K is independent of field. The

maximum deviation of R_K from the mean value in Figure 4.11 is 10%. The accuracy of the values is limited by the inaccuracy of the relaxation time measurements. The obtained results agree quite well with known values from other substances.

c) τ above the λ-point

Non-exponential relaxation above the λ-point suggests that spatial conduction rather than transfer through the interface is the limiting process. This is also supported by the following argument:

The resistance due to a boundary discontinuity can be regarded as an acoustic mismatch for the phonons incident on the boundary. The acoustic impedance Z_a in a material is given by the product of density ρ and velocity of sound v

$$Z_a = \rho v$$

The transmission coefficient T_{12} at a discontinuity interface is given in analogy to transmission line theory by

$$T_{12} = \frac{2Z_2}{Z_2 + Z_1}$$

The acoustic impedances for the different media are

CeES:	$Z_a = 3.7 \times 10^5$	gcm^{-2}	sec^{-1}
HeII, 1.4°K:	$Z_a = 3.4 \times 10^3$	"	"
HeI, 4.2°K:	$Z_a = 2.2 \times 10^3$	"	"
He gas:	$Z_a \approx 10^2$	"	"

which gives the following transmission coefficients:

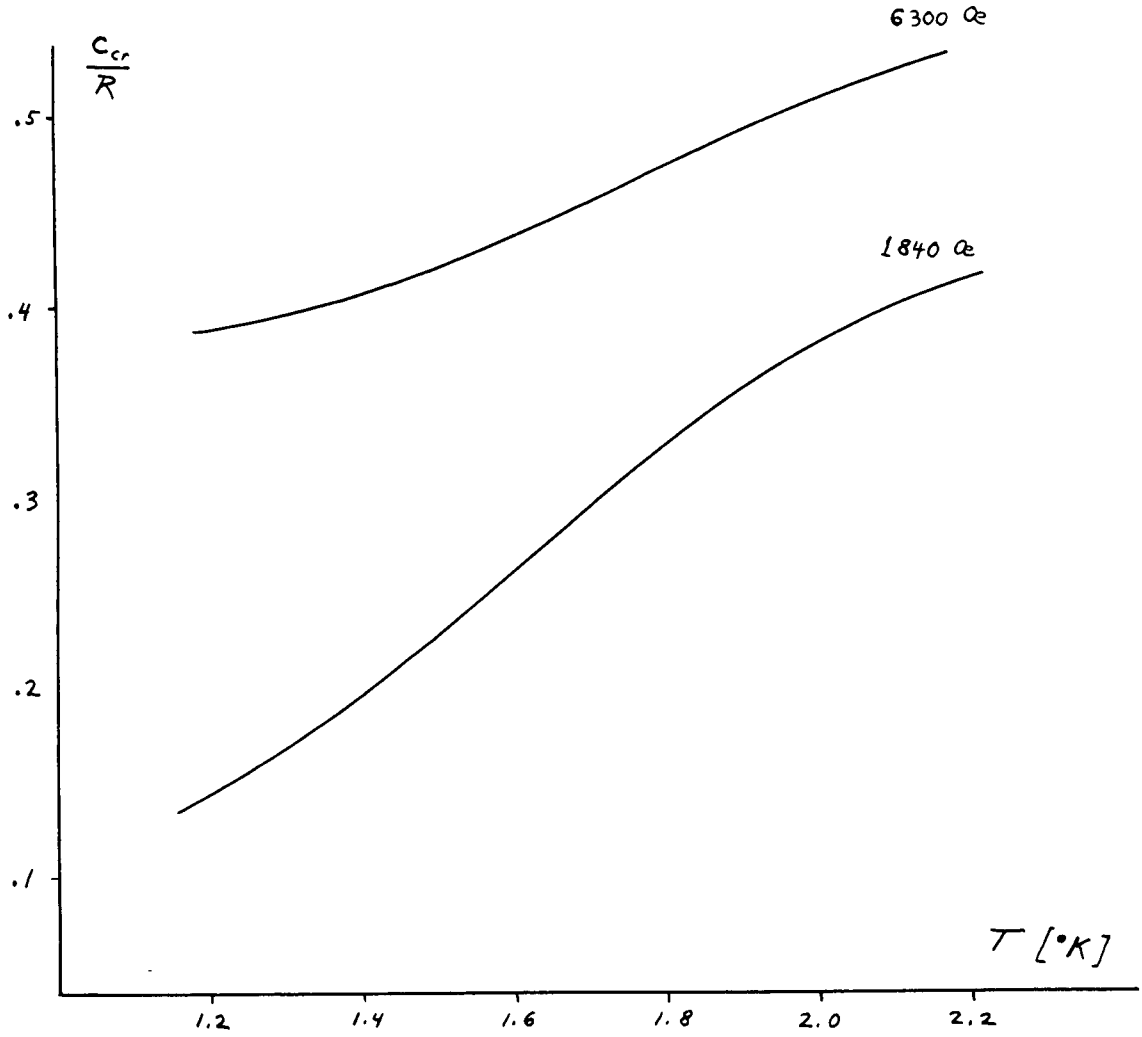

Figure 4.8 Specific heat of CeES as a function of temperature

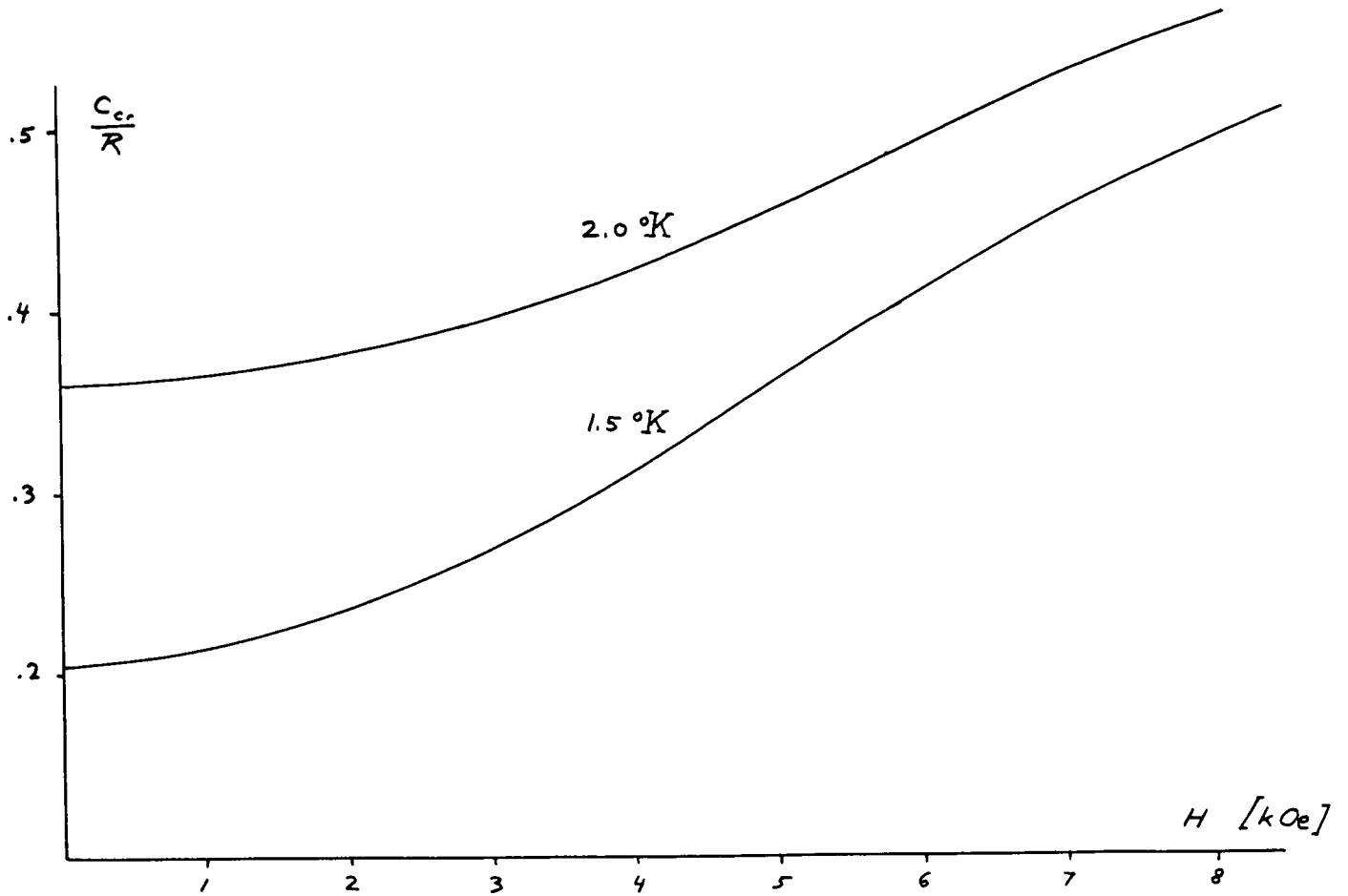

Figure 4.9 Specific heat of CeES as a function of magnetic field

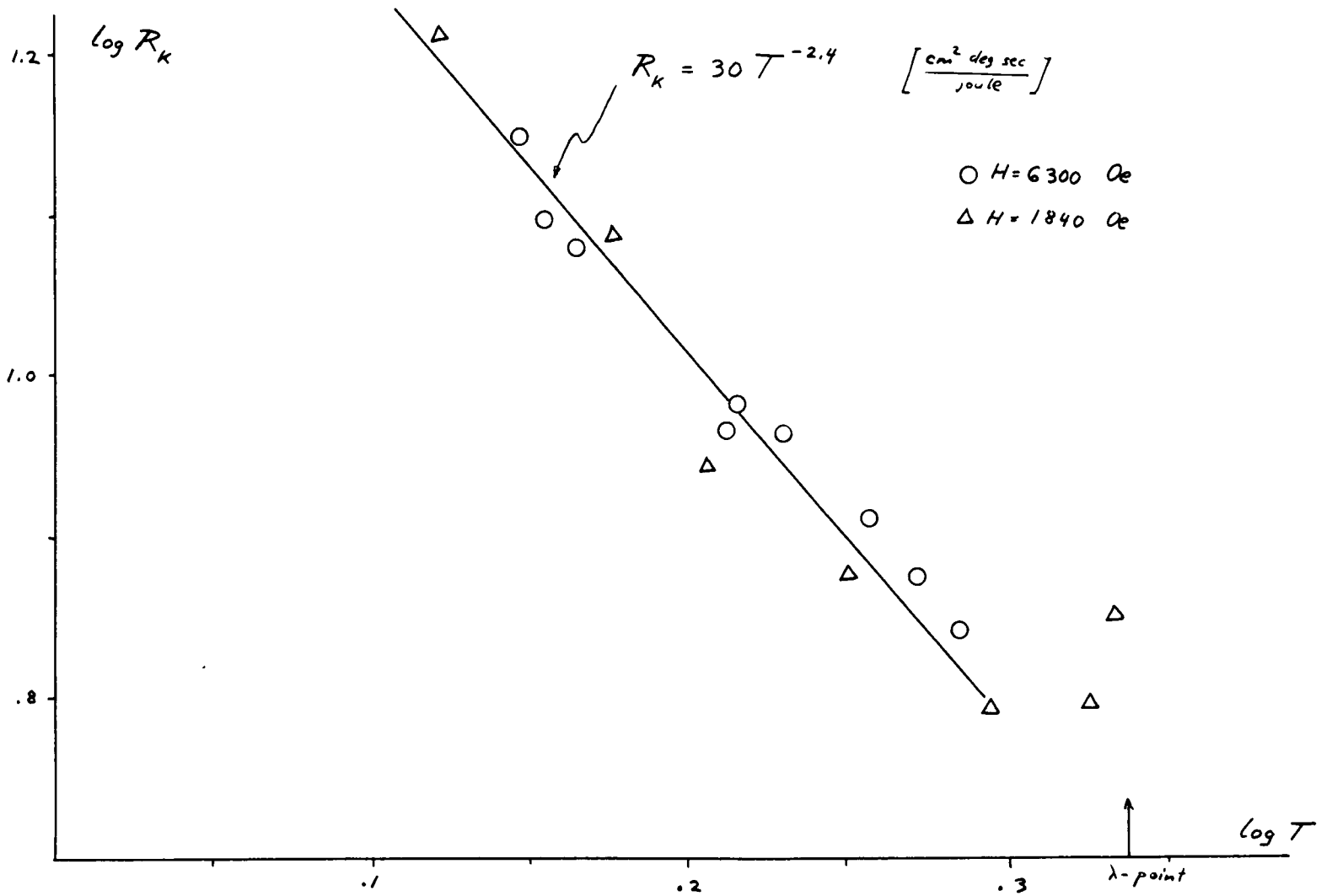

Figure 4.10 Kapitza resistance of CeES-HeII: Temperature dependence

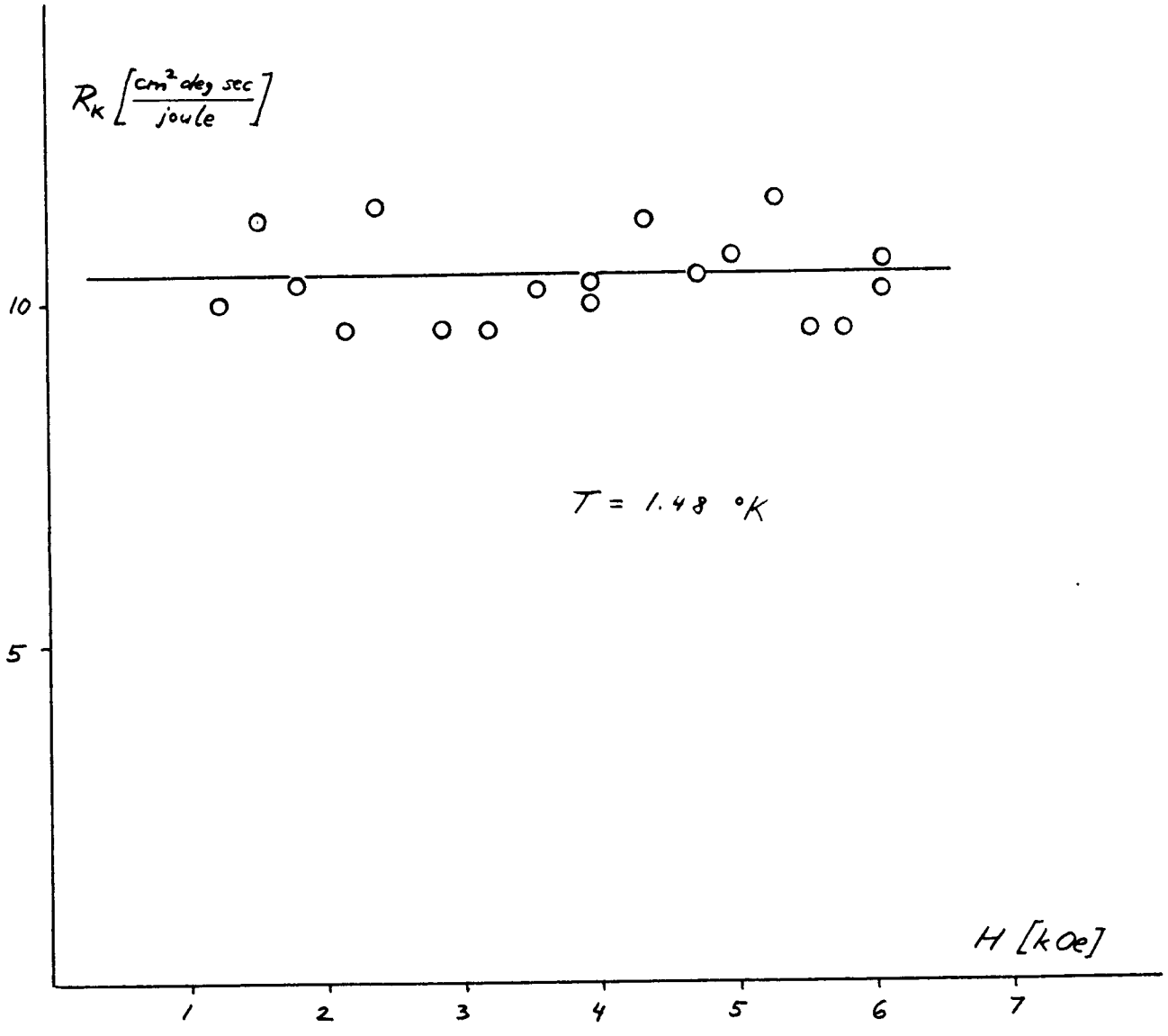

Figure 4.11 Kapitza resistance of CeES-HeII: Field dependence

CeEs HeI : $T_{12} = 1.2 \times 10^{-2}$

CeES He gas : $T_{12} = 5.5 \times 10^{-4}$

From these transmission coefficients it is seen that the boundary resistance and therefore the relaxation time should be considerably longer for the crystal-He gas system as compared to the crystal-liquid He system. This is in disagreement with the measurements at 4.2 °K which show a faster relaxation for the crystal-He gas system.

It has been shown by Mills (1964) that the transmission can be considerably enhanced in the presence of a porous layer on the surface of the crystal, which will serve as an impedance transformer. This effect is certainly present in the ethylsulphates, which dehydrate very easily. It would, however, only reduce the magnitude for the boundary resistance without changing the sign of $(T_{Ce \rightarrow HeI}) - (T_{Ce \rightarrow He\ gas})$ and therefore cannot give a smaller boundary resistance for the CeES - He gas interface as compared to the CeES - HeI boundary.

The spatial diffusion is governed by the diffusion equation

$$\frac{dT}{dt} = \kappa \nabla^2 T$$

The relevant parameter is the diffusion constant

$$\kappa = \frac{K}{\rho c_v}$$

where K is the thermal conductivity.

The values for κ are:

He gas	:	$\kappa = 9 \times 10^{-2} \ \frac{cm^2}{sec}$
HeI	:	$\kappa = 4.5 \times 10^{-4} \ \frac{cm^2}{sec}$
CeES	:	$\kappa \approx 70 \ \frac{cm^2}{sec}$

For the simplest case of linear heat flow in $x > 0$, a possible solution of the diffusion equation is

$$T\ (x,t) = A\ f(x)$$

with $f(x)$ satisfying the equation

$$\frac{d^2f}{dx^2} + \frac{A}{\kappa}\ f(x) = 0\ .$$

In this case, the thermal relaxation time is given by $\tau = \frac{1}{\kappa}$. In general, the boundary conditions are not harmonic and the relaxation is not exponential but has some complicated time dependence. In all cases, however, the thermal relaxation is related to the diffusion constant in such a way that a higher κ means faster relaxation. The slow relaxation in HeI can therefore be attributed to a small value of κ .

In He gas, κ is considerably higher and at the same time the mismatch at the boundary is increased, such that the boundary resistance could again play a role. This would be indicated by a single exponential. The relaxation traces obtained at 4.2°K in the gas are not good enough to decide this question definitely.

An attempt to draw quantitative conclusions from the ex-

perimental relaxation behaviour would involve the solution of the diffusion equation for the crystal-bath system, taking into account the boundary resistance. The unknown or not well known parameters of this solution would have to be adjusted in order to fit the experimental relaxation traces.

The effort involved in such calculations is considerable, even for a rather simplified model. No general results are obtained and numerical methods have to be introduced at an early stage of the calculation. Moreover, it is doubtful if a unique fit to the experimental data could be obtained even from a solution containing all relevant parameters, since too many are unknown within a wide range of values.

The calculations have, therefore, not been carried through.

A few words might be said with regard to the discontinuities in τ below the λ-point when the liquid HeII level was below the crystal. All the parts in the cryostat with a temperature below the λ-point are covered by a film of liquid HeII. The superfluid property of HeII allows a considerable amount of heat to be conducted and therefore keeps the crystal at the temperature of the bulk liquid. If, however, the heat pulses are too big such that the thermal flow in the film exceeds a critical value, the film is not able to conduct the heat away because the thermal behaviour of the film becomes that of a normal liquid and the relaxation behaviour is the same as that observed in HeI.

d) Application to PrES

The relaxation behaviour of PrES shows effects similar to the ones observed in CeES. We have, therefore, re-examined the relaxation times obtained in PrES.

PrES has a very strong spin-lattice interaction and its spin-lattice relaxation times are very short. Larson and Jeffries (1966) have measured T_1 in dilute Pr:LaES and find a bottlenecked direct process and an Orbach process via the excited singlet at 12 cm^{-1}. T_1 is below 100 μsec for temperatures down to 1.4 °K.

The observed relaxation times in the concentrated PrES are much longer and exhibit a completely different temperature and field dependence than would be expected from spin-lattice relaxation theory (Griffiths, 1965). A discontinuity was observed at the λ-point very similar to the one in CeES. Griffiths suggested that above the λ-point, the limited heat conductivity of the surrounding helium is responsible for the bottleneck. Below the λ-point, Griffiths proposed an explanation of the observed magnetic field dependence using the thermal conductivity of the crystal which is strongly field dependent as a result of phonon scattering by the paramagnetic ions.

We would like to show that temperature and field dependence of the relaxation times in PrES below the λ-point can also be explained as arising from the Kapitza boundary resistance. We believe this explanation to be more likely, since spatial conduction leads to non-exponential time dependence and in both cases (CeES and PrES) no deviation from the exponential behaviour

of the relaxation traces below the λ-point has been observed.

As in the case of cerium, we calculate the Kapitza resistance R_K from the formula

$$R_K = \frac{\tau_K}{\varrho\, c_{cr}} \left(\frac{S}{V}\right)$$

The specific heat of PrES between 1.4°K and 2.1°K is the sum of three contributions: the lattice specific heat, which is close to the specific heat of NdES; the low temperature tail of the Schottky anomaly arising from the excited singlet state at 16°K and the high temperature tail of the Schottky peak arising from the ground state splitting. The two former are independent of magnetic field, while the latter is very sensitive to an external magnetic field. Such a field increases the splitting of the ground state and shifts the Schottky peak towards higher temperatures, the specific heat increases strongly with magnetic field as shown in Figure 4.12. A similar increase in τ is observed, leaving the Kapitza resistance field-independent. Just below the λ-point, the specific heat is mainly due to the higher Schottky peak which is practically field independent. In fact, τ loses its field dependence also at 2.15°K (Griffiths, 1965).

Figure 4.13 shows R_K as a function of H, as calculated from the τ-values in Figure 3 of Griffiths and Glättli (1965). There seems to be a weak field dependence in R_K. This effect is not necessarily genuine and might be due to a slight error in calculating c_{cr}. There is, in fact, an uncertainty about

the values of c_{cr} since neither the actual distribution of the crystal field distortions nor an accurate g-value are known for PrES. In accordance with the structureless flat resonance found by Griffiths, we have assumed a rectangular line shape in the calculations for c_{cr}.

Figure 4.14 shows R_K at 6 kgauss as a function of temperature. Reasonably close agreement with the values for CeES is obtained. This is to be expected, since the acoustic mismatch should not change much from one ES to the other.

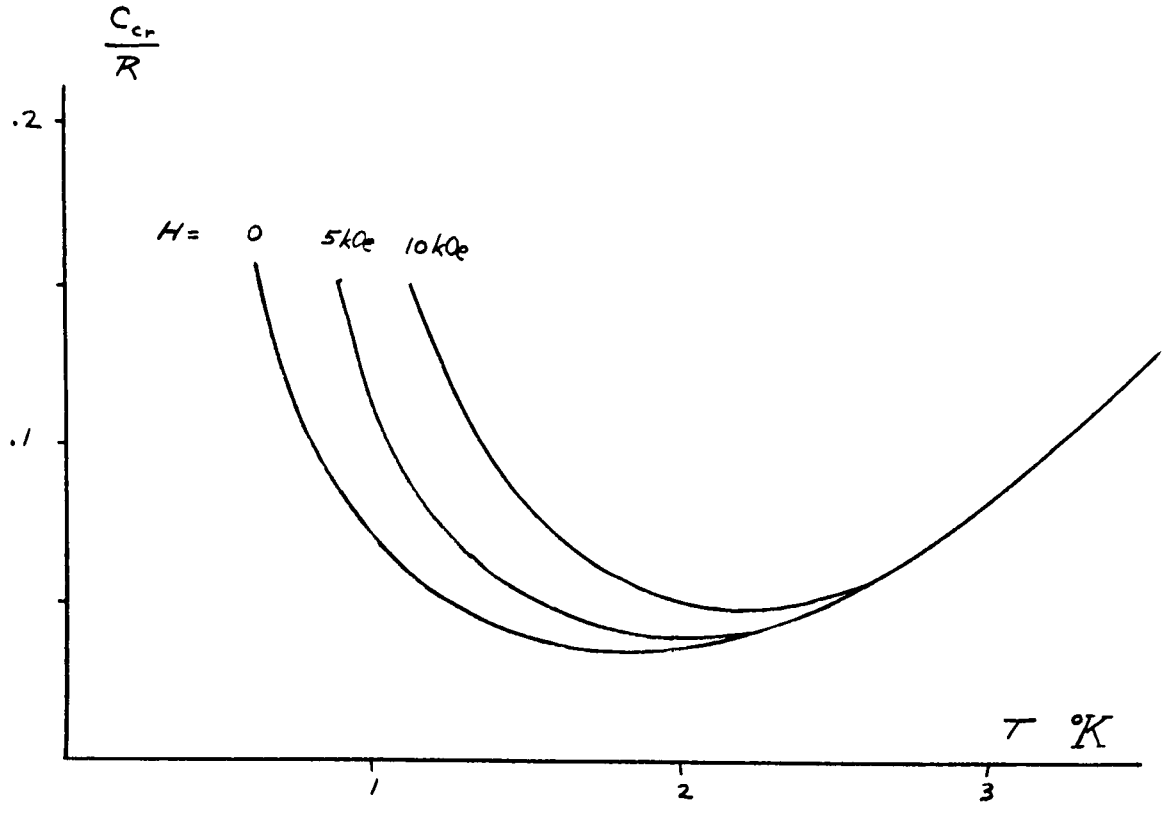

Figure 4.12 Specific heat of PrES as a function of temperature

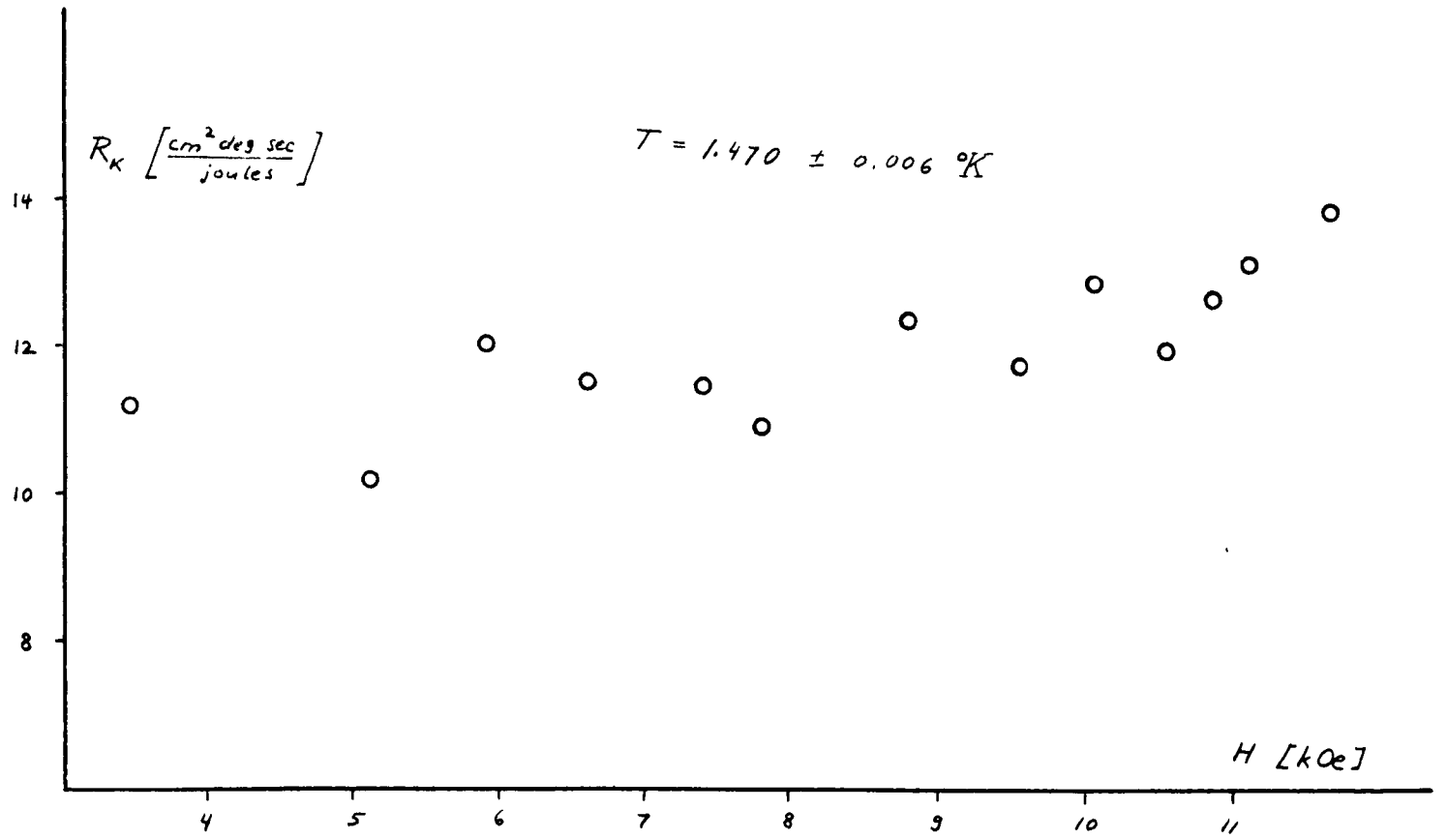

Figure 4.13 Kapitza resistance of PrES-HeII: Field dependence

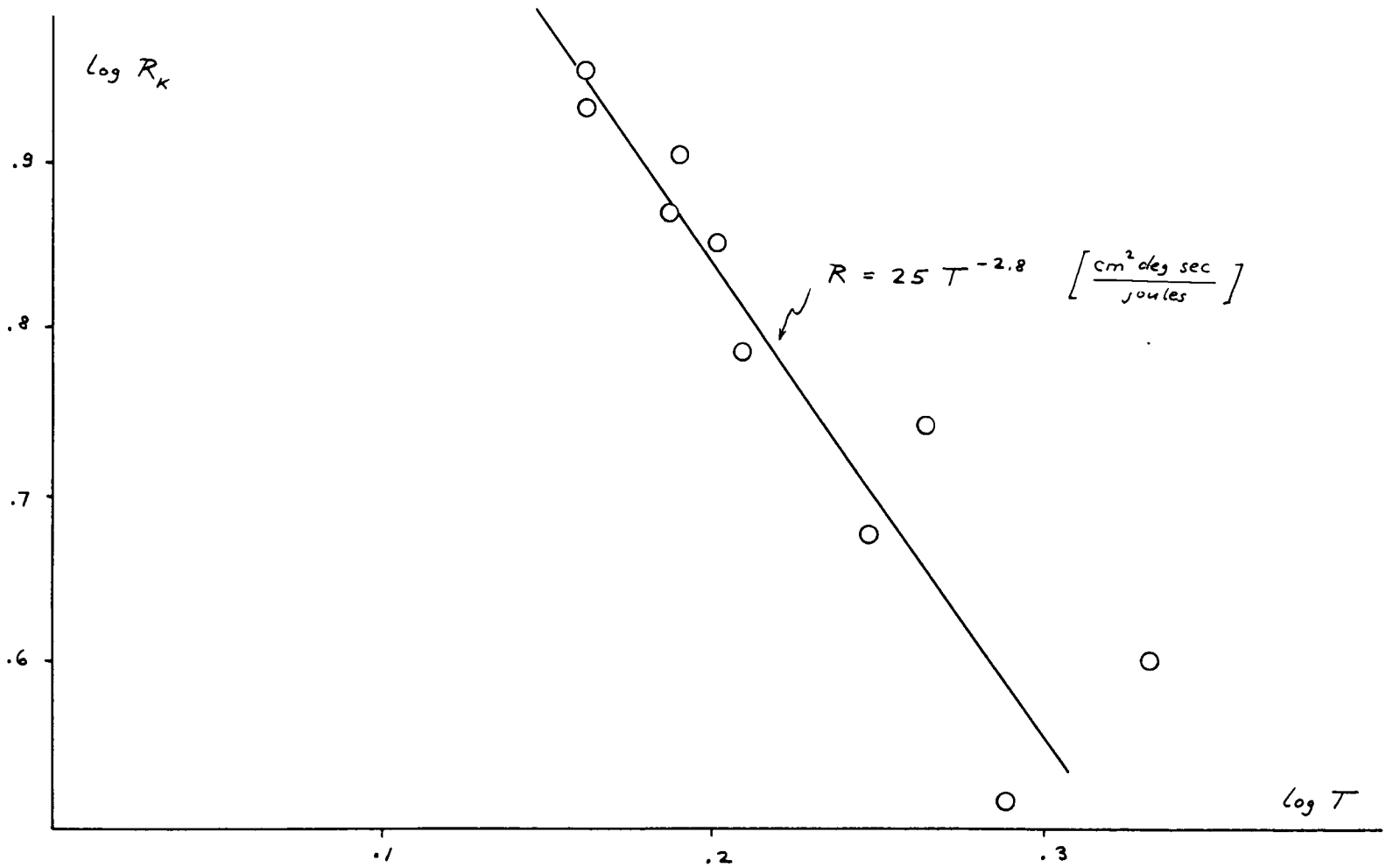

Figure 4.14 Kapitza resistance of PrES-HeII: Temperature dependence

4.2 Europium Doped Calcium Fluoride

4.2.1 Faraday Rotation

The change of the angle of polarization with magnetic field has been measured in order to check that the Faraday rotation was proportional to the magnetization. The measured rotation has been corrected in each case for the Faraday rotation due to the glass walls of the dewar and for the diamagnetic rotation of the crystal. The resulting paramagnetic rotation has been normalized to match the Brillouin function $B_{\frac{7}{2}}$ at the highest values of H/T.

Figure 4.15 shows the normalized paramagnetic rotation of crystal No. 1 as a function of H/T using the purple, green and yellow line of the Hg-light. No systematic difference exceeding the measuring accuracy is observed and this indicates that even the purple light is still far enough from the optical transition causing the Faraday rotation to maintain proportionality between rotation and magnetization. The slight deviation from the Brillouin curve observed above 3 kOe/°K is probably not due to a violation of this proportionality but arises rather from a deviation of the magnetization from the free-ion value. The measurements from the other crystals, plotted in Figure 4.16, confirm the results from crystal No. 1.

The saturation rotation per mm. thickness ϱ_∞ is shown in Table II for the different crystal specimens. The ϱ_∞ are proportional to the Eu^{2+} concentration, if the effect of concentra-

tion dependence of the optical spectrum on the Faraday rotation is negligible. Such an effect would be strongest for light frequencies close to the optical transitions, as can be seen from equation (2.87). We found that the ratio of ρ_∞ for different concentrations does not depend on the light frequency. This supports the assumption that the ρ_∞ are proportional to the Eu^{2+} concentration and, therefore, a direct measure for the relative concentration of the different specimens.

The molar concentration of europium ions added to the CaF_2-melt in the growing process is given in Table II. There is a marked disagreement between the added Eu concentration and the relative Eu^{2+} concentrations obtained from rotation measurements.

It is known that europium enters the fluoride lattice in both the trivalent and the divalent state. (Shen, 1964). The Eu^{3+} ion has a $^7F_0$ singlet groundstate and gives no paramagnetic contribution to the Faraday rotation. The ratio of Eu^{2+} to Eu^{3+} is very sensitive to the growing conditions. In crystal No. 1, europium was added in the form of Eu_2O_3, while in No. 3 the same molar amount was added in the form of EuF_3. As a result, No. 1 has a ten times higher Eu^{2+} concentration than No. 3.

Assuming that the lowest concentration (crystal No. 4) is mostly Eu^{2+}, we have calculated values for both the Eu^{2+} and Eu^{3+} concentrations. These values are also given in Table II and have to be regarded as rather rough approximations. It is seen that two of the heavily doped crystals have a very small

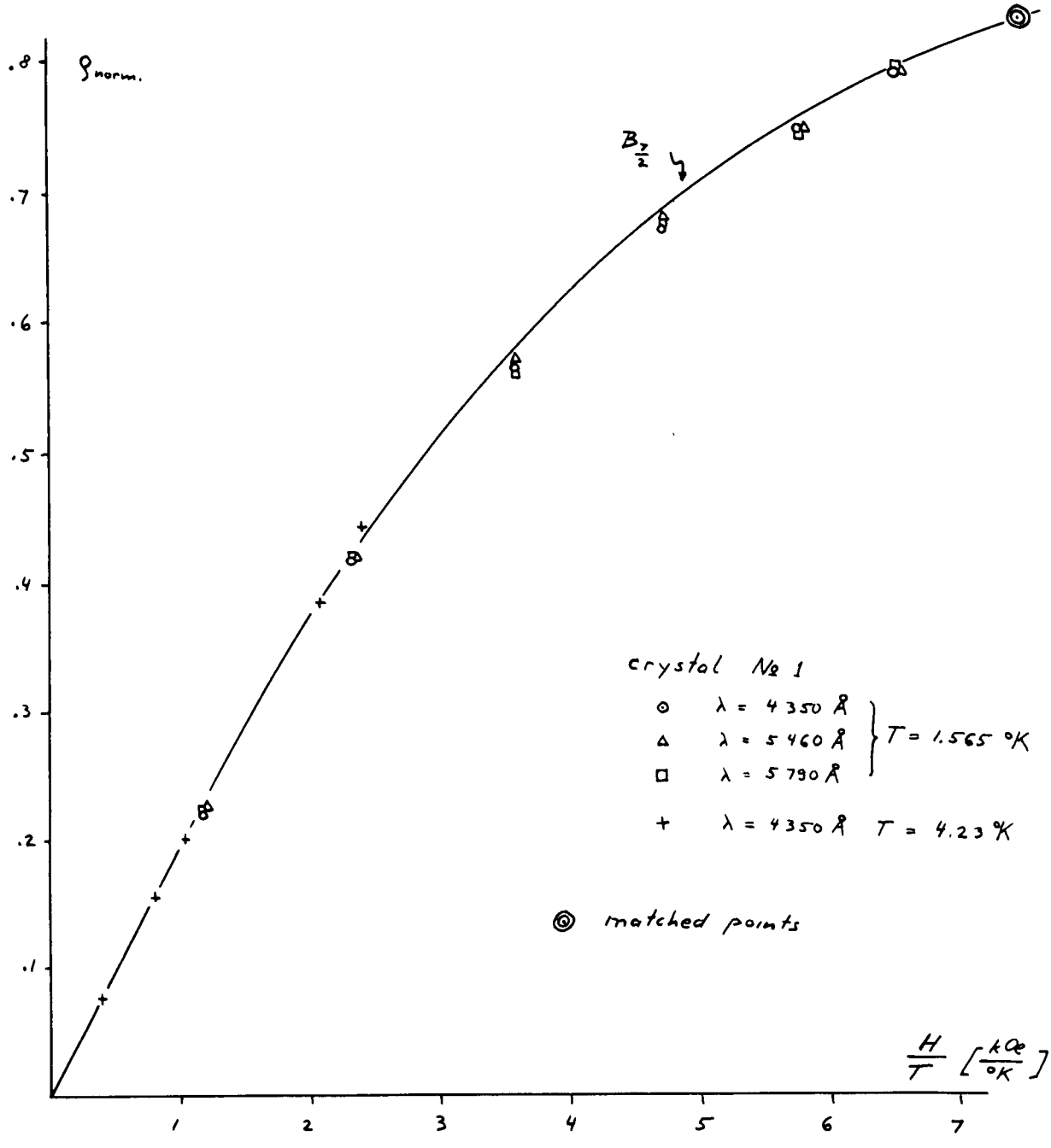

Figure 4.15 Faraday rotation of Eu^{2+}:CaF crystal No. 1

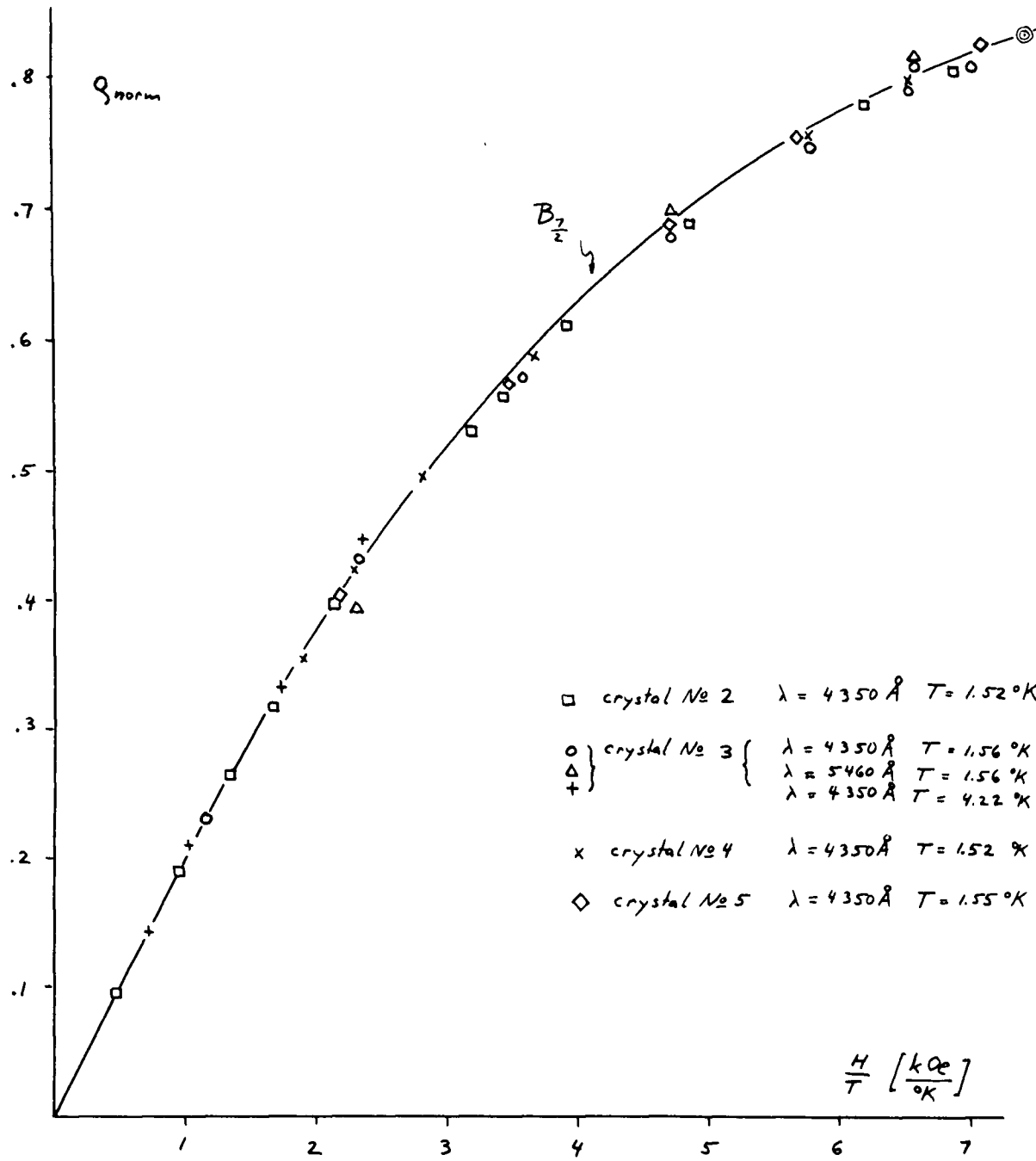

Figure 4.16 Faraday rotation of Eu^{2+}:CaF_2 crystals No. 2 - 5

Specimen No.	Saturation rotation ρ_∞ [deg mm^{-1}]			Eu Total %	Eu^{2+} %	Eu^{3+} %
	4350 Å	5460 Å	5790 Å			
1	137	24.4	18.8	2	0.3	1.7
2	27.8			0.2	0.06	0.14
3	16.2	2.5		2	0.035	2
4	9.6			0.02	0.02	
5	8.8			0.8	0.015	0.8

Table II Saturation rotation and concentration of $Eu:CaF_2$ specimens

Eu^{2+} content. The good fit of their paramagnetic rotation to the Brillouin curve supports the assumption that the Eu^{3+} ion does not contribute to the paramagnetic rotation.

From the saturation rotations ρ_{∞_1} and ρ_{∞_2} for two different light frequencies ω_1 and ω_2, we can calculate the average transition frequency causing the Faraday rotation. From equation (2.87) and (2.89)

$$\rho_{\infty i} \sim \frac{\bar{\omega}^2}{\bar{\omega}^2 - \omega_i^2} \qquad i = 1,2$$

we get

$$\bar{\omega}^2 = \frac{\rho_{\infty_1}\omega_1^2 - \rho_{\infty_2}\omega_2^2}{\rho_{\infty_1} - \rho_{\infty_2}}$$

The values for $\rho_{\infty i}$ from Table II give

$$\bar{\omega} \approx 23\ 900\ \text{cm}^{-1} \quad \text{or} \quad 4180\text{Å}\ .$$

This agrees well with the optical spectrum, which shows a strong absorption band at 24 200 cm^{-1} attributed to $^8S - {}^6P$ transitions. (Low, 1960)

4.2.2 Resonance Spectrum

The saturation s of the spin system as a function of the external magnetic field was determined in the same way as in the case of CeES by measuring the paramagnetic rotation for a given field in presence of microwaves ρ and in absence of microwaves ρ_0.

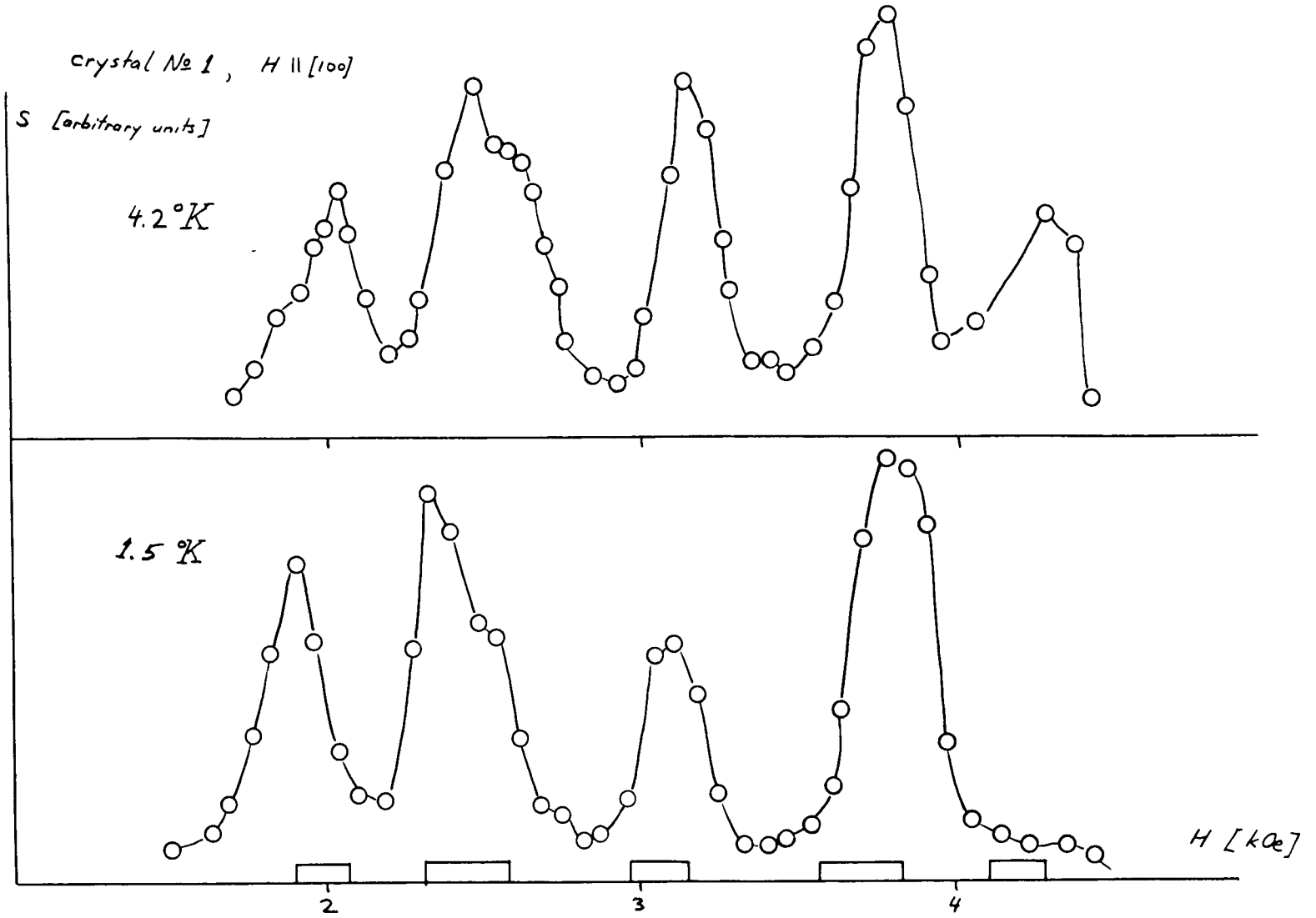

Figure 4.17 Resonance spectrum of $Eu^{2+}:CaF_2$

Since the minimum step possible with our rheostat is about 30 gauss, this point-by-point procedure is not capable of resolving the hyperfine structure. It was, however, possible to obtain an envelope of the hyperfine lines corresponding to a given electronic transition. The results obtained from crystal No. 1 at 1.5 °K and 4.2 °K are shown in Figure 4.17. In both cases, the magnetic field was along a cube edge [100]. The transitions $\pm\frac{3}{2} \rightarrow \pm\frac{5}{2}$ and $\pm\frac{1}{2} \rightarrow \pm\frac{3}{2}$ are too close and are not resolved. The overall width of any one electronic transition agrees with the total hyperfine splitting as measured by Ryter (1957).

The overall splitting of the $^8S_{\frac{7}{2}}$ groundstate is a few °K at the magnetic fields available to us. The upper levels should, therefore, be appreciably depopulated as one cools down from 4.2 °K to 1.5 °K and the corresponding transition should become weaker. This is observed for the line at the high-field side of the spectrum. We identify, therefore, this line as being the $+\frac{7}{2} \rightarrow +\frac{5}{2}$ transition. This corresponds to a negative value of b_4 in equation (2.64).

The slight difference in the resonance center-values between the two spectra is not genuine. It can be accounted for by a shift in the resonance frequency of the cavity and by a slight difference in alignment of the crystal with respect to the external magnetic field.

4.2.3 Relaxation Times

The temperature dependence of the spin-bath relaxation

time τ has been measured in the specimens No. 1 to 5 from 1.5 °K up to the highest temperatures which still gave a reasonable signal-to noise ratio. The results are shown in Figure 4.18. Most points shown are averages from several measurements.

The measurements have been done on the centerline $\frac{1}{2} \rightarrow -\frac{1}{2}$ and with both DC magnetic field and light direction parallel to the four-fold cubic axis. These conditions assure maximum distance between the investigated line and other electronic transitions and therefore minimize cross-relaxations between different electronic transitions.

It is seen that the absolute value as well as the functional dependence of the relaxation rate τ^{-1} depends on the specimen. The different specimens have all nearly the same shape and dimensions but they differ in their europium concentrations as shown in Table II.

The experimental points at the lowest temperatures can in each case be fitted with a straight line with the following slopes:

Crystal No.	1	2	3	4	5
Slope	1.96	1.22	1.88	1.07	1.11
Max. Deviation	0.12	0.03	0.11	0.10	0.10

The mean value of the slope and its possible deviation have been determined graphically. At higher temperatures, deviation from the straight line occurs and a smooth curve has been drawn

through the experimental points.

The error flags attached to the high-temperature point of specimen No. 2 are the maximum errors due to measuring inaccuracy. At lower temperatures, the accuracy is considerably higher and, in general, does not exceed the size of the circles as drawn around the points in Figure 4.18.

The relaxation time has been found to be constant across the whole $+\frac{1}{2} \rightarrow -\frac{1}{2}$ transition. This is important since the cavity-resonance shifts by about 20Mc/s during the warm-up from 1.5 °K to 4.2 °K, and it is impossible with our rough field regulation to correct for this change. A shift of this size is, on the other hand, comparable to the spacing between the hyperfine components and therefore we cannot avoid sitting at different spots on the $\frac{1}{2} \rightarrow -\frac{1}{2}$ line for different temperatures during the same run.

It is also impossible to induce the microwave transition exactly at the same spot in two different runs. No change in absolute value or temperature dependence of τ has been detected in different runs on the same crystal and the good reproducibility of the data are thus a further confirmation that the temperature dependences of τ are genuine properties of the $\frac{1}{2} \rightarrow -\frac{1}{2}$ line.

It has further been checked as to whether τ was dependent on microwave power or pulse length. No change in τ has been observed by varying the microwave power up to 40 db and the pulse length by a factor of 30. In no case has clear evidence been found for nonexponential behaviour of the relaxation trace.

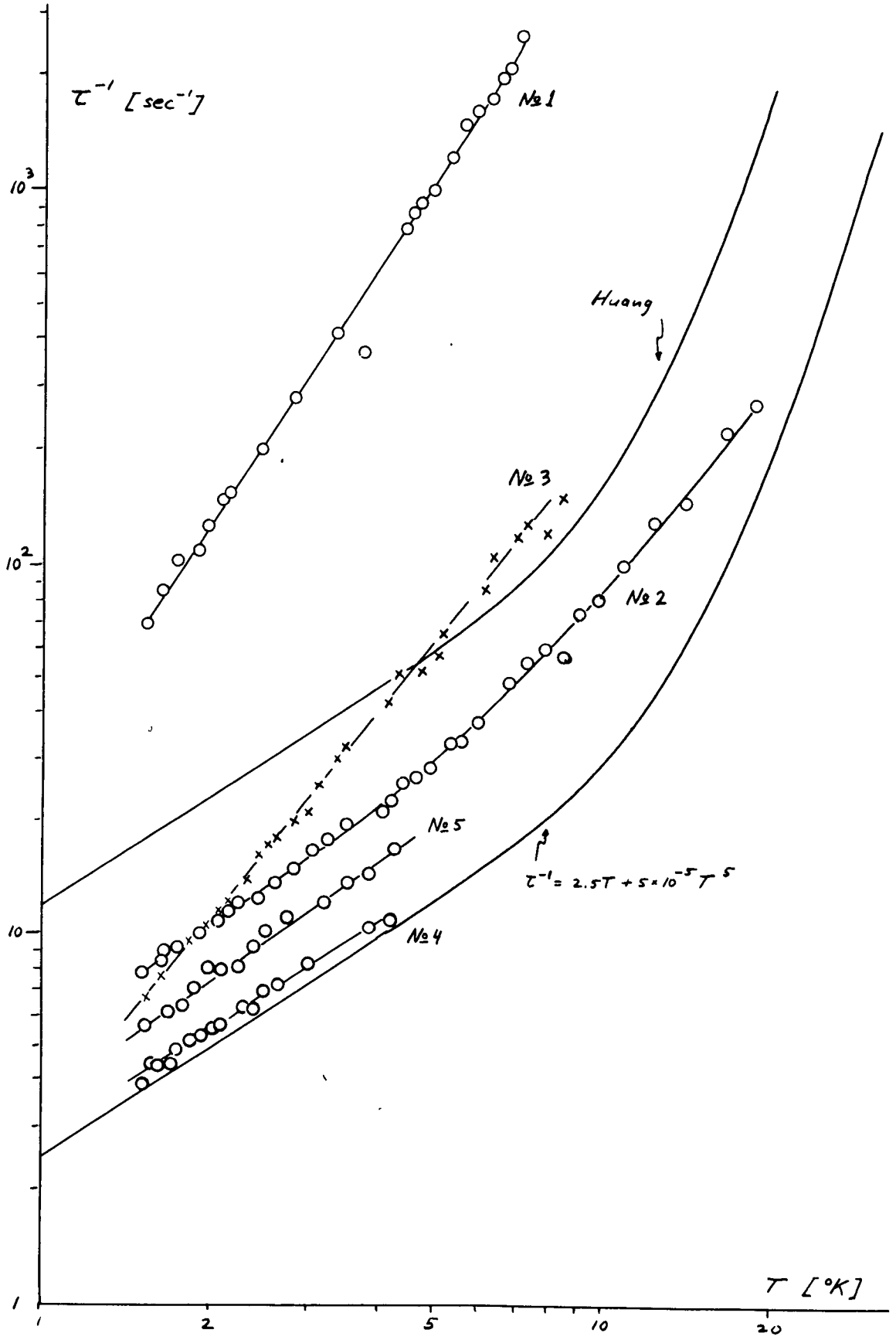

Figure 4.18 Relaxation rate of $Eu^{2+}:CaF_2$ as a function of temperature for different concentrations

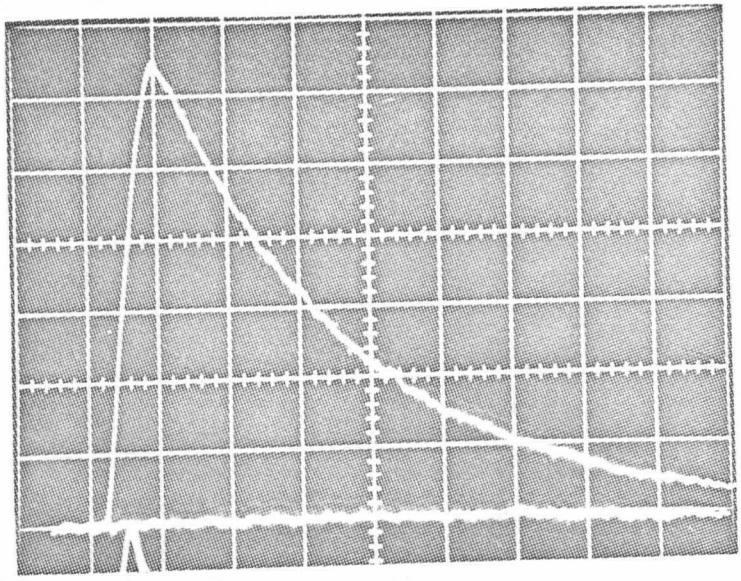

a)

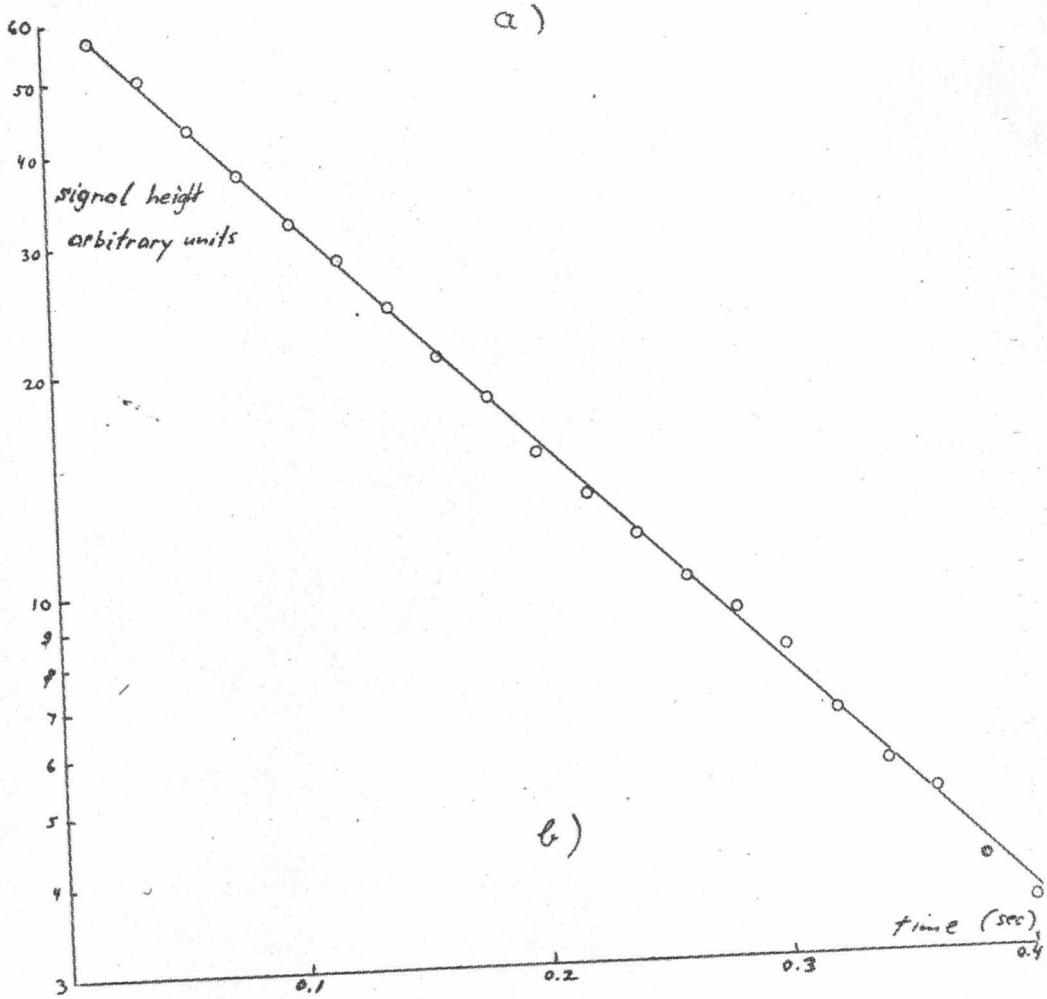

Figure 4.19 a) Typical relaxation trace of $Eu^{2+}:CaF_2$
b) Semilogarithmic plot of trace in a)

A typical relaxation trace is shown in Figure 4.19 together with its semilogarithmic plot.

4.2.4 Discussion

The concentration dependence of the relaxation times cannot be explained by a phonon-bottleneck, although the temperature dependence for the specimens 1 and 3 is very nearly $\tau^{-1} = DT^2$. This temperature dependence can result from the linearized rate equations for the direct process in the presence of a weak phonon-bottleneck (Scott and Jeffries, 1962). The constant D should, however, decrease with increasing concentration in contradiction with our results.

No bottleneck would be expected in this case, anyway. The condition for a phonon bottleneck has been found earlier to be (equation (2.51))

$$\frac{c_C}{c_B}\tau_{AB} \gtrsim \tau_{BC}$$

where c_C and c_B are the heat capacities of spin system and lattice oscillators respectively, τ_{AB} is the phonon lifetime and τ_{BC} is the spin-lattice relaxation time T_1. In our case $\frac{c_C}{c_B} \approx 10^3$ in the direct process region. If one assumes a phonon lifetime of $\tau_{AB} \approx 10^{-6}$sec. (Faughnan and Strandberg, 1961) then $\frac{c_C}{c_B}\tau_{AB} \approx 10^{-3}$. This is two orders of magnitude smaller than our observed relaxation times.

In our measurements, there seem to be, in addition to the conventional spin-lattice relaxation, one or several competing

processes which become increasingly important at high concentrations. If the total relaxation rate due to these processes is λ, we can write for the observed relaxation rate approximately

$$\tau^{-1} = T_1^{-1} + \lambda$$

The spin-lattice relaxation rate has the form

$$T_1^{-1} = AT + BT^5$$

as shown in Chapter 2.4. We do not know anything about λ. The only reasonable assumption is that λ does not decrease with increasing temperature. This yields the following upper limits for the coefficients A and B of the spin-lattice relaxation:

$$A_{max} = 2.5 \qquad B_{max} = 5 \times 10^{-5}$$

The resulting temperature dependence of T_1^{-1} is shown in Figure 4.18.

Table III is a compilation of results obtained by different workers. In the first column, the results obtained by Huang (1965) are shown. He used the pulse-saturation recovery technique. The measurements were done at X-band on the $\frac{1}{2} \rightarrow -\frac{1}{2}$ transition with $H \parallel [100]$. The specimens used had 0.0047%, 0.0074% and 0.18% Eu^{2+} concentration. The second column shows the theoretical estimate obtained for T_1 by Huang. The fourth column shows the estimate of the strength of the direct process deduced from ultrasonic absorption measurements by Dobrow and Browne (1962).

	Huang (Pulse saturation)	Huang (theoretical estimate)	Our measurements (Faraday rotation)	Dobrow (ultrasonic absorption)
A	12	3	2.5	0.1
B	5.3×10^{-4}	4×10^{-4}	5×10^{-5}	

Table III Coefficients for the spin-lattice relaxation in Eu $:CaF_2$

The results are seen to disagree quite considerably. It has to be noted that the three experimental methods measure different physical events.

With the pulse saturation method, the recovery of the paramagnetic absorption line after a strong saturating pulse is observed using a very low monitoring microwave power level. The microwave absorption is proportional to the population difference of the two levels between which the resonance takes place. The measured quantity is, therefore, a population difference between two levels. Spin-lattice relaxation is not the only possibility for recovery of the absorption signal. Other possibilities are (cf. chapter 2.4.5):

a) cross-relaxation between different hyperfine lines within the same electronic transition, or frequency diffusion within an inhomogeneously broadened resonance line in cases where the saturating pulse "burns a hole" in the line.

b) cross-relaxation between different electronic transitions.

c) cross-relaxation to other systems like impurities or

exchange coupled clusters of two or more paramagnetic ions.

Our method of monitoring the change in paramagnetic rotation after a microwave saturating pulse measures the time dependence of the magnetization due to the Eu^{2+}-ions (to the extent that they only contribute to the paramagnetic Faraday rotation). The processes a) and b) above do not contribute to the decay, if they conserve angular momentum. The measured relaxation rates are, however, enhanced by process c) to the same extent as the pulse-saturation measurements.

The ultrasonic absorption measurements are not affected by any of the above mentioned processes. Here, the strength of the orbit-lattice interaction is determined by measuring the absorption coefficient of microwave-phonons.

Processes b) have been observed by Huang to influence the relaxation times for pulses shorter than 0.5 msec. For longer pulses, the whole electronic transition can be considered as homogeneously saturated and the influence of processes b) can be neglected.

The processes a) have also been detected by Huang for different directions and different electronic transitions. They are readily recognized by their temperature independence. For the $\frac{1}{2} \rightarrow -\frac{1}{2}$ transition and with the magnetic field along a cube edge, the distance to all other transitions is maximum. Crossrelaxations of the type a) can, in this case, be expected to be weak. In fact, Huang's relaxation times become temperature

dependent for this configuration.

The influence of processes c) on both relaxation methods but not on the ultrasonic absorption measurements suggests that they might be responsible for the considerable enhancement of the relaxation rates measured by Huang and in the present investigation as compared to Dobrow's values.

We do not believe other paramagnetic ions as impurities are able to account for the whole discrepancy. The spectrum of paramagnetic ions, which could be present only in very high dilution, would have a relatively small number of sharp lines and the crossrelaxation would show a marked field dependence. In addition, the impurity content would be strongly sample dependent.

It seems to be quite general, that spin-lattice relaxation times measured by pulse saturation techniques are found to be shorter than the estimates from acoustic absorption measurements. (For a compilation of data and references see Dobrow (1966), table 1.) This indicates that we have to look for a more general explanation.

It has been shown earlier that pairs of ions might be coupled together through the exchange interaction to form paramagnetic systems with a different level scheme than the single ions. Crossrelaxation from single ions to exchange coupled pairs (or larger clusters) has been proposed by several authors to explain the concentration dependence and enhancement of relaxation rates (Van Vleck, 1959 and 1961; Gill, 1961 and Gill

and Elliott, 1961; Bloembergen and Pershan, 1961; Statz et al, 1961; Ramestad and Wagner, 1963; Schulz and Jeffries, 1966). The following is only a very qualitative investigation of the feasibility of such a mechanism to enhance considerably the spin-bath relaxation rates.

From equation (2.80) follows the condition for a pair or cluster to have an appreciable effect on the single ion relaxation:

$$W_2 \frac{N_2}{N_1} \gtrsim W_1$$

Here N_2 is the population of the levels of the pair spectrum which have a strong spin-spin coupling to the single ion level, N_1 is the population of the single ion level and W_1 and W_2 are the respective spin-lattice relaxation rates.

Statz et al (1961) and Gill (1961) have measured relaxation times of transitions in the Cr^{3+} pair spectrum in ruby. The pair relaxation rates are found to be about three orders of magnitude faster than the single-ion relaxation rates. This efficient relaxation mechanism cannot be due to the ordinary Van Vleck-Orbach relaxation through modulation of the crystal field. Modulation of the exchange interaction by the lattice vibrations has been used by the above authors to explain qualitatively the strong spin-lattice coupling of pairs.

If we adopt the value $W_2/W_1 \approx 10^3$, we have as the limit for crossrelaxation via pairs to become noticeable

$$\frac{N_2}{N_1} \gtrsim 10^{-3}$$

If N_2 is taken as the number of nearest paramagnetic neighbours in a crystal with randomly distributed paramagnetic centers, then for low concentration c we have $N_1/N_2 \approx c$. This means that at concentrations of 0.1%, the pair relaxation could become noticeable.

Not all pair lines might have an efficient crossrelaxation to the single ion line. This would decrease the value of N_2. On the other hand, rather far neighbours might be effectively coupled by indirect Kramers-type exchange interaction. Statz et al have identified pair lines in the Cr^{3+} spectrum in ruby up to the 10th neighbour. This as well as exchange coupled clusters of more than two ions can increase N_2 considerably and if N_2 becomes comparable to N_1, the model of separated single ions and pairs would break down.

The exchange interaction between rare earth ions is, however, weaker than between the iron group ions and exchange interaction, therefore, will not couple neighbours which are too far away. The exchange interactions between Eu^{2+}-ions and CaO and SrO have been studied by Calhoun and Overmeyer (1964). They find $0.5\,^{\circ}K < J_{nn} < 1.5\,^{\circ}K$ and $J_{nnn} < 0.1\,^{\circ}K$, where J_{nn} and J_{nnn} are the exchange coupling constants between nearest neighbours and next nearest neighbours respectively.

The conclusion is that exchange coupled pairs are able to enhance the relaxation rates of the single ions and might, therefore, cause the observed concentration dependence of τ. It is doubtful, however, if this mechanism is strong enough to

account for the large discrepancies between relaxation and acoustic absorption measurements.

As has been mentioned earlier, some of our specimens have an appreciable concentration of Eu^{2+}-ions. These ions have a ground state singlet $^7F_0$. Since the exchange interaction acts on the electronic spin rather than on the total angular momentum Eu^{3+}-ions can be coupled to neighbouring Eu^{2+}-pairs. It is possible that clusters involving Eu^{3+}-ions have a steeper τ versus T dependence than those containing only Eu^{2+}. This could explain the steeper temperature dependence of τ for the two specimens 1 and 2 which have much higher Eu^{3+} concentration than the other crystals, as well as the crossover at 1.9 °K between the specimens 2 and 3. Quantitative or even semi-quantitative explanations are impossible, due to the very complicated structure of our system and to complete lack of knowledge outside the single-ion system. An attempt to detect pair lines in the already very complicated single-ion spectrum using a 34 Gc/s spectrometer was unsuccessful. The considerations above have therefore to remain rather speculative.

4.3 Erbium Ethylsulphate

4.3.1 Introduction

Er^{3+} has a free ion ground state $^4I_{\frac{15}{2}}$, which is split into seven Kramers doublets by the ethylsulphate crystal field. At helium temperatures, only one doublet is populated. It has a highly anisotropic g-value. Bleaney and Scovil (1951) measured for Er^{3+} diluted in LaES $g_{\parallel} = 1.47$ and $g_{\perp} = 8.85$. The paramagnetic resonance spectrum shows one strong center line due to the even isotopes and eight hyperfine lines arising from the only odd isotope Er^{3+} which has a natural abundance of 23%. The total separation of the seven Kramers doublets is 300 cm^{-1} and the doublet closest to the ground state is at 44 cm^{-1}. These values have been measured by Erath (1961) in the concentrated ErES.

The spin-lattice relaxation of Er^{3+} diluted in LaES and YES has been studied by Larson and Jeffries (1966). In LaES and with $H \parallel z$, they find a rather weak direct process $T_1 = 4.2\ T$ which is dominant below 2°K, an Orbach process $T_{10} = 4.5 \times 10^{10} \exp\left(-\frac{59}{T}\right)$ and a strong Raman process $T_{1R} = 4.4 \times 10^{-3}\ T^9$ which is dominant above 2°K. Due to the strong Raman process, the relaxation time changes by more than four orders of magnitude in the liquid helium temperature range. Representative values are

$T_1 = 150$ msec at 1.5°K

and $T_1 = 14\ \mu$sec at 4.2°K

No relaxation time measurements are as yet available for the concentrated ErES.

As in the case of CeES and Eu^{2+} : CaF_2, the paramagnetic Faraday rotation ρ_p of ErES is proportional to the magnetization M. Since only one Kramers doublet is populated ρ_p and M are both proportional to the population difference in the ground state doublet. Becquerel, De Haas and Van den Handel (1937) measured

$$\rho_p = A \tanh \frac{\mu H}{kT}$$

with $\mu = 6.016\beta$ and A = -12.57 deg mm^{-1}

It should therefore be possible to measure the spin-bath relaxation by monitoring ρ_p . In anisotropic crystals, however, ρ_p is not easily measured. In addition to the Faraday rotation birefringence occurs if the light is not propagated along the optic axis. The observed angle of minimum light transmission, i.e. the apparent Faraday rotation, is a function of both birefringence and rotation and is not proportional to the magnetization.

The problem, therefore, is to align the optic axis of the ethylsulphate samples sufficiently parallel to the light direction such that the birefringence is negligible compared to the Faraday rotation. No alignment problem arises in the optically isotropic fluorides. The apparent rotation has been studied as a function of birefringence and rotation by Ramaseshan (1951).

It is convenient to visualize the effect of birefringence

and Faraday rotation on the state of polarization by means of the Poincaré sphere. For a detailed treatment, we refer to the article by Ramachandran and Ramaseshan (1961). We give in the following only a short review in order to explain the negative results in ErES.

4.3.2 The Poincaré Sphere Representation

The electric vector of a totally polarized light wave describes in general an ellipse. The state of polarization of the light wave is specified by two parameters, eg. the ratio $\frac{a}{b}$ of the two axes of the ellipse and the angle ψ between the major axis of the ellipse and a fixed direction.

A one-to-one correspondence between the possible states of polarization (defined by $\frac{a}{b}$ and ψ) and the points P on a sphere (the so-called Poincaré sphere) can be established if P is defined as the point of latitude 2ϑ and longitude 2ψ , where $\tan \vartheta = \frac{b}{a}$ (see Figure 4.20). The poles of the sphere thus correspond to circularly polarized light and the points on the equator characterize linearly polarized light of different orientation. The concept is illustrated in Figure 4.20.

Consider now a light wave of arbitrary polarization $P(\psi,\vartheta)$ entering a crystal which possesses both birefringence and Faraday rotation. The change in polarization of the light wave in passing through the crystal is most easily discussed using the Poincaré sphere. It can be shown that for a given crystal and for a given direction of propagation, there are two orthogonal

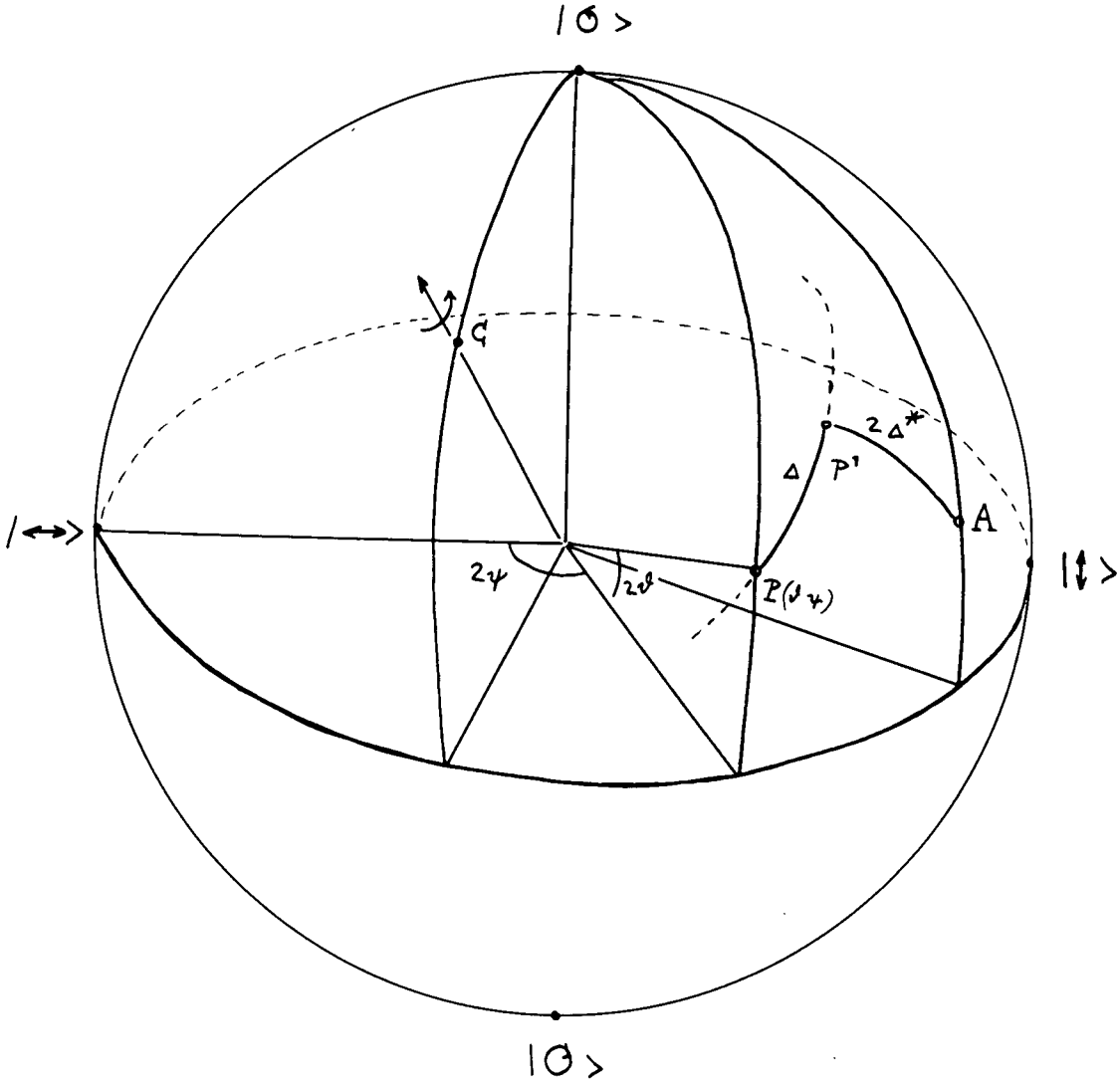

Figure 4.20 The Poincaré sphere - General relations

states of polarization which propagate unchanged through the crystal. These states are called the stable modes C and C'. For an arbitrary polarization P of the light entering the crystal, the state P' of the emerging light after a path length d in the crystal can be found by rotating the point P by an angle Δ about the axis joining the two stable modes C and C'. This axis passes through the center of the sphere due to the fact that the stable modes are orthogonal. The angle of rotation is given by

$$\Delta = d\Delta_0 = d\sqrt{\delta_0^2 + (2\rho_0)^2}$$

where δ_0 is the birefringence per unit path length in absence of Faraday rotation and ρ_0 is the Faraday rotation per unit path length in absence of birefringence. The latitude of the stable mode C is given by

$$\tan 2\vartheta = \frac{2\rho_0}{\delta_0}$$

An analyser can be represented by the point A on the sphere which corresponds to the light polarization passing the analyser without attenuation. If light of polarization P' is incident on the analyser A, only a fraction proportional to $\cos^2\Delta^*$ is passed by the analyser where $2\Delta^*$ is the angle of the great circle between A and P'.

Figure 4.21 illustrates the special case which applies in our relaxation measurements. The light incident on the crystal is linearly polarized (point L). The crystal has a stable

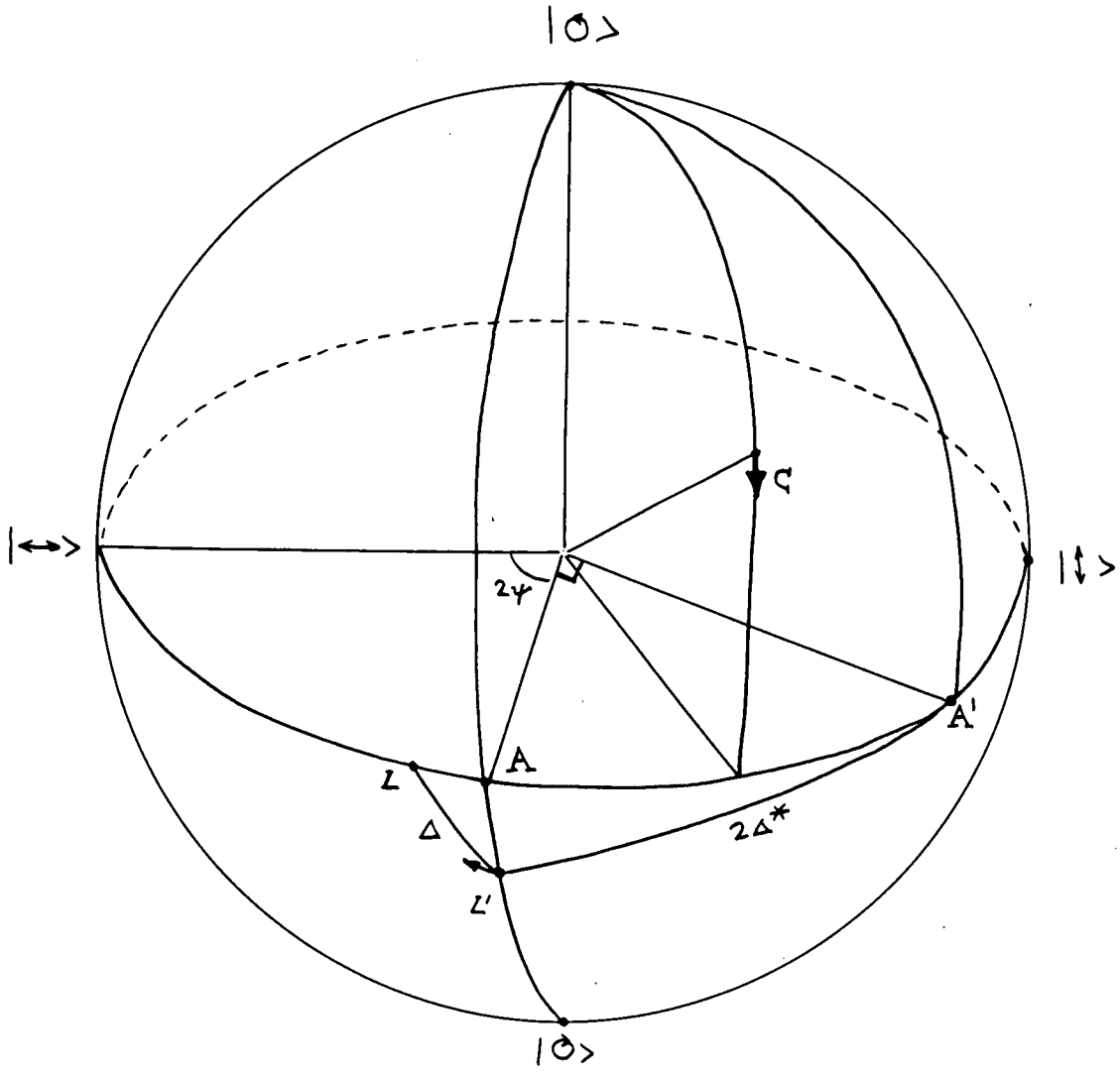

Figure 4.21 The Poincaré sphere applied to relaxation measurements

mode C with

$$\tan 2\vartheta = \frac{2\varrho_0}{\delta_0} = \frac{2\varrho_0}{\delta_\perp \sin^2\alpha}$$

where α is the angle between the light direction and the optic axis and is supposed to be small. $\delta_\perp = \frac{2\pi}{\lambda}(n_\omega - n_\varepsilon)$ is the birefringence per unit path length. n_ω and n_ε are the two principal refractive indices. After passing through the crystal, the light can be represented by the point L' which is rotated by an angle Δ about CC' from L

$$\Delta = d\sqrt{\delta_\perp^2 \sin^4\alpha + 4\varrho_0^2}$$

The analyser at A gives minimum light transmission (apparent Faraday rotation ϱ'). For observation of the relaxation, the analyser is set at $\varrho' + 45^\circ$ (point A') and the transmitted light intensity is proportional to $\cos^2\Delta^*$. Application of a microwave saturating pulse reduces the Faraday rotation, thus moving both L' and C in the direction indicated by arrows in Figure 4.21. The functional dependence $\cos^2\Delta^* = f(\varrho)$ is in general very complicated and expansions are possible only in the special cases of $\delta \ll 2\varrho$ (negligible birefringence) or $\delta \gg 2\varrho$ (negligible Faraday rotation). In the case of ErES, the Faraday rotation is 10 deg mm^{-1} at resonance field and 1.5 °K (Becquerel <u>et al</u>, 1937). The refractive indices are $n_\omega = 1.490$ and $n_\varepsilon = 1.480$, giving a path retardation of $\delta_\perp = 115\ mm^{-1}$. Hence $\frac{2\varrho}{\delta_\perp} = 0.003$. A few representative values for the latitude 2ϑ of the stable modes C for small misalignments α are

$\alpha = 1$ deg $\qquad 2\vartheta = 84$ deg

$\alpha = 2$ deg $\qquad 2\vartheta = 68$ deg

$\alpha = 3$ deg $\qquad 2\vartheta = 48$ deg

It is seen that for ErES, the alignment has to be very accurate in order to keep the stable modes on the pole of the Poincaré sphere. It has to be noted that the 2ϑ values given are the optimum values during the relaxation trace since microwave saturation decreases ϱ and hence 2ϑ.

As has been described in chapter 3.1, the crystal could be rotated at He-temperature about two fixed axes. It is generally impossible to obtain any direction in space by rotation about two fixed axes. The possibility of proper alignment thus depends on the orientation of the two axes of rotation (i.e. on the position of the teflon plug in the cavity) and on the position of the crystal specimen with respect to the teflon plug. It is impossible to adjust the alignment at room temperature, since cooling down to He temperatures can change the orientations considerably. The sources of misalignment are not reproducible from one experimental run to another.

We have tried to achieve proper alignment in seven runs with four different crystal specimens. (The same crystal cannot be used for more than two runs, in general, due to deterioration of the polished faces.) The conclusion is that a more accurate mechanical aligning system has to be found. This seems rather tricky since the experiments are performed at He temperatures in the tight space of a magnet gap.

BIBLIOGRAPHY

Abel, W.R., Anderson, A.C., Black, W.C. and Wheatley, J.C. (1966) Phys. Rev. Lett. 16, 274.

Abragam, A. (1961) The Principles of Nuclear Magnetism (Oxford Univ. Press) P. 404.

Anderson, A.C., Connolly, J.I. and Wheatley, J.C. (1965) Phys. Rev. 135, A910.

Andronikashvili, E.L. (1956) Soviet Physics Jetp 2, 406.

Baker, J.M., Bleaney, B. and Hayes, W. (1958) Proc. Roy. Soc. A247, 141.

Becquerel, J., De Haas, W.S., and Van den Handel, J. (1937) Physica 4, 345.

Becquerel, J., De Haas, W.J., and Van den Handel, J. (1938) Physica 5, 857.

Bleaney, B. and Scovil, H.E.D. (1951) Proc. Phys. Soc. A64, 204.

Bleaney, B. and Bowers, K.D. (1952) Proc. Roy. Soc. A214, 451.

Bloembergen, N., Shapiro, S., Pershan, P.S., and Artman, J.O. (1959) Phys. Rev. 114, 445.

Bloembergen, N. and Pershan, P.S. (1961) Advances in Quantum Electronics (Columbia Univ. Press) J.R. Singer ed. p. 373.

Bogle, G.S., Cooke, A.H. and Whitley, S. (1951) Proc. Roy. Soc. A64, 931.

Brya, W.S. and Wagner, P.E. (1965) Phys. Rev. Lett. 14, 431.

Burgiel, J.C. and Meyer, H. (1966) Bull. Am. Phys. Soc. II, 11, 453.

Calhoun, B.A. and Overmeyer, J. (1964) J. appl. Phys. 35, 989.

Casimir, H.B.G. (1939) Physica 6, 156.

Challis, L.J. (1962) Proc. Phys. Soc. 80, 759.

Challis, L.J., Dransfeld, K. and Wilks, J. (1961) Proc. Roy. Soc. A260, 31.

Daniels, J.M., and Wesemeyer, H. (1958) Can. J. Phys. 36, 405.

Devor, D.P. and Hoskins, R.H. (1961) Bull. Am. Phys. Soc. II 6, 364.

Dobrow, W.I. and Browne, M.E. (1962) Magnetic and Electric Resonance and Relaxation, Prox. XI Coll. Ampere, Eindhoven (1962) J. Smidt, ed. (North-Holland Publishing Co. Amsterdam, 1963) p. 129.

Dobrow, W.I. (1966) Phys. Rev. 146, 268.

Dweck, J. and Seidel, G. (1966) Phys. Rev. 146, 359.

Dransfeld, K. (1958) Bull. Am. Phys. Soc. II 3, 324.

Elliott, R.J. and Stevens, K.W.H. (1952) Proc. Roy. Soc. A215, 437.

Erath, E.H. (1961) J. Chem. Phys. 34, 1985.

Eschenfelder, A.H. and Weidner, R.T. (1953) Phys. Rev. 92, 869.

Faughnan, B.W. and Strandberg, M.W.P. (1961) J. Phys. Chem. Solids 19, 155.

Feofilov, P.P. and Kaplyanskii, A.A. (1963) Optics and Spectr. (USSR) 13, 129.

Finn, C.B.P., Orbach, R. and Wolf, W.P. (1961) Proc. Phys. Soc. 77, 261.

Fitzwater, D.R. and Rundle, R.E. (1959) Z. Krist. 112, 362.

Garwin, R.L., Hutchinson, D., Penman, S. and Shapiro, G. (1959) Rev. Sci. Instr. 30, 105.

Geschwind, S., Collins, R.J. and Schawlow, A.L. (1961) Advances in Quantum Electronics (Columbia Univ. Press, J.R. Singer ed.) p. 232.

Geschwind, S., Devlin, G.E., Cohen, R.L. and Chinn, S.R. (1965) Phys. Rev. 137, A1087.

Gill, J.C. (1961) Proc. Phys. Soc. 79, 58.

Gill, J.C. and Elliott, R.J. (1961) Advances in Quantum Electronics(Columbia Univ. Press) J.R. Singer ed. p. 399.

Giordmaine, J.A. and Nash, F.R. (1965) Phys. Rev. 138, A1510.

Gorter, C.J., Van der Marel, L.C. and Bölger, B. (1955) Physica 2., 103.

Griffiths, D.J. (1965) Ph. D. Thesis, University of British Columbia (unpublished).

Griffiths, D.J. and Glättli, H. (1965) Can. J. Phys. 43, 2361.

Huang, C.Y. (1964) Ph. D. Thesis, Harvard University (unpublished)

(1965) Phys. Rev. 139, A241

Hüfner, S. (1962) Z. f. Physik 169, 417.

Johnson, R.C. and Little, W.A. (1963) Phys. Rev. 130, 596.

Kalbfleisch, H. (1964) Z. f. Physik 181, 13.

Kalbfleisch, H. (1965) Z. f. Physik 188, 186.

Kapitza, P. (1941) J. phys. USSR 4, 181.

Kastler, A. (1951) C. R. Acad. Sci., Paris, 232, 953.

Ketelaar, J.A.A. (1937) Physica 4, 619.

Kramers, H.A. (1930) Proc. Roy. Acad. Amst. 33, 959.

Kronig, R. deL. (1939) Physica 6, 33.

Kuang, Wey-Yen (1962) Soviet Physics Jetp 15, 635.

Lacroix, R. (1957) Helv. Phys. Acta. 30, 374.

Larson, G.H. and Jeffries, C.D. (1966) Phys. Rev. 141, 461.

Lee, K., Muir, H. and Catalano, E. (1965) J. Phys. Chem. Solids 26, 523.

Low, W. Paramagnetic Resonance in Solids, Suppl. 2 of Solid State Physics, Seitz and Turnbull ed.

Low, W. (1960) Nuovo Cimento 17, 607.

Meyer, H. and Smith, P.L. (1959) J. Phys. Chem. Solids 9, 285.

Mills, D.L. (1964) Phys. Rev. 133, A876.

Mims, W.B. (1965) Rev. Sci. Instr. 36, 1472.

Opechowski, W. (1953) Rev. Mod. Phys. 25, 264.

Orbach, R. (1961) Proc. Roy. Soc. A264, 458.

Orbach, R. and Blume, M. (1962) Phys. Rev. Lett. 8, 478.

Owen, J. (1961) J. appl. Phys. 32 Suppl., 213S.

Persico, F., Stevens, K.W.H. and Tucker, J.W. (1963) Phys. Lett. 5, 16.

Peterson, R.L. (1965) Phys. Rev. 137, A1444.

Ramachandran, G.N. and Ramaseshan, S. (1961) Encyclopedia of Physics (Flügge ed.) vol. XXV/1, p. 1.

Ramaseshan, S. (1951) Proc. Indian Acad. Sci. A34, 32.

Rannestad, A. and Wagner, P.E. (1963) Phys. Rev. 131, 1953.

Rieckoff, K.E. (1962) Ph.D. Thesis, University of British Columbia (unpublished).

Rieckoff, K.E. and Weissbach, R. (1962) Rev. Sci. Instr. 33, 1393.

Ryter, C. (1957) Helv. Phys. Acta 30, 353.

Schulz, M.B. and Jeffries, C.D. (1966) Phys. Rev.,to be published.

Scott, P.L. and Jeffries, C.D. (1962) Phys. Rev. 127, 32.

Shen, Y.R. (1963) Ph.D. Thesis, Harvard University, unpublished .

Shen, Y.R. (1964) Phys. Rev. 133, A511.

Shiren, N.S. and Tucker, E.B. (1959), Phys. Rev. Lett. 2, 206.

Statz, H., Rimai, L., Weber, M.J., De Mars, G.A., and Koster, G.F. (1961) J. appl. Phys. 32 Suppl., 218 S.

Stoneham, A.M. (1965) Proc. Phys. Soc. 86, 1163.

Van den Broek, J. and Van der Marel, L.C. (1963) Physica 29, 948.

Van Kranendonk, J. and Van Vleck, J.H. (1958) Rev. Mod. Phys. 30, 1.

Van Vleck, J.H. (1939) J. Chem Phys. 7, 72.

Van Vleck, J.H. (1940) Phys. Rev. 57, 426.

Van Vleck, J.H. (1941) Phys. Rev. 59, 724.

Van Vleck, J.H. (1959) Quantum Electronics, C.H. Townes ed. (Columbia Univ. Press) p. 391.

Van Vleck, J.H. (1961) Advances in Quantum Electronics (Columbia Univ. Press, J.R. Singer ed.) p. 388.

Van Vleck, J.H. and Hebb, M.H.(1934) Phys. Rev. 46, 17.

Wyckoff, Crystal Structures, Interscience Publishers, New York.

Ziman, J.M. (1954) Proc. Roy. Soc. A226, 436.